uOttawa

L'Université canadienne
Canada's university

FACULTÉ DES ÉTUDES SUPÉRIEURES ET POSTOCTORALES

uOttawa

L'Université canadienne
Canada's university

FACULTY OF GRADUATE AND POSDOCTORAL STUDIES

Rui Sun

AUTEUR DE LA THÈSE / AUTHOR OF THESIS

M.A.Sc. (Civil Engineering)

GRADE / DEGREE

Department of Civil Engineering

FACULTÉ, ÉCOLE, DÉPARTEMENT / FACULTY, SCHOOL, DEPARTMENT

Bearing Capacity and Settlement Behavior of Unsaturated Soils from Model Footing Tests

TITRE DE LA THÈSE / TITLE OF THESIS

Sai Vanapalli

DIRECTEUR (DIRECTRICE) DE LA THÈSE / THESIS SUPERVISOR

CO-DIRECTEUR (CO-DIRECTRICE) DE LA THÈSE / THESIS CO-SUPERVISOR

Mohammad Rayhani

Mamadou Fall

Jules Anges Infante Sedano

Gary W. Slater

Le Doyen de la Faculté des études supérieures et postdoctorales / Dean of the Faculty of Graduate and Postdoctoral Studies

BEARING CAPACITY AND SETTLEMENT BEHAVIOR OF UNSATURATED SOILS FROM MODEL FOOTING TESTS

by

Rui Sun

A Thesis
Submitted under the Supervision of
Dr. Sai K. Vanapalli, P.Eng.

In partial fulfillment of the requirements for
the degree of Master of Applied Science
in Civil Engineering

Department of Civil Engineering
University of Ottawa
Ottawa, Canada K1N 6N5

April 2010

Your file Votre référence
ISBN: 978-0-494-65950-2
Our file Notre référence
ISBN: 978-0-494-65950-2

This thesis is dedicated to my parents and girlfriend
for their love, endless support and encouragement.

ABSTRACT

A series of model footing tests were conducted to determine the bearing capacity and settlement behaviour of four different soils of which the first two were coarse-grained soils (i.e. Filtration sand and Quarry sand) and the remainder two were fine-grained soils (i.e. Sil-co-sil 106 and Mil-u-sil 30) using four different sizes of model footings (i.e. 20 mm × 20 mm, 37 mm × 37 mm, 41.75 mm in diameter, and 50 mm × 50 mm) over a suction range of 0 to 8 kPa. This range of matric suction 0 to 8 kPa extends over the boundary effect, transition and residual stages (Vanapalli et al. 1999) for the two coarse-grained soils (i.e. Filtration sand and Quarry sand). A soil container which is 300 mm in diameter and 700 mm in height has been used in the experiment. The targeted matric suction values in the soils were achieved by controlling the level of water table in the soil container and confirmed using Tensiometers installed in the soil at different depths.

The experimental results demonstrated that: 1) The variation of bearing capacity of coarse-grained soils (i.e. Filtration sand and Quarry sand) with respect to matric suction was nonlinear in nature. The bearing capacity increases up to the residual suction value and then decreases with further increase in matric suction values. The trends for settlement are however opposite; the settlement decreases up to residual suction value and gradually start increasing along with an increase in the matric suction. 2) For the unsaturated fine-grained soils (i.e. Sil-co-sil 106 and Min-u-sil 30), bearing capacity increases and settlement decreases as the matric suction increases because the suction range (i.e. 0 to 8 kPa) is in the boundary effect zone. In other words, the suction range in the boundary effect zone is lower than the air-entry value (i.e. saturation zone). More detailed discussions are offered with respect to the bearing capacity and settlement behaviour of unsaturated soils including the influence of footing size on the bearing capacity and settlement results. In addition, these test results were used to verify the semi-empirical models proposed by Vanapalli and Mohamed (2007) and Oh et al. (2009) for predicting the bearing capacity and settlement behaviour of unsaturated soils, respectively.

ACKNOWLEDGEMENTS

I am very grateful to my supervisor Dr. Sai K. Vanapalli for his guidance, encouragement, valuable advice and suggestions throughout this research program.

I would like to thank Geotechnical Lab technicians Kulan Ambalavanar and Jean Claude Celestin for helping me purchase and set up various materials and facilities required for the research program. I appreciate the help received from John Perrins in the student workshop who helped me to fabricate the model footings used in the experiment.

Thanks to my colleagues Won Taek Oh, Fathi, Lu Lu, Joseph, Nil, and other graduate students in Civil Engineering Department at the University of Ottawa for their assistance.

Finally, I thank the faculty and staff in Civil Engineering Department for providing support to my graduate study.

Table of Contents

List of Figures

List of Tables

CHAPTER 1

INTRODUCTION

1.1 Statement of the Problem

Conventional soil mechanics principles are commonly used in engineering practice assuming soils are typically found in a state of saturated condition in nature. However, soils typically have other fluids in the voids (e.g., air) along with water. There are numerous soils; for example, expansive, compacted, residual, cemented, weakly bonded or collapsible soils that are frequently encountered in engineering practice are typically in a state of unsaturated condition. About 33% of the earth's surface is considered either arid or semi-arid and the natural soils in these regions are unsaturated soils (Dregne, 1976).

The bearing capacity and settlement are two key parameters required in the design of shallow foundations. The shallow foundations are usually located above the ground water table where the soil is typically in a state of unsaturated condition. The stresses associated with the loading of these foundations are also distributed within the unsaturated zone (i.e., above groundwater table). Therefore, the bearing capacity and settlement behavior should be interpreted taking account of the influence of capillary stresses (i.e., matric suction). However, in conventional engineering practice, foundations are designed assuming the soil is in a state of saturated condition such that the design approach is conservative both for bearing capacity and settlement behavior. The estimated bearing capacity is lower and the settlement is larger by extending the conventional soil mechanics approach. Such simplistic approaches are followed in engineering practice because a valid framework for interpreting the bearing capacity of unsaturated soils is not available.

A rational approach for interpreting the mechanical behavior of unsaturated soils, using two independent stress state variables, namely matric suction and net normal stress was put forward by Fredlund and Morgenstern (1977). The matric suction is defined as the difference between the pore air pressure, u_a and pore water pressure, u_w. Several studies were undertaken to understand the contribution of matric suction towards the bearing capacity of unsaturated soils (Broms 1964, Steensen-Bach et al. 1987, Fredlund and Rahardjo 1993, Schnaid et al. 1995, Oloo et al. 1997, Miller and Muraleetharan 1998, Costa et al. 2003, Yongfu 2004). However, it is only recently a framework has been put forward to both interpret and predict the bearing capacity and settlement behavior of unsaturated soils based on several research studies undertaken at the University of Ottawa. More details of these studies are briefly summarized in the next section.

1.2 Background

Mohamed and Vanapalli (2006) designed a tank (900 mm × 900 mm × 750 mm) with special provisions to determine the bearing capacity and settlement behavior of model footings in both saturated and unsaturated conditions. Based on the bearing capacity tests using two different sizes of square model footings (100 mm × 100 mm and 150 mm × 150 mm) on a compacted, fine-grained sand), Vanapalli and Mohamed (2007) have provided a relationship to both interpret and predict the variation of bearing capacity of unsaturated soils with respect to matric suction using the saturated shear strength parameters (c', ϕ) and the Soil-Water Characteristic Curve (SWCC). There was a good comparison between the measured and predicted bearing capacity values. The proposed relationship shows a smooth transition between the bearing capacity of unsaturated soils and the conventional Terzaghi's (1943) bearing capacity equation for saturated soils.

Vanapalli et al. (2007) have conducted a series of model footing tests on statically compacted unsaturated Indian Head till soil samples at different matric suction values to

determinate the contribution of matric suction towards bearing capacity of unsaturated soils under undrained loading conditions. Based on the results of these studies, Vanapalli et al. (2007) proposed a relationship for estimating the bearing capacity of unsaturated soils under undrained loading conditions using the unconfined compression test results under saturated condition and the soil-water characteristic curve (SWCC). There was a good comparison between the measured and estimated bearing capacity values.

Oh & Vanapalli (2008) conducted finite element analysis using SIGMA/W of GEO-SLOPE to model the stress versus settlement behavior of foundations in unsaturated sands simulating the testing conditions summarized in Vanapalli & Mohamed (2007) and Vanapalli et al. 2007. The results of the modeling studies show that the conventional stress distribution theory concepts extending elastic analysis can be used to estimate the stresses below foundation. In addition, the assumption of calculating the average matric suction value from 0 to 1.5B depth region is reasonable as it provided good comparison between the measured and predicted bearing capacity values for sands in unsaturated conditions (Poulos & Davis, 1974). These results also show that the bearing capacity of model footings of 50 mm width or lower can be conducted using relatively smaller size tanks of 300 mm diameter. In other words, the results using tank sizes greater than 300 mm also provide similar results when the model footings sizes are less than 50 mm. This study results were encouraging as small scale model footing tests can be used to generate experimental data more quickly and to understand the various parameters that influence the bearing capacity and settlement behavior of unsaturated soils; which are time consuming and difficult to conduct using large size model footing tests.

Li (2008) conducted model footing tests to investigate the bearing capacity of three compacted (coarse-grained, sub-coarse-grained, and fine-grained) sands under both

saturated and unsaturated conditions. These tests were conducted using four different sizes of square model footings (20 mm × 20 mm, 25 mm × 25 mm, 37.5 mm × 37.5 mm, and 50 mm × 50 mm) in two different soil containers (short container with 300 mm in diameter and 300 mm in height and the tall container with 300 mm in diameter and 700 mm in height) that were specially designed and for conducting these tests. The trends of experimental results were consistent with the earlier results of Mohamed and Vanapalli (2006).

A semi-empirical model has been proposed by Oh et al. (2009) to predict the variation of modulus of elasticity with respect to matric suction for unsaturated soils using the soil-water characteristic curve (SWCC) and the modulus of elasticity under saturated conditions. Using this model, three different sandy soils were used to compare the predicted and measured moduli of elasticity and elastic settlements from model footing test results. There was good agreement between the predicted and measured moduli of elasticity and elastic settlements.

All the above studies were encouraging; however, there is a need to conduct more model footing tests on different soils. In addition, it is also important to understand the various parameters that influence the bearing capacity and settlement behavior of unsaturated soils. Such studies will encourage the practicing engineers to extend the mechanics of unsaturated soils into practice.

1.3 Objectives of the Research

The focus of the present research is to study bearing capacity and settlement behavior of four different unsaturated soils under a controlled laboratory environment using four different sizes of model footings in a specially designed apparatus.

The following objectives were addressed in the research presented in this thesis:

1) To determine the bearing capacity of four different soils using different size of model footings under saturated and unsaturated conditions. Two of the soils studied were coarse-grained sands and the other two were commercially available Sil-co-sils that are commonly used in paste backfills.
2) To predict the variation of bearing capacities with respect to different matric suction values using the SWCC and the saturated shear strength parameters and provide comparison with the measured bearing capacity values.
3) To study the variation of settlement with respect to different matric suction values under a certain applied stress and provide comparison with the measured and predicted settlement values.
4) To investigate the influence of size and shape of model footings on the bearing capacity and settlement behavior of unsaturated soils.

1.4 Scope of the Thesis

The experimental studies related to the research objectives listed in the earlier section were undertaken at the Geotechnical Laboratory of the University of Ottawa. The shear strength parameters, namely; the effective cohesion c' and the angle of internal friction ϕ of the tested soils were determined using triaxial shear test. The SWCCs for the tested soils were obtained using Tempe Cell Apparatus and WP4-T. Moreover, other soil properties such as grain size analysis, suction profile (i.e. the relationship between matric suction and depth of ground water table) were also determined in the laboratory using the procedure developed by Li (2008). Different values of matric suction in the soil below the model footings were achieved by lowering water table to different depths below the soil surface. The matric suction values in the stress bulb zone under the footing were confirmed by tensiometers located at different depths in the soil container before conducting model footing tests under unsaturated conditions.

1.5 Outline of the Thesis

This thesis is organized into six chapters. This chapter provides the background information related to studies undertaken with model footings at the University of Ottawa and summarizes the objectives of the research program.

The second chapter, "Literature Review", provides a brief summary on the bearing capacity and settlement of saturated and unsaturated soils.

The third chapter, "Equipments and Methodology", outlines the details of all the equipments used in the experimental study, including the methodology for carrying out the research.

The fourth chapter, "Soil Properties", details the properties of four soils which include the grain size distribution, suction profile, soil-water characteristic curve (SWCC), and the shear strength characteristics.

The fifth chapter, "Results and Analysis", reports all the test results. The relationship of bearing capacity and settlement with respect to matric suction is discussed for different soil studied as a part of the present research. In addition, the influence of footing size and shape on the bearing capacity values and settlements are also discussed.

The last chapter, "Conclusions", presents summary and conclusions of this research. Furthermore, experimental problems encountered during the research program are briefly addressed and some recommendations are also advised for future research studies.

CHAPTER 2

LITERATURE REVIEW

2.1 General

Bearing capacity and settlement are two of the key parameters required in the design of foundations, dams, retaining walls, bridge abutments, and temporary support structures. This chapter compiles background information related to bearing capacity and settlement behavior of soils both in saturated and unsaturated conditions. More focus has been directed towards compiling recent research related to the interpretation and prediction of the bearing capacity and settlement behavior of unsaturated soils.

2.2 Bearing Capacity of Saturated Soils

In this section, some of the important studies undertaken by various researchers that are conventionally used in engineering practice with respect to the bearing capacity of saturated soils are summarized.

2.2.1 Terzaghi (1943)

The failure surface at ultimate load under a continuous or strip foundation suggested by Terzaghi (1943) is shown in Figure 2.1. The failure area in the soil under the foundation load was divided into five zones, one Zone I and two pairs of Zone II and Zone III.

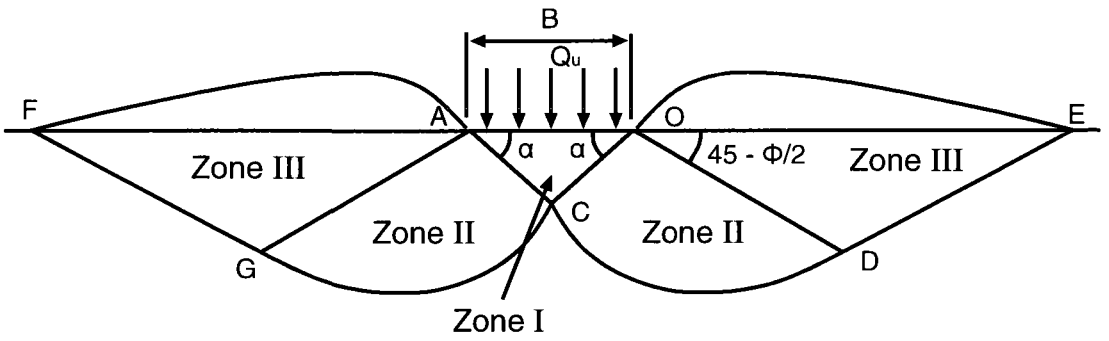

Figure 2.1 Bearing capacity failure in soil under a rough rigid continuous foundation (modified after Terzaghi 1943)

i. The triangular Zone I under the footing base is considered as a part of the footing and penetrates the soil like a wedge because of friction and adhesion between the footing base and the soil.

ii. Zones II's that are located between Zone I and Zone III are known as the radial shear zones which constitute the shear pattern lines that radiate from the outer edge of the base of the footing.

iii. Zones III's are identical to Rankine passive state with respect to shear pattern lines that develop in these zones.

Terzaghi extended the limit equilibrium method and suggested using equation [2.1] for estimating the ultimate bearing capacity per unit area of the foundation. The bearing capacity of the soil is dependent on the dimensions of the footing, the unit weight and the saturated shear strength parameters, c' and ϕ'.

$$q_u = c'N_c + qN_q + 0.5B\gamma N_\gamma \qquad [2.1]$$

where:

q_u = ultimate bearing capacity, kPa

c' = effective cohesion, kPa

ϕ' = internal friction angle for saturated condition, deg.

q = effective overburden pressure, kPa

B = width of the footing, m

γ = unit weight of the soil, kN/m^3

N_c = bearing capacity factor due to cohesion

N_q = bearing capacity factor due to surcharge

N_γ = bearing capacity factor due to unit weight

Terzaghi also proposed bearing capacity factors in terms of angle of internal friction, ϕ' as below:

$$N_q = \frac{e^{2\left(\frac{3\pi}{4}-\frac{\phi'}{2}\right)\tan\phi'}}{2\cos^2(45+\frac{\phi'}{2})} \qquad [2.2]$$

$$N_c = (N_q - 1)\cot\phi' \qquad [2.3]$$

$$N_r = \frac{1}{2}K_{p\gamma}\tan^2\phi' - \frac{\tan\phi'}{2} \qquad [2.4]$$

where:

$$K_{p\gamma} = \tan^2(45+\phi/2) \qquad [2.5]$$

Table 2.1 summarizes the variation of the bearing capacity factors with soil friction angle ϕ'. The values N_c and N_q are from Terzaghi (1943) and N_γ values were obtained by

Kumbhojkar (1993). Kumbhojkar (1993) study shows that bearing capacity computations provide better comparisons with the measured bearing capacity values using the N_γ values based on his study results. Vanapalli and Mohamed (2007) and Oh and Vanapalli (2008) studies also support these results.

Table 2.1 Bearing Capacity Factors used in the research study, N_c and N_q from Terzaghi (1943) and N_γ from Kumbhojkar (1993)

Φ'	N_c	N_q	N_γ	Φ'	N_c	N_q	N_γ	Φ'	N_c	N_q	N_γ
0	5.70	1.00	0.00	17	14.60	5.45	2.18	34	52.64	36.50	38.04
1	6.00	1.1	0.01	18	15.12	6.04	2.59	35	57.75	41.44	45.41
2	6.30	1.22	0.04	19	16.57	6.70	3.07	36	63.53	47.16	54.36
3	6.62	1.35	0.06	20	17.69	7.44	3.64	37	70.01	53.80	65.27
4	6.97	1.49	0.10	21	18.92	8.26	4.31	38	77.50	61.55	78.61
5	7.34	1.64	0.14	22	20.27	9.19	5.09	39	85.97	70.61	95.03
6	7.73	1.81	0.20	23	21.75	10.23	6.00	40	95.66	81.27	115.31
7	8.15	2.00	0.27	24	23.36	11.40	7.08	41	106.81	93.85	140.51
8	8.60	2.21	0.35	25	25.13	12.72	8.34	42	119.67	108.75	171.99
9	9.09	2.44	0.44	26	27.09	14.21	9.84	43	134.58	126.50	211.56
10	9.61	2.69	0.56	27	29.24	15.90	11.60	44	151.95	147.74	261.60
11	10.16	2.98	0.69	28	31.61	17.81	13.70	45	172.28	173.28	325.34
12	10.76	3.29	0.85	29	34.24	19.98	16.18	46	196.22	204.19	407.11
13	11.41	3.63	1.04	30	37.16	22.46	19.13	47	224.55	241.19	512.84
14	12.11	4.02	1.26	31	40.41	25.28	22.65	48	258.28	287.85	650.87
15	12.86	4.45	1.52	32	44.04	28.52	26.87	49	298.71	344.63	831.99
16	13.68	4.92	1.82	33	48.09	32.23	31.94	50	347.50	415.14	1072.80

Table 2.2 below summarizes the shape factor as defined by Terzaghi (1943).

Table 2.2 Terzaghi (1943) shape factors for various shallow foundations

Shape factor	Strip footing	Square footing	Circular footing
s_c	1.0	1.3	1.3
s_γ	1.0	0.8	0.6

Note 1: s_c = shape factor due to cohesion

Note 2: s_γ = shape factor due to unit weight

Terzaghi (1943) included the shape factors and proposed the following relationships for

square and circular foundations.

$$q_u = 1.3cN_c + qN_q + 0.4\gamma BN_\gamma \quad \text{(square foundation)} \qquad [2.6]$$

and

$$q_u = 1.3cN_c + qN_q + 0.3\gamma BN_\gamma \quad \text{(circular foundation)} \qquad [2.7]$$

2.2.2 Meyerhof (1951)

Meyerhof (1951) suggested a bearing capacity theory which could be applied to rough shallow and deep foundations. The failure surface at ultimate load under a continuous shallow foundation assumed by Meyerhof (1951) is shown in Figure 2.2. In this figure, *abc* is the elastic triangular wedge, *bcd* is the radial shear zone with *cd* being an arc of a log spiral, and *bde* is a mixed shear zone in which the shear varies between the limits of radial and plane shear, depending on the depth and roughness of the foundation. The plane *be* is called an equivalent free surface. The normal and shear stresses on plane *be* are p_o and s_o, respectively.

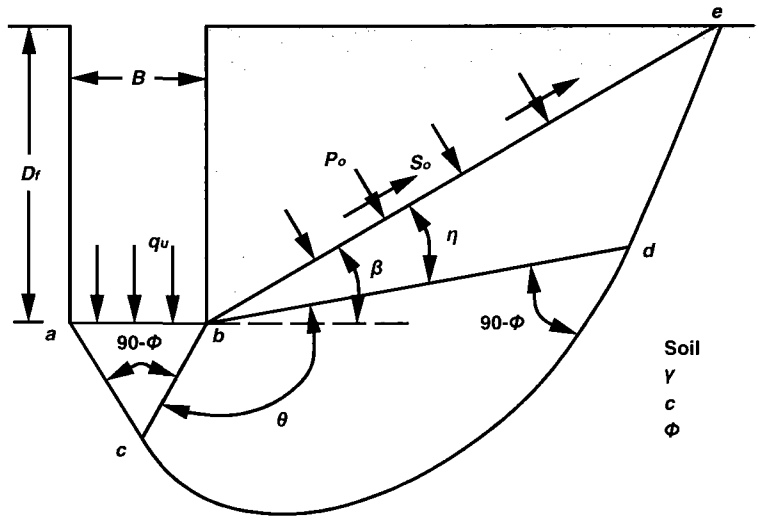

Figure 2.2 Slip line fields for a rough continuous foundation (Meyerhof 1951)

The ultimate bearing capacity, q_u, of the continuous foundation is expressed similar to the Terzaghi's equation.

$$q_u = c' N'_c + qN'_q + 0.5B\gamma N'_\gamma \quad [2.8]$$

where:

N'_c, N'_q, N'_γ = bearing capacity factors associated with cohesion, surcharge and unit weight which can be determined using the equations below:

$$N'_q = e^{\pi \tan\phi'} \left(\frac{1+\sin\phi'}{1-\sin\phi'} \right) \quad [2.9]$$

$$N'_c = (N'_q - 1)\cot\phi' \quad [2.10]$$

$$N'_\gamma = (N'_q - 1)\tan(1.4\phi') \quad [2.11]$$

Table 2.3 Variation of Meyerhof's Bearing Capacity Factors N_q', N_c' and N_γ' (Meyerhof 1951)

Φ'	N_c	N_q	N_γ	Φ'	N_c	N_q	N_γ	Φ'	N_c	N_q	N_γ
0	5.14	1.00	0.00	17	12.34	4.77	1.66	34	42.16	29.44	31.15
1	5.38	1.09	0.002	18	13.10	5.26	2.00	35	46.12	33.30	37.15
2	5.63	1.20	0.01	19	13.93	5.80	2.40	36	50.59	37.75	44.43
3	5.90	1.31	0.02	20	14.83	6.40	2.87	37	55.63	42.92	53.27
4	6.19	1.43	0.04	21	15.82	7.07	3.42	38	61.35	48.93	64.07
5	6.49	1.57	0.07	22	16.88	7.82	4.07	39	67.87	55.96	77.33
6	6.81	1.72	0.11	23	18.05	8.66	4.82	40	75.31	64.20	93.69
7	7.16	1.88	0.15	24	19.32	9.60	5.72	41	83.86	73.90	113.99
8	7.53	2.06	0.21	25	20.72	10.66	6.77	42	93.71	85.38	139.32
9	7.92	2.25	0.28	26	22.25	11.85	8.00	43	105.11	99.02	171.14
10	8.35	2.47	0.37	27	23.94	13.20	9.46	44	118.37	115.31	211.41
11	8.80	2.71	0.47	28	25.80	14.72	11.19	45	133.88	134.88	262.74
12	9.28	2.97	0.60	29	27.86	16.44	13.24	46	152.10	158.51	328.73
13	9.81	3.26	0.74	30	30.14	18.40	15.67	47	173.64	187.21	414.32
14	10.37	3.59	0.92	31	32.67	20.63	18.56	48	199.26	222.31	526.44
15	10.98	3.94	1.13	32	35.49	23.18	22.02	49	229.93	265.51	674.91
16	11.63	4.34	1.38	33	38.64	26.09	26.17	50	266.89	319.07	873.84

Table 2.3 summarizes the variation of N'_q , N'_c and N'_γ obtained from Eqs. [2.9] and [2.10] and [2.11], respectively. The new set of bearing capacity factors were suggested by Meyerhof (1951) because failure zone surface is different in shape from the failure wedge proposed by Terzaghi (1943).

2.2.3 Vesić (1973)

Vesić (1973) proposed an improved bearing capacity based on Terzaghi (1943) theory by introducing different bearing capacity factors and shape factors which were recommended for reliable computation of the bearing capacity. The shape factors proposed by Vesić (1973) take into account the bearing capacity factors and the footing dimensions.

$$q_{ult} = c' N_{cv} \xi_c + q N_{qv} \xi_q + 0.5 \gamma B N_{\gamma v} \xi_\gamma \qquad [2.12]$$

where:

$$N_{qv} = e^{\pi \tan \phi'} \tan^2 (45 + \phi'/2) \qquad [2.13]$$

$$N_{cv} = (N_{qv} - 1) \cot \phi' \qquad [2.14]$$

$$N_{\gamma v} = 2(N_q + 1) \tan \phi' \qquad [2.15]$$

$$\xi_c = 1 + (B/L)(N_q / N_c) \qquad [2.16]$$

$$\xi_q = 1 + (B/L) \tan \phi' \qquad [2.17]$$

$$\xi_\gamma = 1 - 0.4(B/L) \qquad [2.18]$$

N_{cv} and N_{qv} are not very different from Terzaghi's bearing capacity factors (i.e. N_c and N_q). However, the value of $N_{\gamma v}$ is different due to differences in the assumption

with respect to the failure angle α (as shown in Figure 2.1). The N_γ values of Terzaghi (1943) and Meyerhof (1951) are lower than the values proposed by Vesić (1973). The question of which set of N_γ values are more appropriate has remained unsettled, because of difficulties in selecting a representative value of angle of shearing resistance, ϕ' for the bearing capacity factor N_γ (Vesić 1973). However, more recently the N_γ values proposed by Kumbojkar (1993) are more widely used.

Vesić (1973) studies also show the position of the ground water table can influence the bearing capacity of a footing significantly. It was recommended to base the bearing capacity analysis assuming the highest possible ground water table level during the lifetime of the foundation. If the highest ground water table level is within the depth, $z_w \leq B$ below the foundation base, then the effective unit weight, γ of the soil below the foundation base was suggested to be calculated using the equation below (Figure 2.3):

$$\gamma = \gamma' + [\frac{z_w}{B}](\gamma_m - \gamma') \qquad [2.19]$$

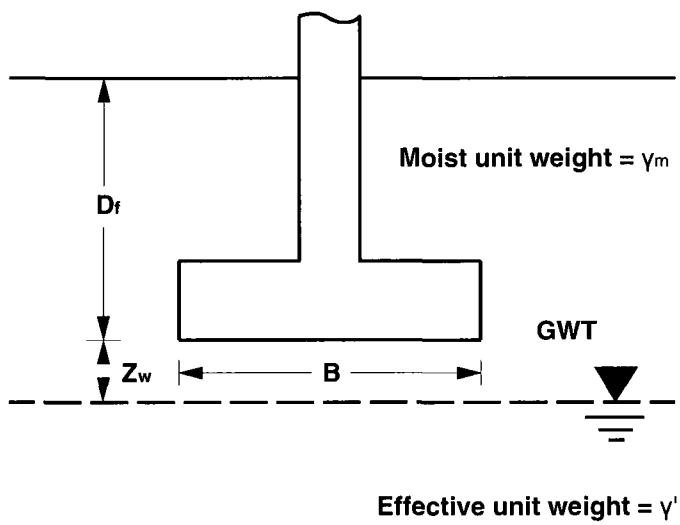

Figure 2.3 Effect of ground water table on ultimate bearing capacity (modified after Vesić 1973)

If $z_w = B$, the effective unit weight should be taken as γ_m (moist unit weight) and for a water table at or above the foundation level, the submerged unit weight should be used in the Equation [2.12].

2.3 Settlement of Shallow Foundations

2.3.1 Introduction

The safety against bearing capacity failure as well as excessive settlement of the foundation should be considered in the design of foundations. In many practical scenarios, it is the settlement which will be the governing design criteria rather than the bearing capacity of the soil. This section describes the procedures for estimating the settlement of foundations due to simple axial load.

The settlement of a foundation can have three components: (a) elastic settlement, S_i; (b) primary consolidation settlement, S_c; (c) secondary consolidation settlement, S_s. Thus the total settlement S_t can be expressed as

$$S_t = S_i + S_c + S_s \qquad [2.20]$$

For any given foundation, one or more of the components may be zero or negligible. Elastic settlement is caused by deformation of dry, saturated or unsaturated soil without any change in moisture content (Das 1999). Primary consolidation settlement is a time-dependent process which occurs in clayey soils located below the ground water table as a result of the volume change in soil because of the expulsion of water that occupies the void spaces. Secondary consolidation settlement follows the primary

consolidation process in saturated clayey soils is a result of the plastic adjustment of soil fabric.

2.3.2 Settlement from elastic theory

Mayne and Poulos (1999) provided a general relationship for elastic settlement calculation of footings using displacement influence factors derived from elasticity continuum theory. It is assumed that the soil stiffness increases linearly with depth, from a value of E_o at footing level. According to this theory (Figure 2.4):

$$\rho_{center} = \frac{qdI_G I_F I_E (1-\nu^2)}{E_o} \qquad [2.21]$$

where:

d = equivalent diameter of a rectangular footing

ν = Poisson's ratio of soil

I_G = displacement influence factor (Figure 2.5)

I_E = settlement coefficient factor to account for depth of embedment

I_F = rigidity coefficient factor

The relationships to estimate I_E and I_F are:

$$I_E = 1 - \frac{1}{3.5\exp(1.22\nu - 0.4)\left[\left(\frac{d}{z_e}\right)+1.6\right]} \qquad [2.22]$$

$$I_F = \frac{\pi}{4} + \frac{1}{4.6 + 10\left(\frac{E_f}{E_o + \frac{d}{2}k_E}\right)\left(\frac{2t}{d}\right)^3} \qquad [2.23]$$

where E_f = modulus of elasticity of the footing material (which is, in most cases, reinforced concrete), t = footing thickness, z_e = embedment depth of the footing, and k_E = increase in soil stiffness per unit depth (i.e., $E_S = E_o + k_E z$).

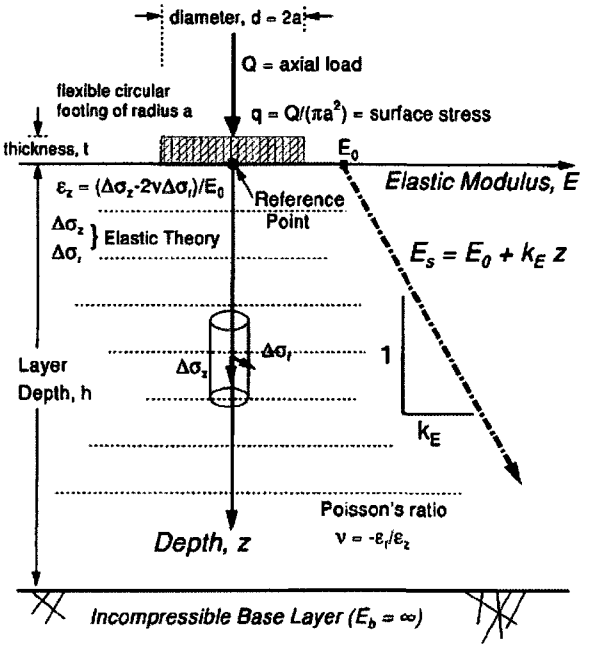

Figure 2.4 Footing on a compressible layer (Mayne and Poulos 1999)

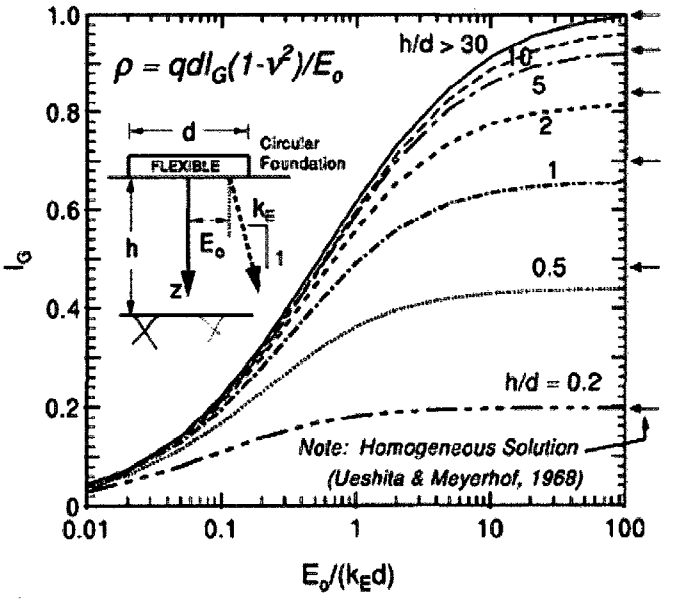

Figure 2.5 Variation of I_G with $E_o/k_E d$ and h/d (Mayne and Poulos 1999)

2.3.3 Modulus of elasticity

The magnitudes of immediate settlement for practical applications are evaluated from Young's modulus E_s and Poisson's ratio v_s. Young's elastic modulus is commonly used for estimation of settlement from static loads. Lade and Nelson (1987), Lade (1988), and Lancelotta (1995) studies show that the elastic settlement is significantly influenced by the stress-strain modulus, E_s, while Poisson's ratio, v (which varies from 0.25 to 0.49) does not play an important role. The modulus of elasticity, E, can be estimated both from laboratory and field tests. In general, the modulus of elasticity from conventional triaxial tests can be underestimated due to sample disturbance caused by stress relief and other mechanical disturbances. To overcome this disadvantage, Davis and Poulos (1968) suggested the use of K_0-consolidation triaxial test results to derive the modulus of elasticity. According to the test results by Simons and Som (1970), the modulus of elasticity from K_0-consolidation triaxial tests are significantly higher than those determined from conventional undrained triaxial tests (Oh et al. 2009).

Plate load tests, cone penetration tests, pressuremeter tests or geophysical methods (i.e., seismic methods) are usually used to estimate the in situ modulus of elasticity. In the case of plate load tests (or model footing tests), the modulus of elasticity, E, can be calculated using Eq. [2.24] (Timoshenko and Goodier 1951).

$$E = \frac{1-v^2}{\Delta\delta / \Delta q_p} B_p I_w \qquad [2.24]$$

where $\Delta\delta / \Delta q_p$ is the slope of the settlement versus plate pressure, B_p is the width or diameter of the plate, and I_w is the influence factor (i.e., 0.79 for a circular plate and 0.88 for a square plate).

2.4 Failure Mechanisms in Shallow Foundations

2.4.1 General shear failure

Figure 2.6 shows a shallow foundation of width B located at a depth D_f below the ground surface and supported by a dense sand or stiff clayey soil. If this foundation is subjected to a load Q which is gradually increased, the load per unit area, $q = Q/A$ (A = area of the foundation), will increase and the foundation will undergo increased settlement.

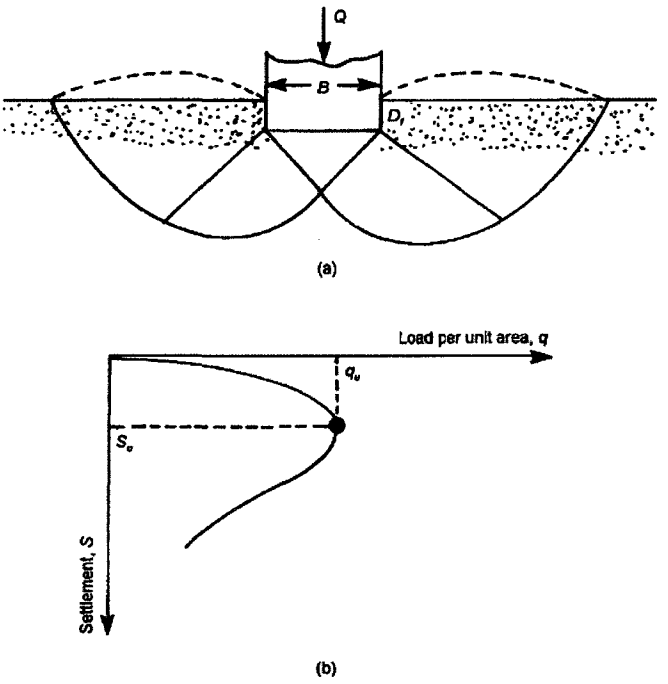

Figure 2.6 General shear failure in soil (modified after Terzaghi 1943 and Vesić 1963 by Das 1999)

When q reaches a value equal to q_u at foundation settlement $S = S_u$, the soil supporting the foundation undergoes sudden shear failure. The failure surface in the soil is shown in Figure 2.6a, and the q versus S plot is shown in Figure 2.6b. This type of failure is called general shear failure, and q_u is the ultimate bearing capacity. In this

type of failure, a peak value $q = q_u$ is clearly defined in the load-settlement curve.

2.4.2 Local Shear Failure

If the foundation shown in Figure 2.6a is supported by a medium dense sand or clayey soil of medium consistency (Figure 2.7a), the plot of q versus S will be as shown in Figure 2.7b.

The magnitude of q increases with settlement up to $q = q_u'$, which is usually referred to as the first failure load. At this time, the developed failure surface in the soil will be like that shown by the solid lines in Figure 2.7a. If the load on the foundation is further increased, the load-settlement curve becomes steeper and erratic with the gradual outward and upward progress of the failure surface in the soil (shown by the broken lines in Figure 2.7a) under the foundation.

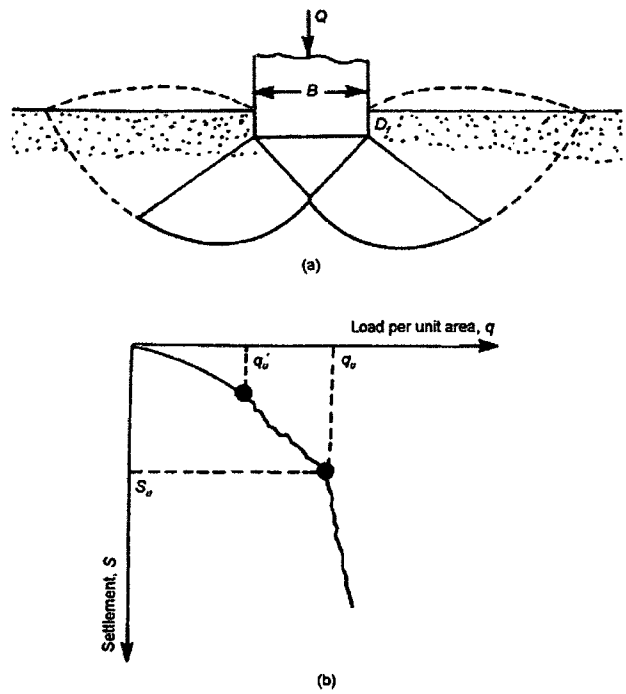

Figure 2.7 Local shear failure in soil (modified after Terzaghi 1943 and Vesić 1963 by Das 1999)

When q becomes equal to q_u (ultimate bearing capacity), the failure surface reaches the ground surface. Beyond that, the plot of q versus S takes almost a linear shape, and a peak load is never observed. This type of bearing capacity failure is called local shear failure.

2.4.3 Punching Shear Failure

Figure 2.8a shows the same foundation located on a loose sand or soft clayey soil. For this case, the load-settlement curve will be like that shown in Fig. 2.8b.

A peak value of load per unit area, q, is never observed. The ultimate bearing capacity, q_u, is defined as the point where $\Delta S/\Delta q$ becomes the largest and almost constant thereafter.

This type of failure in soil is called punching shear failure. In this case, the failure surface never extends up to the ground surface.

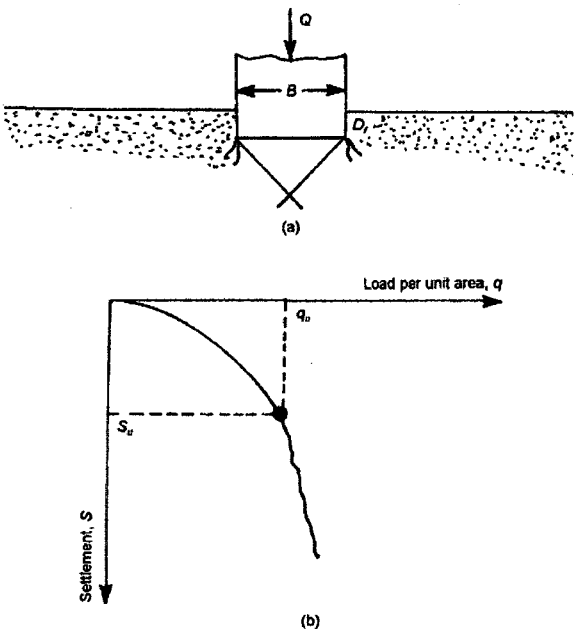

Figure 2.8 Punching shear failure in soil (modified after Terzaghi 1943 and Vesić 1963 by Das 1999)

The nature of failure in soil at ultimate load is a function of several factors such as the strength and the relative compressibility of soil, the depth of the foundation (D_f) in relation to the foundation width (B), and the width-to-length ratio (B/L) of the foundation. Vesić (1973) explained this behavior conducting extensive laboratory model tests using model rectangular footings loaded on the surface of sand. The summary of Vesić's findings is shown in Figure 2.9. In this figure, D_r is the relative density of sand, and the hydraulic radius, R, of the foundation is defined as

$$R = \frac{A}{P} \qquad [2.25]$$

where: A = area of the foundation = BL

P = perimeter of the foundation = $2(B + L)$

Thus

$$R = \frac{BL}{2(B+L)} \qquad [2.26]$$

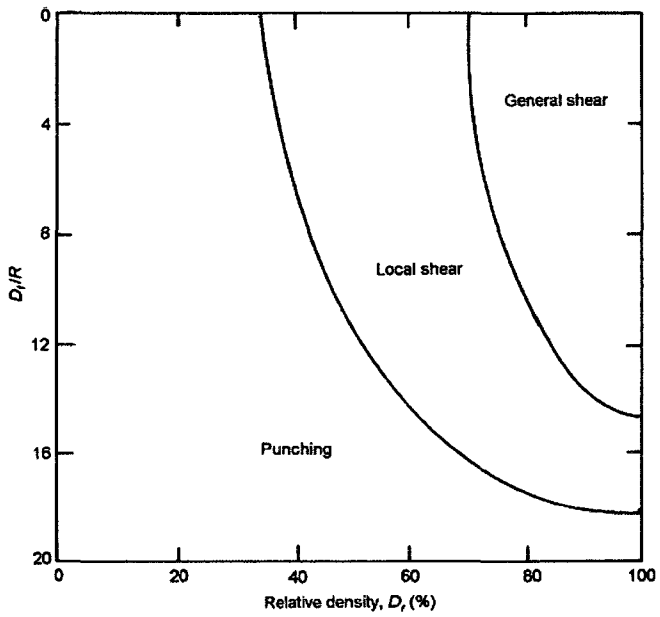

Figure 2.9 Nature of failure in soil with relative density of sand (D_r) and D_f/R (modified after Vesić 1973)

Equation [2.26] yields the relationship below for a square foundation, $B = L$.

$$R = \frac{B}{4} \qquad [2.27]$$

From Fig. 2.9 it can be seen that, when $D_f / R \geq$ about 18, punching shear failure occurs in all cases, irrespective of the relative density of compacted sand.

2.5 Bearing Capacity of Unsaturated Soils

The measured bearing capacity from field tests is typically higher than the estimated or computed bearing capacity values using classical methods (Terzaghi 1943, Meyerhof 1951, Vesić 1973). This behavior may be attributed to neglecting the contribution of suction towards the bearing capacity of soils (Steensen-Bach et al. 1987, Fredlund and Rahardjo 1993). Significant advances were made during the last twenty years towards understanding the engineering behavior of unsaturated soils; however, a valid framework for interpreting the bearing capacity of unsaturated soils has not been developed until recently. Some of the key research works related to the bearing capacity of unsaturated soils are summarized in this section.

2.5.1 Broms (1964)

Broms (1964) was one of the earliest investigators to propose a method to evaluate the bearing capacity of flexible pavement in unsaturated soils. This method assumed that the failure takes place in fully saturated subgrade soil. The bearing capacity was found to be a function of the degree of saturation, S, the apparent cohesion, c and internal friction angle, ϕ. From this study, it was found that a decrease in the degree of saturation from 100 to 90% increased the bearing capacity of two fine-grained soils (i.e., silt and clay) by approximately 2 and 8% respectively. Broms (1964) studies suggest that the bearing

capacity of the subgrade is reduced due to an increase in the degree of saturation. Figure 2.10 shows the relationship between the tire pressure and the ultimate wheel load with respect to the degree of saturation, *S*. Apparently, the degree of saturation has a significant effect on the bearing capacity of the pavement. These studies did not consider the influence of suction, but were explained with reference of the degree of saturation, *S* values.

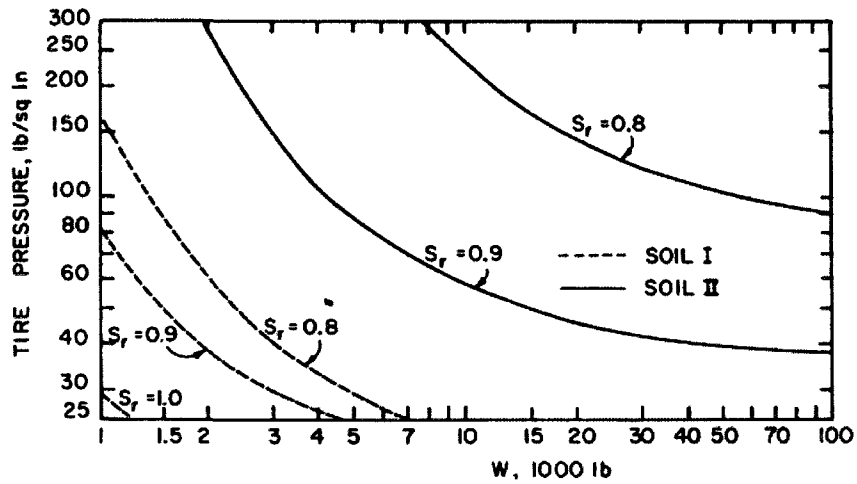

Figure 2.10 The tire pressure versus wheel load of flexible pavement (Broms 1964)

2.5.2 Steensen-Bach et al. (1987)

Steensen-Bach et al. (1987) performed surface model footing (22 mm × 22 mm × 20 mm) tests on Sollerod and Lund sand using a circular steel test pit (200 mm diameter × 120 mm height) under saturated and unsaturated conditions. The capillary pressure (i.e., matric suction) below the footings was determined by in-situ measurements using Tensiometers and using the soil-water characteristic curves (SWCC) (Figure 2.11). It was found that the measured bearing capacity of unsaturated sand is typically 4 to 6 times higher than the saturated bearing capacity of the same soil. Based on experimental studies on model tests on three different sands, Steensen-Bach (1987) concluded that the presence of capillary pressures is certainly fact, not fiction, and its effect should be

carefully considered.

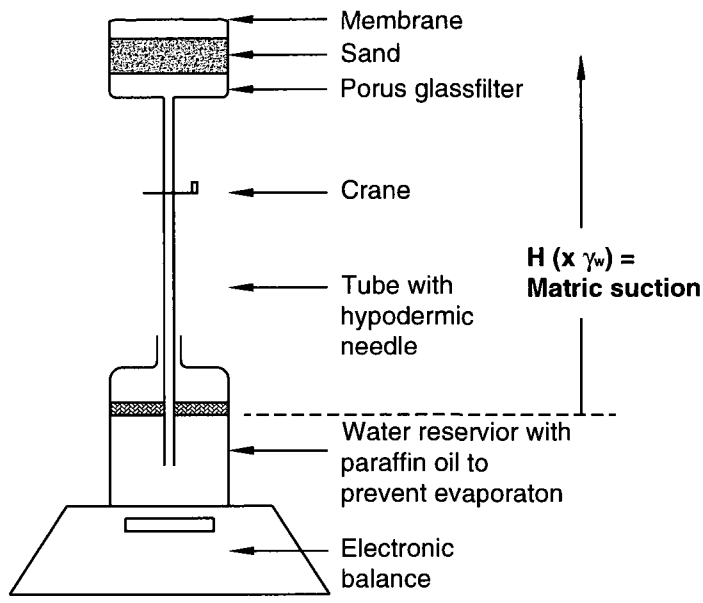

Figure 2.11 General scheme of the SWCC measuring equipment (Steensen-Bach et al. 1987)

2.5.3 Fredlund and Rahardjo (1993)

Fredlund and Rahardjo (1993) proposed bearing capacity equations for unsaturated soils by extending conventional bearing capacity equations including the influence of matric suction in the term apparent cohesion extending total stress approach.

The apparent cohesion consists of two components expressed by Equation [2.28]. The first component is the effective cohesion, c' and the other component is the contribution due to matric suction, $(u_a - u_w)$. The contribution of matric suction, $(u_a - u_w)$ can be considered as an additional cohesion component in total stress approach. In other words, the conventional bearing capacity theory can be extended to unsaturated soils by adding the component of matric suction to effective cohesion, c'. The increase of the cohesion is due to matric suction which is illustrated in Figure 2.12 for various ϕ^b values.

$$c_{unsat} = c' + (u_a - u_w)\tan\phi^b \qquad [2.28]$$

where:

c_{unsat} = total cohesion, *kPa*

ϕ^b = internal friction angle with respect to matric suction, *(deg.)*

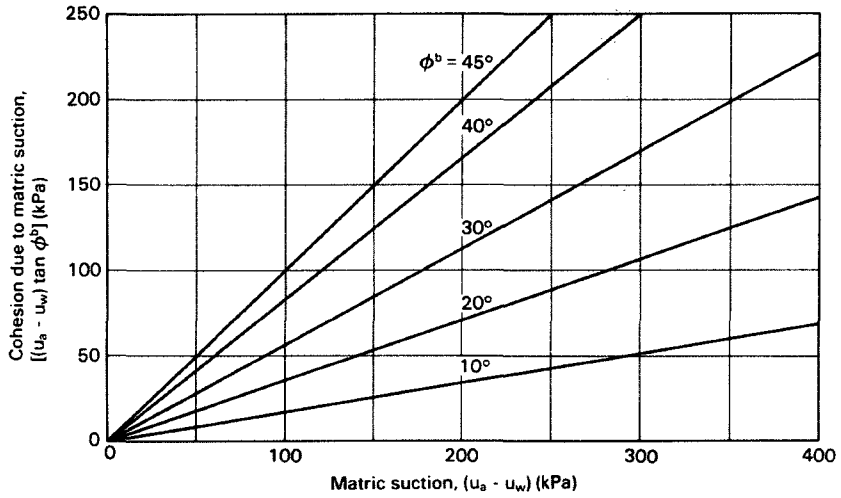

Figure 2.12 The component of cohesion due to matric suction for angles (Fredlund and Rahardjo 1993)

A theoretical study was undertaken to evaluate the effect of soil matric suction on the ultimate bearing capacity using a square footing embedded in clay type of soil. Based on this study, it was reported an increase in the bearing capacity by 27% when the matric suction increased by an amount equal to the undrained shear strength of the fine-grained soil. Figure 2.13 shows the relationship between the bearing capacity of a strip footing for various matric suction values, obtained by Fredlund and Rahardjo (1993).

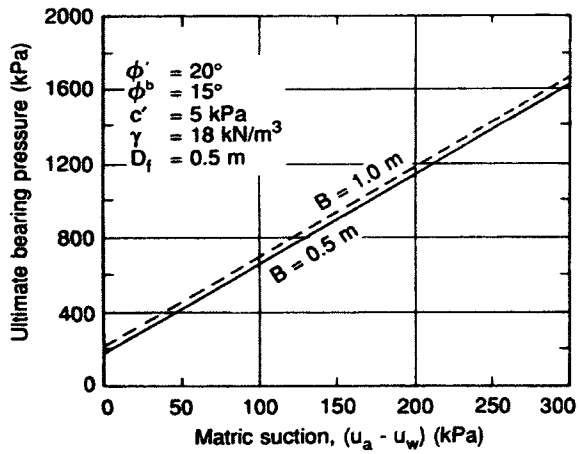

Figure 2.13 Bearing capacity versus matric suction for a strip footing (Fredlund and Rahardjo 1993)

Profile 1 shows the variation of matric suction above the ground water table, while Profile 2 is conventional analyses ignoring the influence of matric suction (Figure 2.14). The use of Profile 1 should be encouraged in engineering practice, particularly in semi-arid and arid regions because it is more rational. Conventional analyses for saturated soils ignore the influence of contribution of matric suction towards bearing capacity.

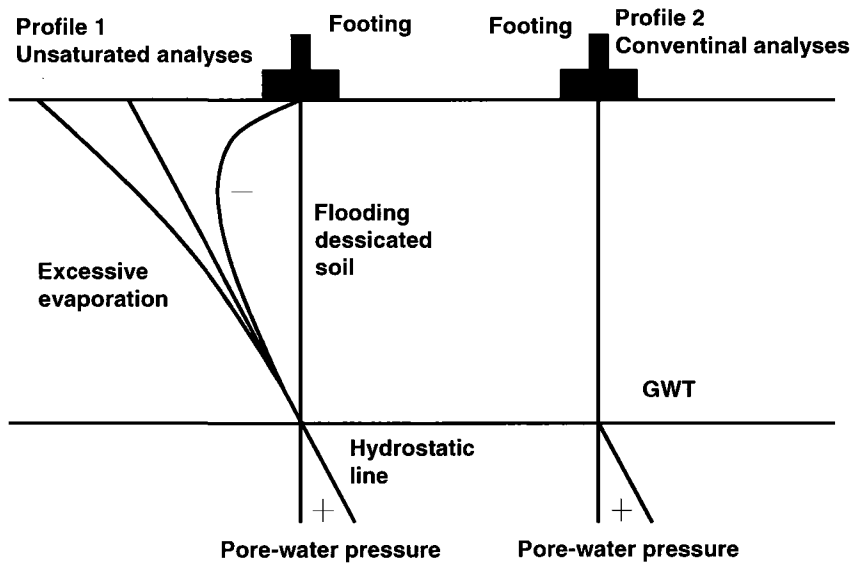

Figure 2.14 Typical schematic pore-water profiles below a spread footing (Fredlund and Rahardjo 1993)

2.5.4 Oloo et al. (1997)

Oloo et al. 1997 proposed a method based on bearing capacity for designing unpaved roads consisting of a base layer overlying a subgrade taking account of the influence of matric suction. Furthermore, a general bearing capacity equation (Equation 2.29) that can be used for computing the bearing capacity of unsaturated soils was proposed. The proposed equation was tested on two fine-grained soils (i.e., Botkin silt and glacial till). Two different scenarios were considered in this equation. In the first scenario, the matric suction is considered to be uniform below the footing. In the second scenario, the equation considers the variation of the matric suction under the footing as hydrostatic above the ground water table.

$$q_u = [c' + (u_a - u_w)_b(\tan\phi' - \tan\phi^b) + (u_a - u_w)_s \tan\phi^b]N_{co} + 0.5(\gamma - \lambda_m \frac{\tan\phi^b}{\tan\phi'})N_{\gamma o} \qquad [2.29]$$

where:

λ_m = rate of decrease of suction with depth

N_{co}, $N_{\gamma o}$ = bearing capacity factors proposed by Oloo (1994)

$(u_a - u_w)_b$ = matric suction at the air entry value, kPa

$(u_a - u_w)_s$ = matric suction at the surface, kPa

Oloo et al. (1997) further simplified Equation [2.29] to take the form as Equation [2.30] assuming matric suction to be uniform within a layer of an unsaturated soil and the air entry value, $(u_a - u_w)_b$ is close to zero.

$$q_u = [c' + (u_a - u_w)\tan\phi^b]N_{co} + 0.5B\gamma N_{\gamma o} \qquad [2.30]$$

The bearing capacity of an unsaturated soil increases linearly with matric suction if this equation used. Equation [2.30] suggests that the soil desaturates immediately after application of even small values of matric suction. Such an assumption is valid more for coarse-grained soils in comparison to fine-grained soils. This assumption is simple for practical purposes; however, it is not valid as several studies related to unsaturated soils have shown that the engineering properties vary in a non-linear fashion with the matric suction (Vanapalli et al. 1996).

2.5.5 Costa et al. (2003)

Costa et al. (2003) carried out a study to investigate the influence of matric suction on the plate load test results performed on Lateritic soil deposit at a depth of 1.5 m, which was in a state of unsaturated condition. Matric suction was monitored during the tests with tensiometers installed at the bottom of the testing pit as shown in Figure 2.15. The bearing plate was 0.8 m in diameter and 25 mm in thickness.

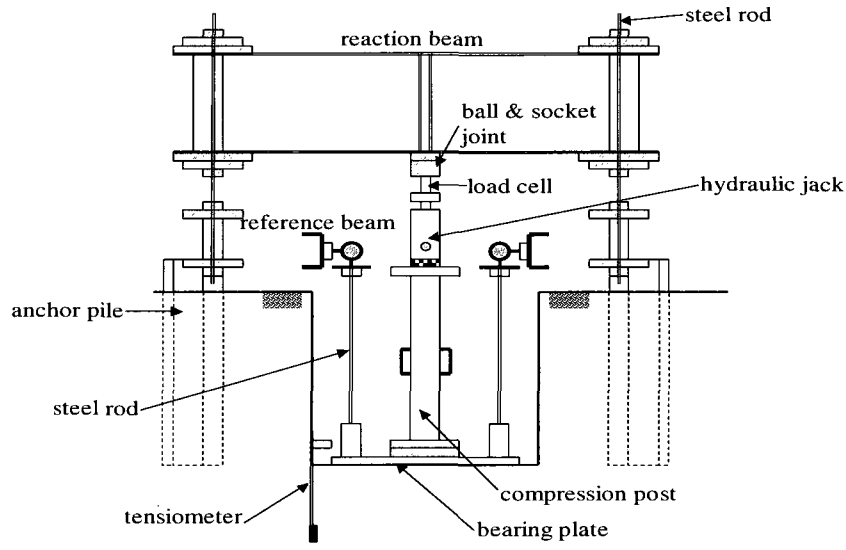

Figure 2.15 General schematic of the testing assembly and used apparatus (Costa et al. 2003)

Field test results show that small increases in matric suction lead to substantial increases in bearing capacity of the soil-plate system. Changes in matric suction were observed to significantly influence settlement response, particularly for high levels of surcharge load. The rate of settlement shows a non-linear decreasing trend with increasing soil matric suction.

Costa et al. (2003) proposed a bearing capacity equation (Equation [2.31]) for comparisons with the experimental results.

$$\sigma_p = \gamma H N_q \zeta_q + 0.5\gamma B N_\gamma \zeta_\gamma + \{c' + (u_a - u_w)\tan\phi^b\} N_c \zeta_c \qquad [2.31]$$

where:

σ_p = predicted failure stress,

H = depth of the bearing plate,

N_q, N_c, N_γ = bearing capacity factors (estimated according to Vesić 1973), and

ζ_q, ζ_γ, ζ_c = shape factors (estimated according to Vesić 1973)

Equation [2.31] however does not provide reasonable comparisons between the measured and predicted bearing capacity values.

2.5.6 Mohamed and Vanapalli (2006)

Mohamed and Vanapalli (2006) carried out model footing tests in a specially designed bearing capacity tank (University of Ottawa Bearing Capacity Equipment, UOBCE, 900×900×750 mm), which has provisions to simulate both saturated and unsaturated conditions in the tank (Figure 2.16). Two different sizes of model footings (i.e. 100mm×100mm and 150mm×150mm) were used to determine the values of bearing capacity with respect to matric suction of compacted coarse-grained sand.

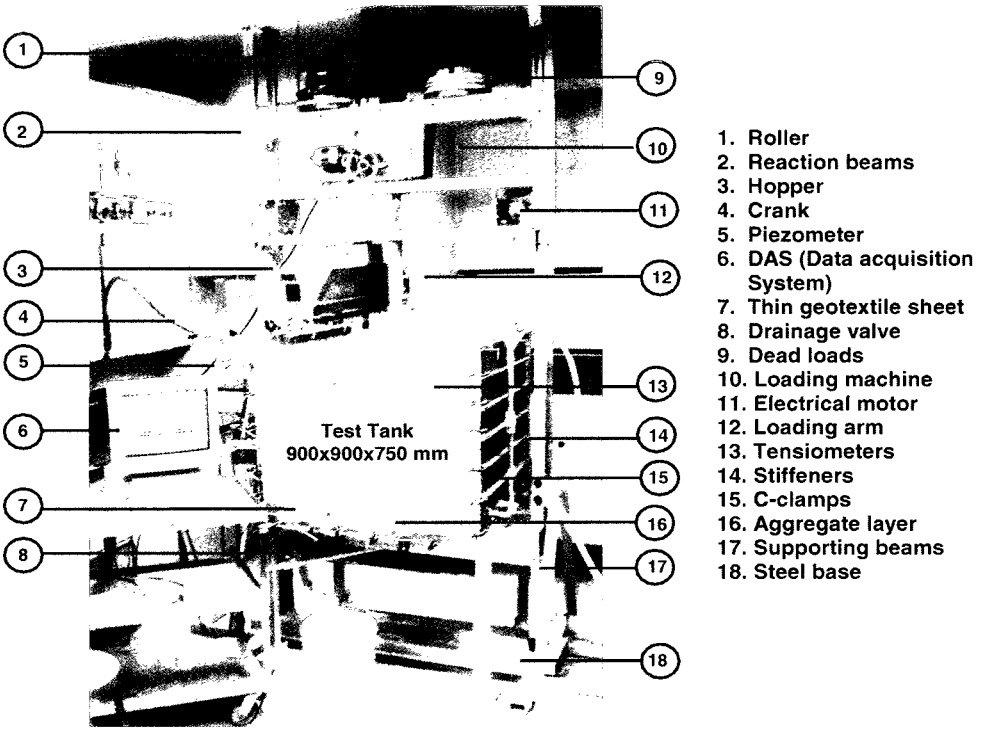

Figure 2.16 University of Ottawa Bearing Capacity Equipment (UOBCE) (Mohamed and Vanapalli 2006)

Figure 2.17 shows the variation of matric suction values with depth which were measured using several tensiometers in the UOBCE. The matric suction value at the centroid of the matric suction distribution diagram from 0 to 1.5B depth region was considered as the average value of matric suction (i.e., 6 kPa in this case) for the analysis of the experimental results. This is the zone of depth in which the stresses due to loading are predominant (Poulos and Davis, 1974).

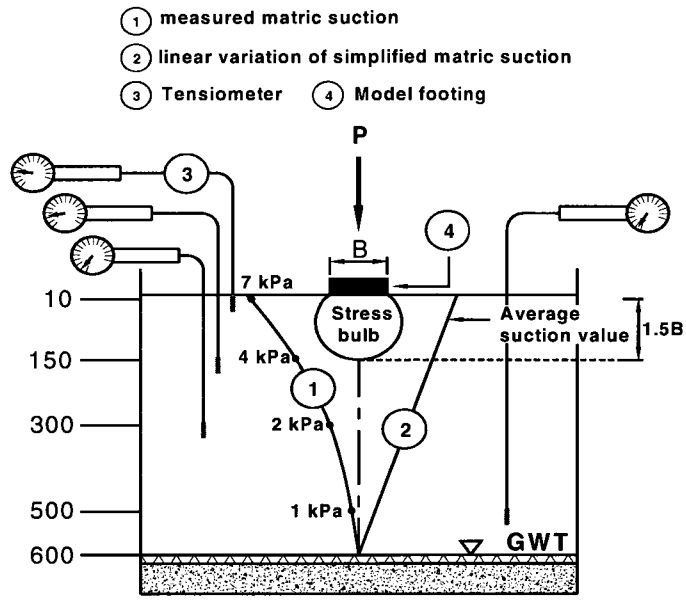

Figure 2.17 Variation of measured matric suction values in the UOBCE with depth along with hydrostatic matric suction distribution. (after Oh and Vanapalli 2008)

Oh and Vanapalli (2008) conducted computer modelling studies using the results of Vanapalli and Mohamed (2007) which is shown in Figure 2.18. The vertical stress distribution contours due to an applied unit stress on rigid footing using axisymmetric analysis (Diameter = 112.8 mm, which represents an equivalent diameter for 100 x 100 mm square footing) in the UOBCE were modeled. The results shown in Figure 2.18 were obtained from the finite element analysis (SIGMA/W of GEO-SLOPE) using linear elastic model. It can be seen that the stress intensity under the center of a footing at a depth lower than 1.5B is less than 0.15 in comparison to the applied unit stress at the surface. These results are consistent with the conventional stress distribution theory concepts based on elastic analysis and support the assumption that the average matric suction value can be estimated from 0 to 1.5B depth region (Vanapalli and Mohamed, 2007). The stress distribution diagram illustrates that bearing capacity model studies can be undertaken using relatively smaller size tanks such as 300 mm diameter yielding similar results.

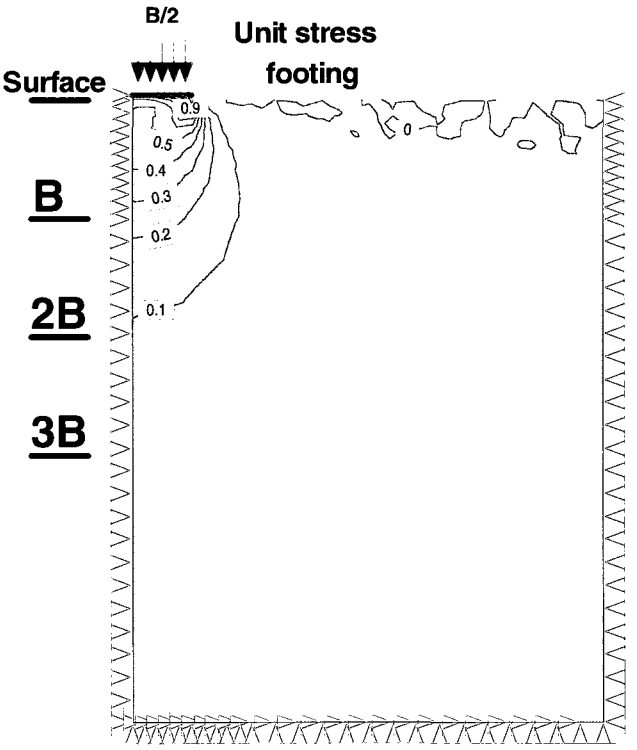

Figure 2.18 Vertical stress distribution contours obtained from SIGMA/W due to an applied unit stress on a rigid footing in UOBCE (after Oh and Vanapalli 2008)

Vanapalli and Mohamed (2007) proposed an equation to both interpret and predict the variation of bearing capacity with respect to matric suction for surface model footings on unsaturated soils using the saturated shear strength parameters (i.e. c' and ϕ') and the SWCC as below:

$$q_{ult} = [c' + (u_a - u_w)_b (1 - S^{\psi}) \tan\phi' + (u_a - u_w)_{AVR} S^{\psi} \tan\phi'] \times N_c \xi_c + 0.5 B \gamma N_\gamma \xi_\gamma \qquad [2.32]$$

where:

q_{ult} = the ultimate bearing capacity

ψ = a fitting parameter, $(u_a - u_w)_{AVR}$ is average (representative) suction value, B is the width of footing.

L = the length of footing

γ = soil unit weight

N_c, N_q = bearing capacity factors from Terzaghi (1943)

N_γ = bearing capacity factor from Kumbhokjar (1993)

ξ_c, ξ_γ = shape factors from Vesic (1973) which can be determined using the equations below

$$\xi_c = \left[1.0 + \left(\frac{N_q}{N_c}\right)\left(\frac{B}{L}\right)\right] \quad [2.33]$$

$$\xi_\gamma = \left[1.0 - 0.4\left(\frac{B}{L}\right)\right] \quad [2.34]$$

Vanapalli and Mohamed (2007) provided comparisons between the measured bearing capacity values and predicted bearing capacity values using some of their own results and others from literature of unsaturated soils for both coarse and fine-grained soils. There was a reasonable good comparison. Figure 2.19 shows a typical result of their studies on coarse-grained sand.

Moreover, Vanapalli and Mohamed (2007) also provided a relationship (Figure 2.20) between the fitting parameter, ψ and I_p that can be used for predicting the bearing capacity of unsaturated soils as given below:

$$\psi = -0.0031(I_p^2) + 0.3988(I_p) + 1 \quad [2.35]$$

where I_p = plasticity index

A best-fit between the measured and predicted bearing capacity values for sands was achieved using ψ value equal to 1 according to the test results by Mohamed and

Vanapalli (2006). The approach for predicting the bearing capacity of unsaturated soil is similar to the approach proposed by Vanapalli et al. (1996) to predict the variation of shear strength with respect to suction using the effective shear strength parameter c' and ϕ' along with the SWCC.

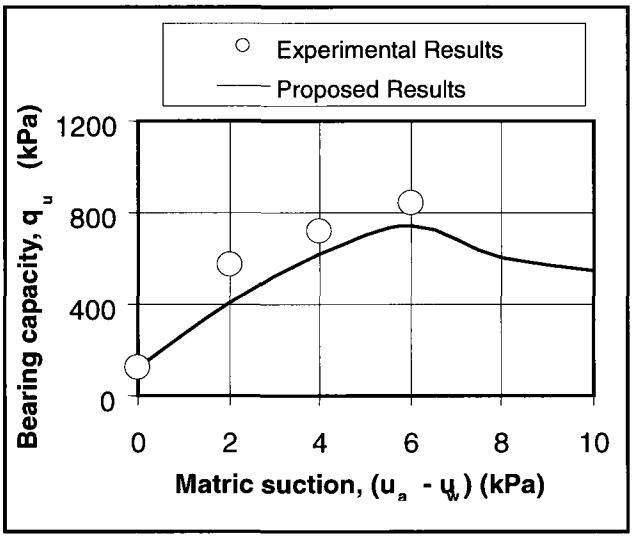

Figure 2.19 Comparison between measured and predicted bearing capacity of a compacted unsaturated sand (Vanapalli and Mohamed 2007)

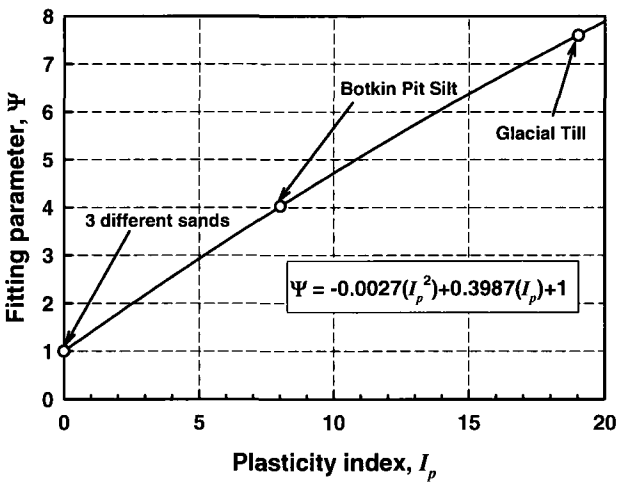

Figure 2.20 Relationship between the bearing capacity fitting parameter, ψ and the plasticity index, I_p (Vanapalli and Mohamed 2007)

2.5.7 Vanapalli et al. (2007)

Vanapalli et al. (2007) have conducted a series of model footing tests on statically compacted unsaturated Indian Head till soil samples at different matric suction values to determinate the contribution of matric suction towards bearing capacity of unsaturated soils under undrained loading conditions by using specially designed equipment (Figure 2.21).

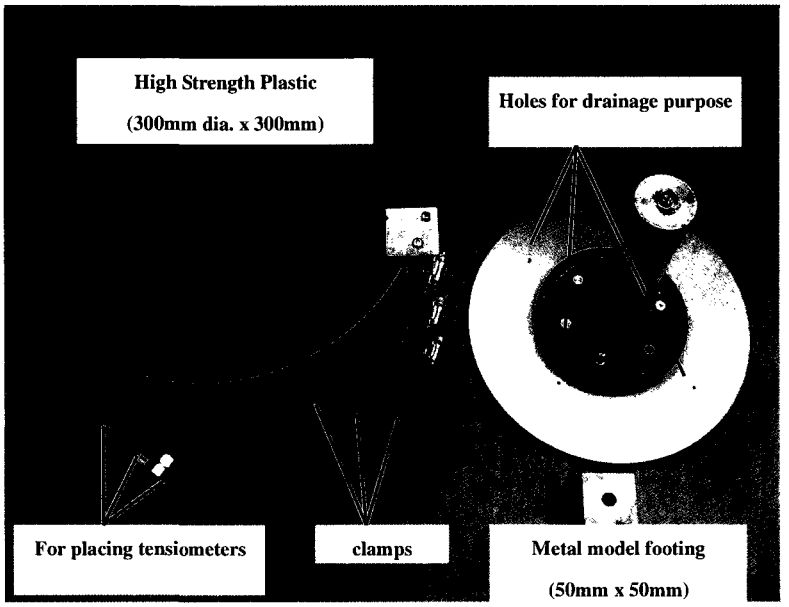

Figure 2.21 Equipment used for determining the bearing capacity of unsaturated soils under undrained loading conditions (Vanapalli et al. 2007)

The soil was compacted in a high strength plastic mould. During the saturation process of the compacted specimen, a compactor plate was securely placed on the surface of compacted soil and fixed to the cross bar of the loading machine to prevent any possible volume change of soil due to swelling. The compacted soil was saturated using a downward flow of water simulating natural flow behavior in field conditions. This flow was achieved through drainage holes on the compaction plate. Once the compacted soil in the plastic container was fully saturated, it was subjected to natural air drying for several days. The changes in the suction values with respect to depth in the soil sample due to air

drying were monitored using tensiometers.

The bearing capacity was determined using a 50 mm × 50 mm footing which was loaded in a conventional loading frame. After the tests, three specimens were collected from the compacted soils using 50mm diameter stainless steel thin-wall tubes. Two of the specimens were used for measuring the undrained strength by conducting unconfined compression tests (1.14 mm/min). The third specimen was used for measuring matric suction following axis translation technique to verify the accuracy of the suction measurements of tensiometers. In addition, the water content variation with respect to depth was also investigated.

Using the results of these studies, Vanapalli et al. (2007) proposed a relationship for estimating the bearing capacity of unsaturated soils under undrained loading conditions from unconfined compression test results.

The bearing capacity can be predicted with the equation:

$$q_{ult} = [q_{u(unsat)} / 2][1 + (B/L)(N_q / N_c)]N_{cs} \quad [2.36]$$

where:

q_{ult} = ultimate bearing capacity, kPa

$q_{u(unsat)}$ = unconfined compression shear strength for an unsaturated soil, kPa

N_c, N_q = cohesion and surcharge factors

N_{cs} = factors associated with cohesion under undrained condition

B, L = footing width and length, m

Equation [2.36] is similar in form as Skempton (1948) equation for estimating the bearing capacity of saturated soils from conventional unconfined compression test results. Figure

2.22 shows that there is a good comparison between the measured bearing capacity values from model footing tests and estimated bearing capacity values from unconfined compression tests.

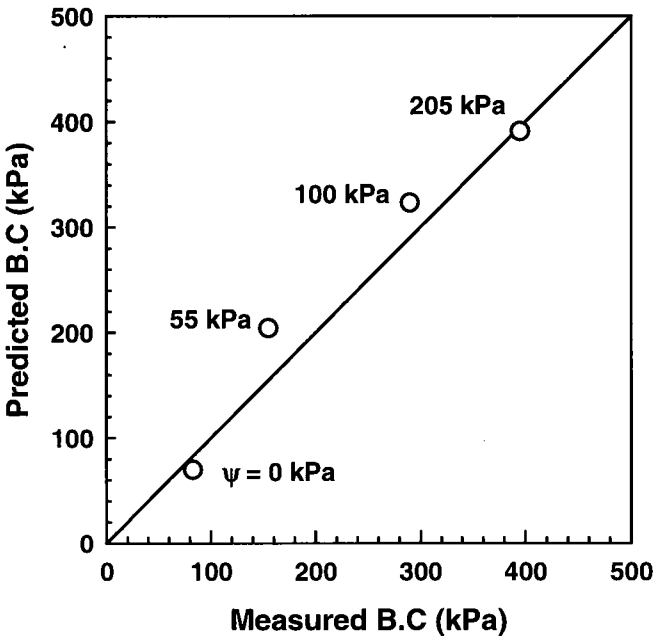

Figure 2.22 Comparison between the measured and predicted bearing capacity under undrained loading conditions of compacted Indian Head till specimens (Vanapalli et al. 2007)

2.6 Settlement Behavior of Unsaturated Soils

The settlement behavior typically governs the design of a foundation in comparison to the bearing capacity of the soil in several scenarios. This is particularly true for coarse-grained soils such as sands in which foundation settlements are immediate in nature. Foundations are conventionally designed assuming that the soil in which they are placed is in a saturated condition. The concepts of conventional soil mechanics may not be valid in the estimation of elastic settlement of foundations in unsaturated soils. Several investigations have shown that the elastic settlement in shallow foundations can be significantly reduced due to the contribution of matric suction (Oh et al. 2009).

2.6.1 Oh et al. (2009)

Oh et al. (2009) have proposed a semi-empirical model to predict the variation of modulus of elasticity with respect to matric suction for unsaturated sandy soils using the soil-water characteristic curve (SWCC) and the modulus of elasticity under saturated conditions.

Equation [2.24] was used to determine the modulus of elasticity for saturated conditions. A value of 0.3 was used for ν in the study, assuming drained loading conditions for the tested sands. The procedure used in the calculation of elastic settlement for saturated conditions is illustrated in Figure 2.23.

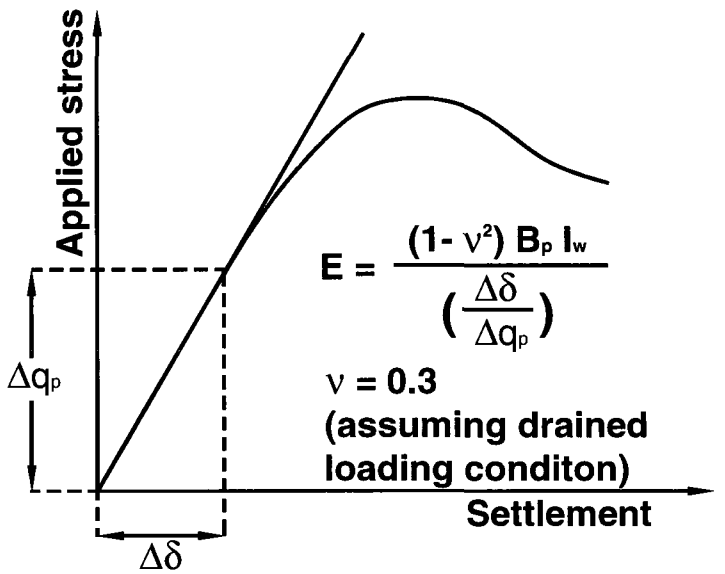

Figure 2.23 Estimation of elastic settlement from plate load test (Oh et al. 2009)

A simple equation is proposed by Oh et al. (2009) for predicting the variation of modulus of elasticity of unsaturated sandy soils using the SWCC and the modulus of elasticity under saturated conditions.

$$E_{unsat} = E_{sat} + E_{sat}\alpha\frac{(u_a - u_w)}{(P_a/100)}(S^{\beta}) = E_{sat}\left[1 + \alpha\frac{(u_a - u_w)}{(P_a/100)}(S^{\beta})\right] \quad [2.37]$$

where E_{unsat} is modulus of elasticity under unsaturated conditions, E_{sat} is modulus of elasticity under saturated conditions, α and β are fitting parameters, and P_a is atmospheric pressure (i.e., 100 kPa). In Eq. [2.37], the terms S^{β} and the parameter, α control the nonlinear variation of the modulus of elasticity. The term (P_a/100) was used for maintaining consistency with respect to the dimensions and units on both sides of the equation. The value of β is similar to using fitting parameter ψ (i.e., 1 for predicting the bearing capacity of sandy soils; see Equation [2.35]). Fitting parameter α is related with model footing size. A relationship between the parameter α and footing width for coarse-grained soils is shown in Figure 2.24. However, more tests using larger footing sizes would be valuable to verify this relationship.

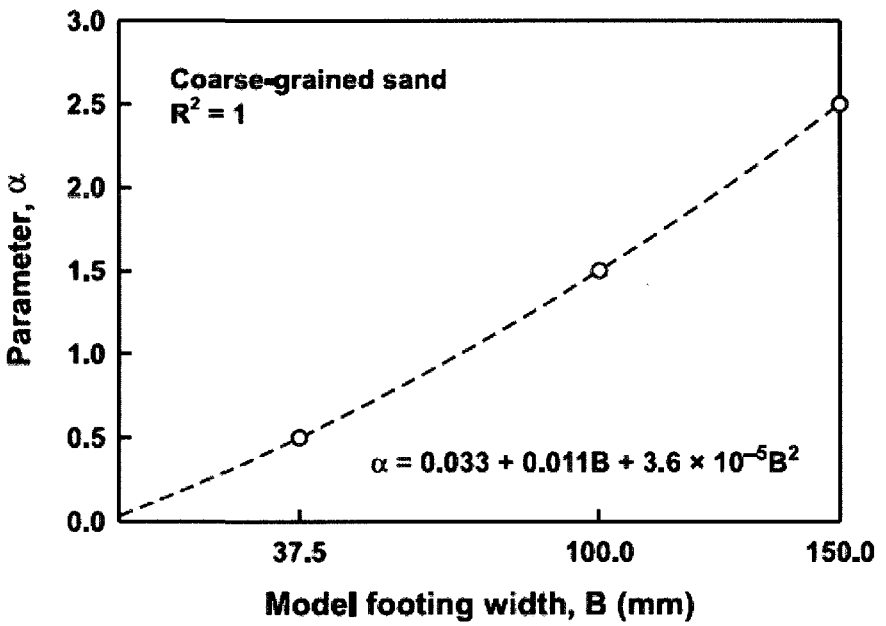

Figure 2.24 Variation of the fitting parameter, α, with respect to model footing width for coarse-grained sand (Oh et al. 2009)

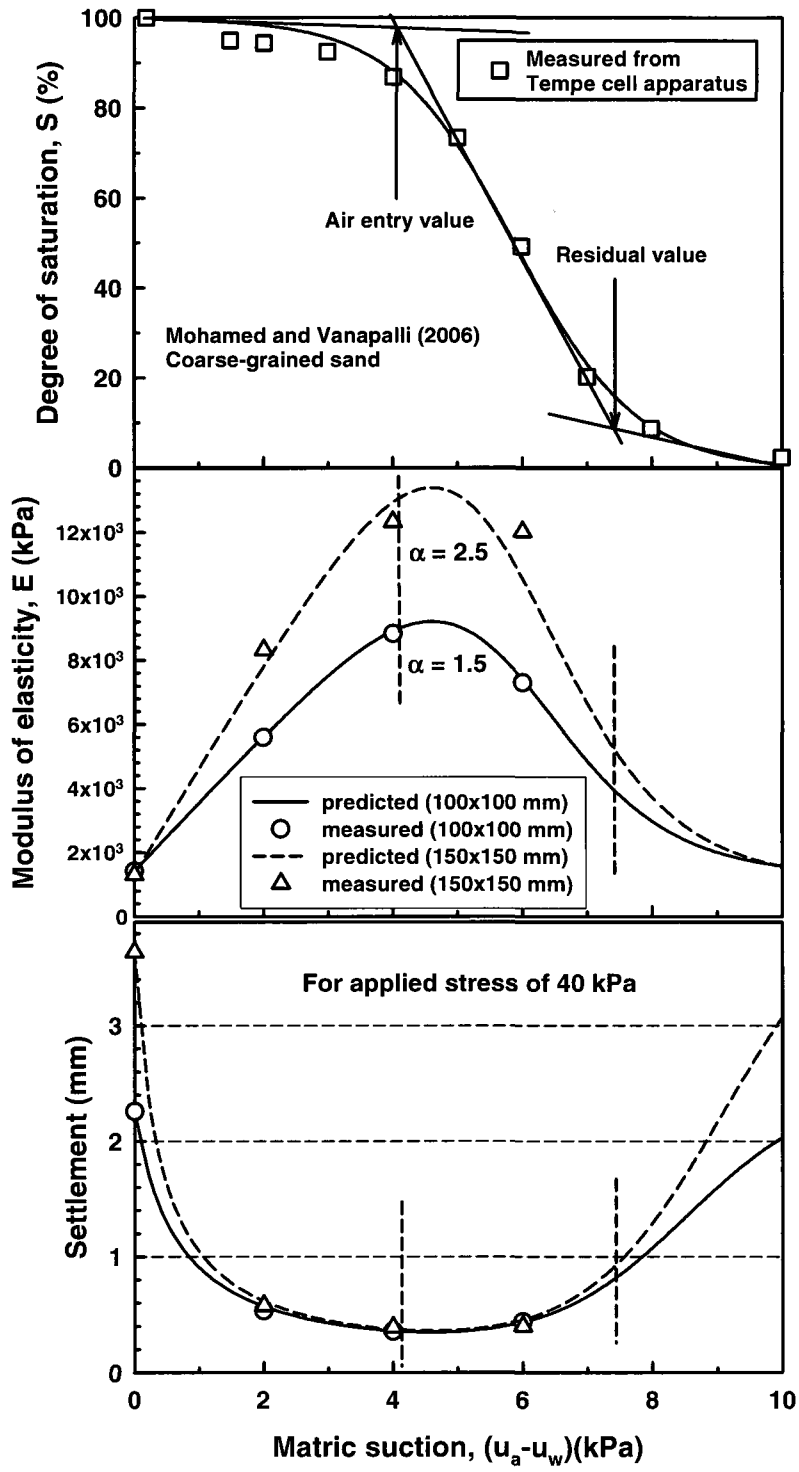

Figure 2.25 SWCC, variation of modulus of elasticity, and immediate settlement with matric suction from model footing tests in coarse-grained sand (Oh et al. 2009)

Figure 2.25 shows the SWCC, the variation of modulus of elasticity, and elastic settlement with respect to matric suction for model footing tests conducted on coarse-grained sand. Comparisons are provided between the measure and predicted values of elastic settlements for an applied stress of 40 kPa. The results show there is good agreement between the predicted and measured moduli of elasticity and settlements.

Figure 2.26 shows the variation of elastic settlement with respect to matric suction for different applied stress values in the range of 40 to 400 kPa for the 100 mm × 100 mm model footing tested in coarse-grained sand. For the applied stress of 400 kPa, the minimum elastic settlement is 3.50 mm at a matric suction value of 5 kPa. This elastic settlement value is the same as the value measured for an applied stress of 100 kPa at a matric suction value of 0.5 kPa. The study shows that elastic settlements in shallow foundations can be significantly reduced even if low matric suction values are maintained in sandy soils.

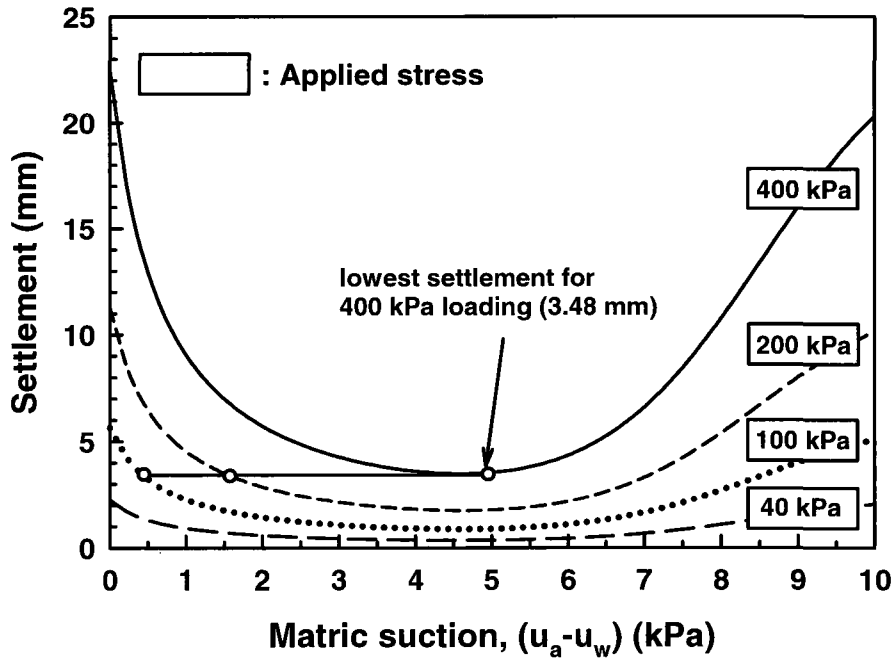

Figure 2.26 Variation of elastic settlement with respect to various applied stresses for the 100 mm × 100 mm model footing in coarse-grained sand (Oh et al. 2009)

2.7 Summary

A comprehensive review of the background related to bearing capacity and settlement of saturated and unsaturated soils is presented in this chapter. There are many methods available for determining the bearing capacity and settlement behavior such as standard penetration tests (SPT) or cone penetration tests (CPT). Several studies are conducted and are in progress at the University of Ottawa for estimating the bearing capacity and settlement behavior of unsaturated sands from CPT results (Mohamed and Vanapalli 2009; Mohamed et al. 2010). However, only those methods that can be used for interpreting the model footing results with respect to the bearing capacity and settlement behavior are summarized in this Chapter.

In summary, the contribution of matric suction towards bearing capacity and settlement behavior of unsaturated soils cannot be ignored. The simple models proposed by Vanapalli and Mohamed (2007) and Oh et al. (2009) for predicting the bearing capacity and settlement behavior are useful tools. However, there is a need to perform more laboratory studies to better understand how the various parameters such as the footing size and type of soil influence the bearing capacity and settlement behavior of unsaturated soils. These studies form the focus of research presented in this thesis.

CHAPTER 3

EQUIPMENTS AND METHODOLOGY

3.1 Introduction

This chapter provides details of the bearing capacity testing system that was specially designed at the University of Ottawa for determining the bearing capacity and settlement behavior of model footings in saturated and unsaturated conditions. Another unit, referred to as the suction profile set for determining the variation of capillary suction (i.e., matric suction) with respect to depth above the ground water table unit is also described. In addition, equipment details of the Tempe Cell and Decagon's WP4-T Dewpoint PotentiaMeter used for measuring the Soil-Water Characteristic Curve (SWCC) are also provided. Other equipment such as the triaxial shear apparatus used for measuring the saturated shear strength parameters is briefly discussed. The methodologies associated with conducting the various laboratory tests required for the research program presented in this thesis are also summarized.

3.2 Bearing Capacity Test System

Figure 3.1 shows the bearing capacity test system along with a soil container and other accessories. An electrically operated and mechanically controlled loading machine with a robust loading frame is used for this test system. More elaborate design details of this equipment are available in Li 2008 and Vanapalli et al. 2010.

The model footing can be placed on the surface of the compacted soil specimen in the soil container under both saturated and unsaturated conditions and loaded to failure using a loading frame. Some key details related to the system and the other elements are discussed in later sections of this chapter.

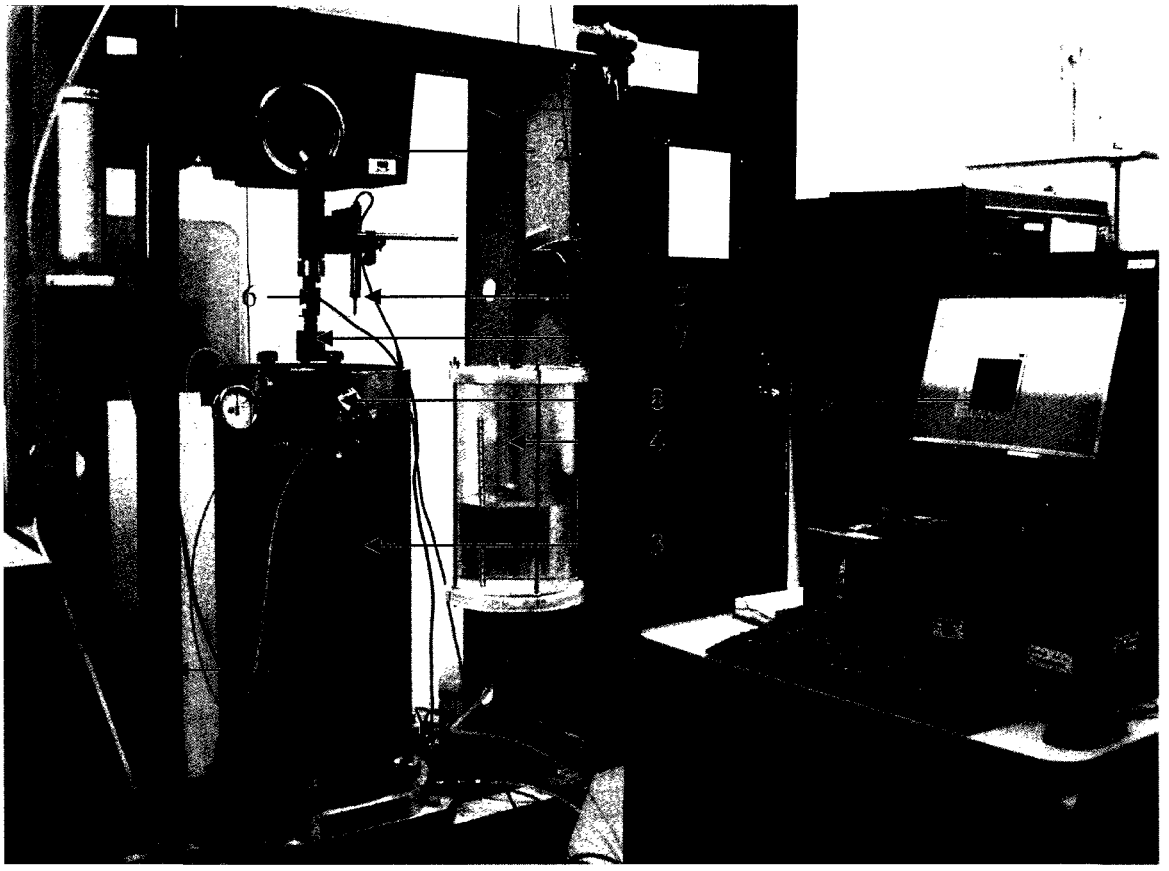

1. Loading frame	2. Loading machine
3. Soil container	4. Water container
5. Settlement transducer	6. Load cell
7. Model footing	8. Tensiometer
9. Data acquisition system	10. Suction profile set

Figure 3.1 Bearing capacity test system (modified after Li 2008)

3.3 Model Footings

Four aluminum footings were used in the research program. They include three square footings with dimensions of 20 mm × 20 mm, 37 mm × 37 mm and 50 mm × 50 mm and one circular footing with diameter of 41.75 mm. The footings of 37 mm × 37 mm and 41.75 mm in diameter have equivalent area which is equal to 1369 mm^2. The objective of using different size and shape footings in this study is to understand the influence of footing size and shape on the bearing capacity and settlement behavior of unsaturated soils (Figure 3.2).

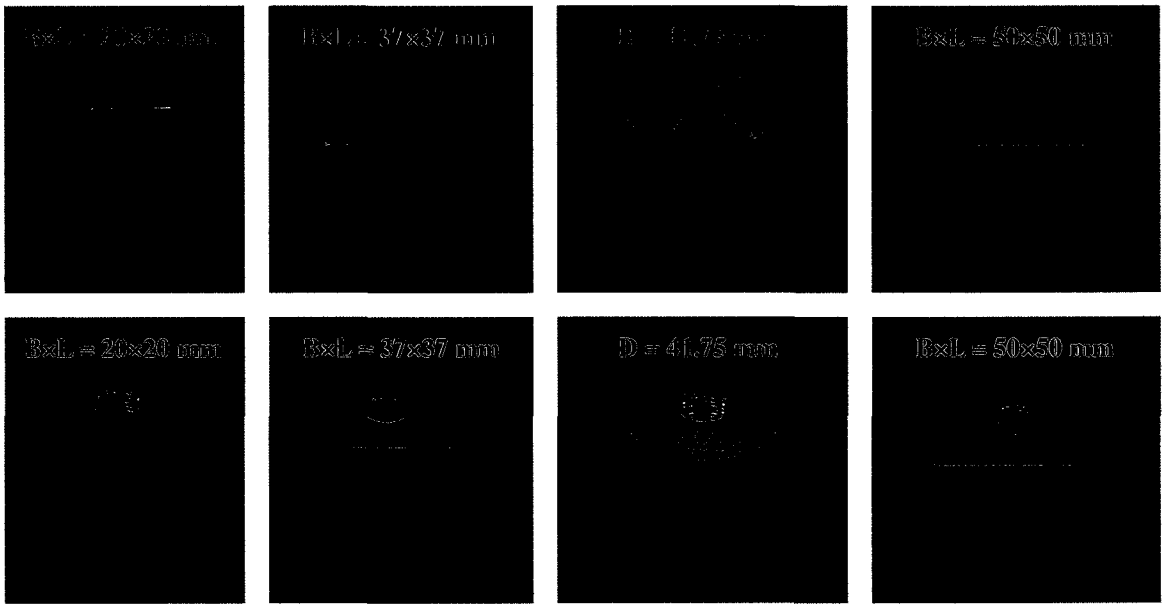

Figure 3.2 Different footings used in the research program

All the model footings are relatively smaller in size in comparison to the diameter of the bearing capacity tank soil container. The ratio of the soil container size to the model footing sizes used in the present study is greater than 6. Adams and Collin (1997), Carter (2006) and Vanapalli et al. (2007) experimental studies show that there would be no influence of stresses on the boundaries of the soil container due to the applied loads on the footing by using ratio of the soil container size to the model footing size of 6 or greater. In other words, the size of soil container which is greater than the present soil container will also provide the same bearing capacity values. Earlier studies by Poulos and Davis (1974) and more recent modeling studies by Oh and Vanapalli (2008) also support these findings. More details on the influence of size of the footing were discussed in the results and discussions (i.e. Chapter 5).

3.4 Soil Container

The bearing capacity tank soil container has several other features to systematically conduct the bearing capacity tests using model footings. This unit facilitates saturation and desaturation of the soil sample in the container. Figure 3.3 shows the schematic of the container with all the various elements.

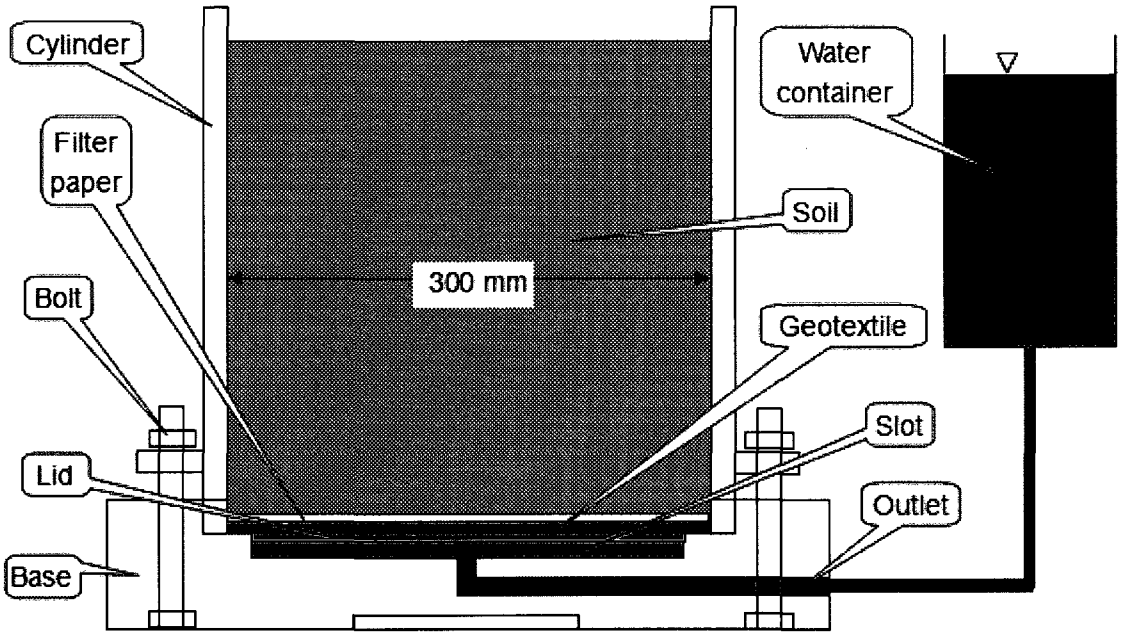

Figure 3.3 Schematic of the soil container with various elements (modified after Li 2008)

Figure 3.4 shows the different individual elements of the soil container system. The soil container assembly is fabricated from cylindrical tube of 300 mm in diameter, 700 mm in height and 8 mm in thickness is shown in Figure 3.4a. Figure 3.4b shows the base plate with circular grooves to facilitate gradual and even drainage of water into and out of the container. The circular grooves of the bottom plate are covered using a stainless steel lid (Figure 3.4c) of 260 mm in diameter and 1.25 mm in thickness with small holes (2 mm in diameter). Above the lid, a geotextile and filter paper are provided (Figure 3.4d) to prevent the soil particles from getting into the circular grooves of the base plate and valves.

The soil container allows lowering the water table to a depth of 700 mm below soil surface. By varying the depth of water table, different values of capillary suction (i.e., matric suction) can be achieved below the footing for conducting the bearing capacity tests. In other words, the variation of bearing capacity with respect to matric suction for model footings can be determined using this equipment. The settlement behavior of model footings can also be studied simultaneously.

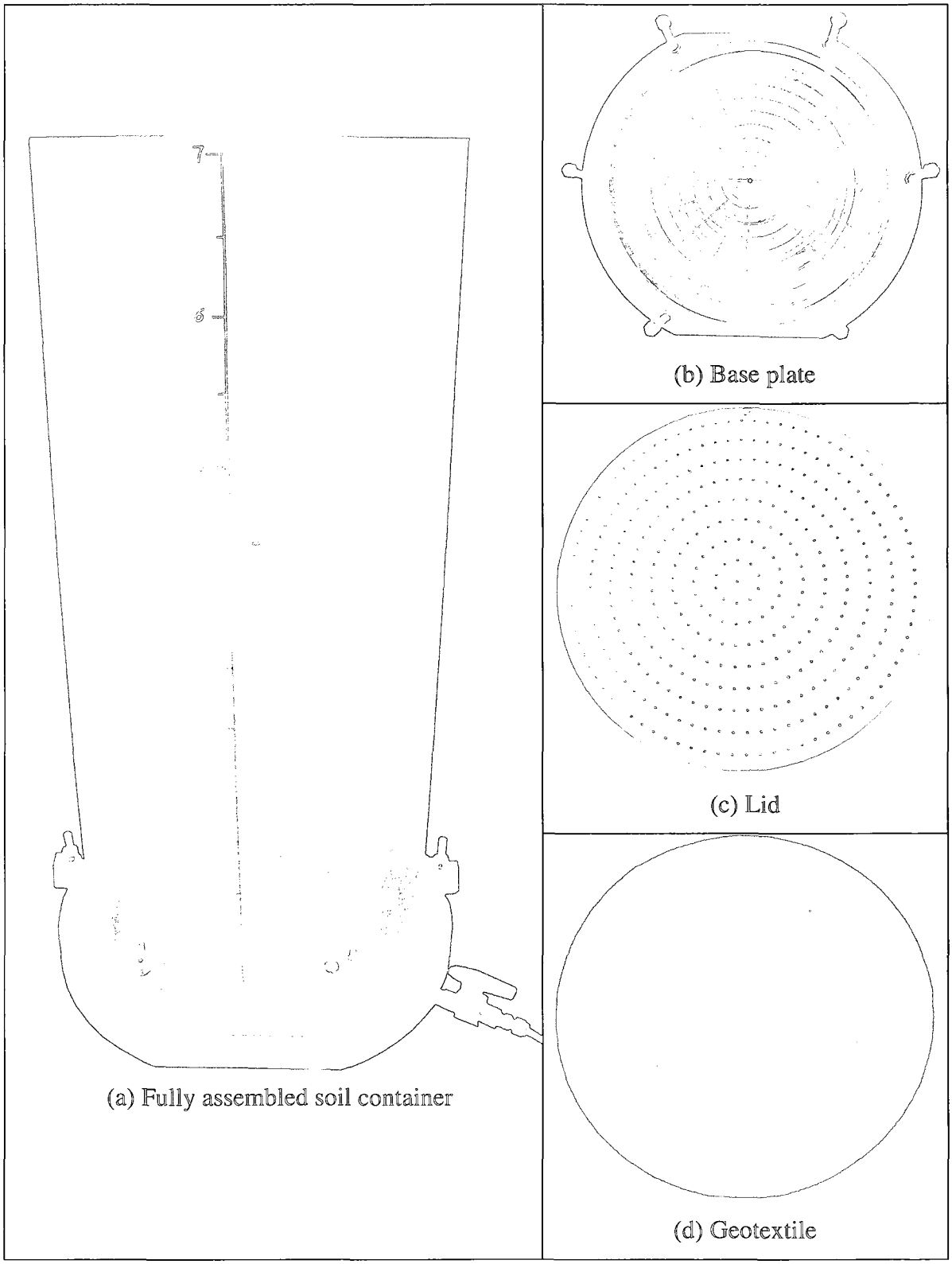

Figure 3.4 Various components of the soil container (modified after Li 2008)

3.5 Loading Frames

Figure 3.5 shows ENERPAC loading frame. The frame is a part of H-Frame Presses made by Enerpac Hydraulic Technology. It is made of steel and its height is 1930 mm (76") and 1030 mm (i.e., 40.50") of wide. It has a capacity of 50 tons.

Engineering Laboratory Equipment Ltd. loading machine is attached on the top of this frame. This unit is an electrically operated and mechanically controlled loading system for loading the model footings. The engine is mounted on and fixed to the frame by a piece of specially designed steel (250 mm × 400 mm × 8 mm) and bolts which were designed and manufactured at the University of Ottawa student workshop.

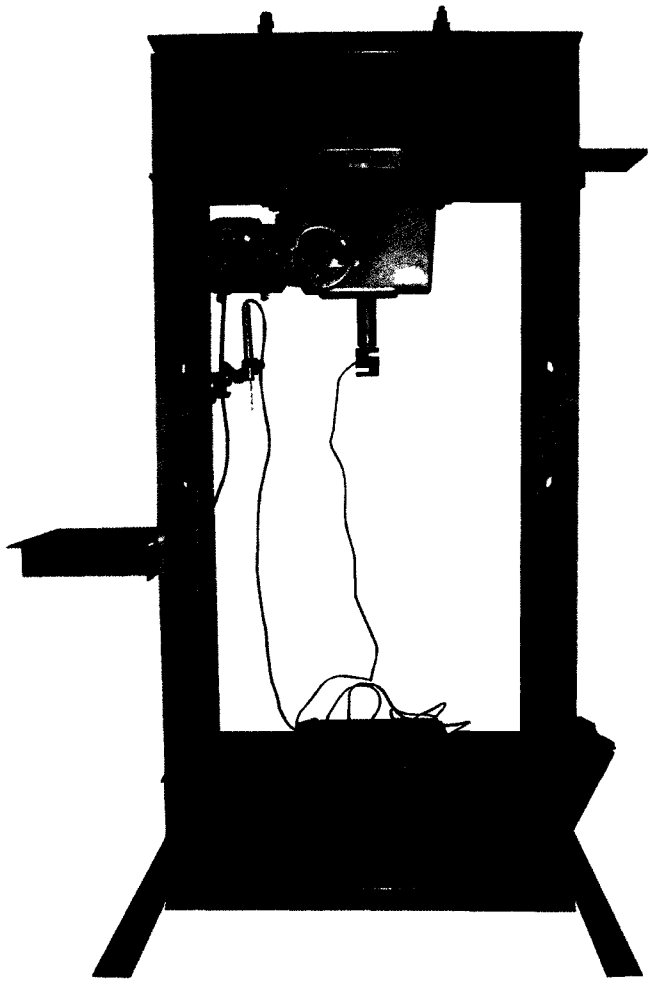

Figure 3.5 ENERPAC loading frame

3.6 Triaxial Shear Apparatus

Triaxial shear apparatus used for determining the saturated shear strength parameters is TRI-FLEX 2 system manufactured by ELE International, Ltd. The TRI-FLEX 2 Triaxial System is a versatile unit with loading machine, triaxial cell and other accessories and can accommodate up to 4" (102 mm) diameter test specimen, a free-standing multi-function compact control panel and three pressure interface devices (Figure 3.6).

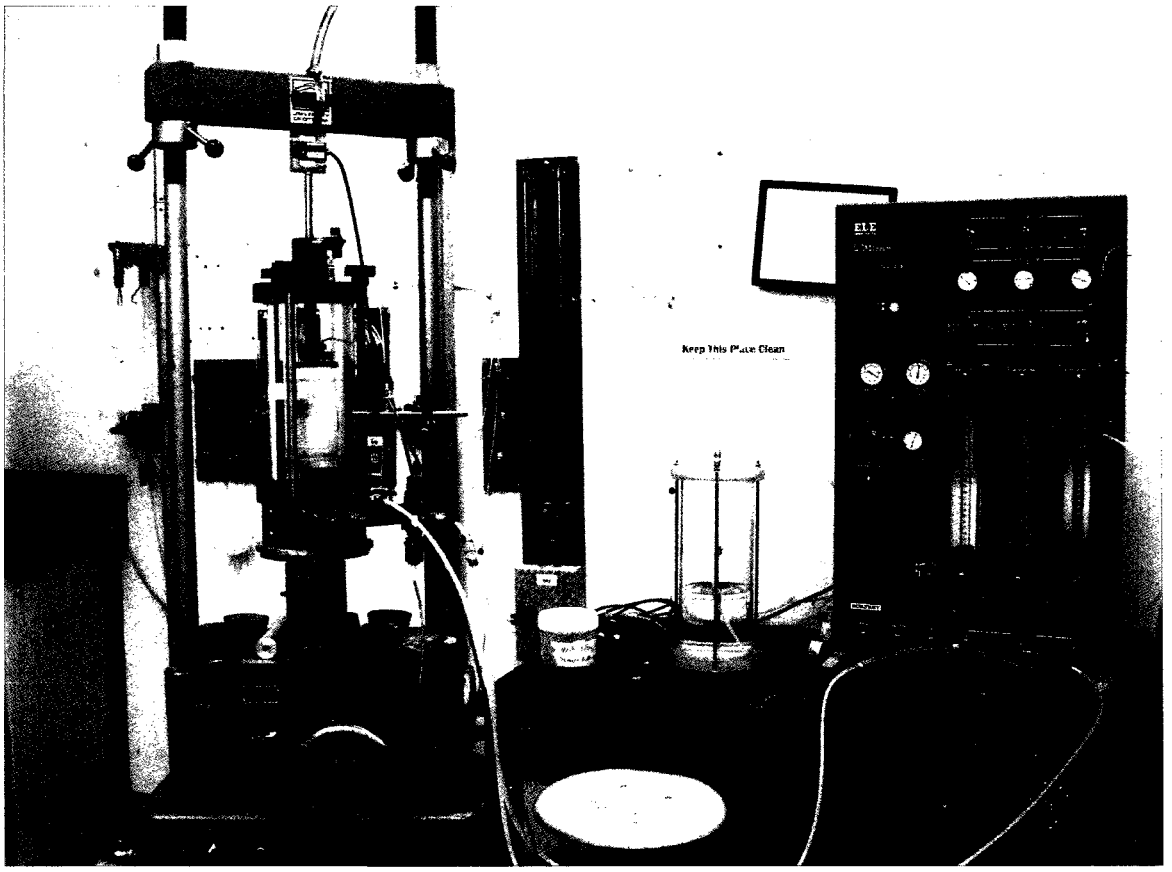

Figure 3.6 Triaxial Shear Apparatus

The effective shear strength parameters of the four soils (i.e., c' and ϕ') used in this research program were determined under consolidated drained conditions in the present research program following the procedures summarized in ASTM D4767-04. The experiments were conducted assuring fully drained conditions (i.e., the pore-water pressure was equal to zero). More details about the soil specimen preparation and strain rate are discussed in Chapter 4.

3.7 Tempe Cell

The setup details used in the present research program for measuring the SWCC in the laboratory using the Tempe Cell Apparatus is shown in Figure 3.7. A soil specimen with the same density as the soil in the bearing capacity cylinder (see Fig. 3.1, item 3) can be placed on the saturated ceramic disk in the Tempe Cell for measuring the SWCC.

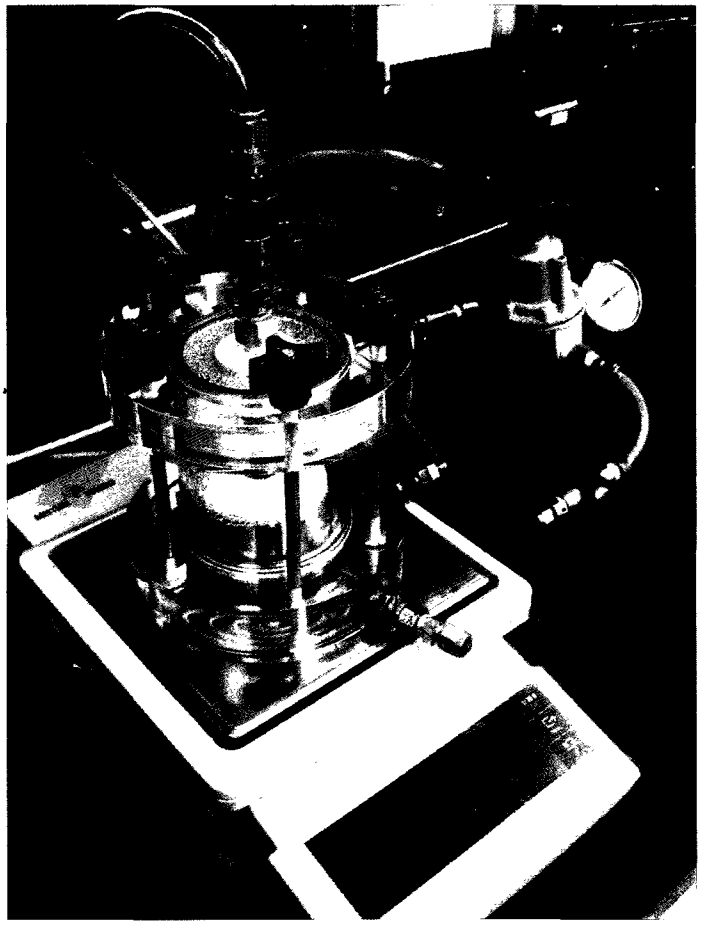

Figure 3.7 Tempe Cell Setup

The soil specimen in the Tempe Cell was saturated prior to the measurement of the SWCC by allowing access of water from a container that was placed at a higher level. This technique facilitates removal of any air bubbles from the specimen, which will collect on the soil specimen surface. After the specimen was saturated, a known value of matric suction value was applied by increasing the air pressure in the Tempe cell. The applied air pressure, u_a will be equal to the matric suction, $(u_a - u_w)$ as the pore-water

pressure, u_w at the bottom of the soil specimen is equal to atmospheric pressure (i.e., zero value). The water expelled from the specimen due to the application of the matric suction is collected in a separate tube from the bottom of the ceramic disk.

A time period of one day or two days is required for achieving equilibrium conditions with respect to each applied matric suction value. The mass of the Tempe cell is continuously monitored on an electronic balance. The water content is determined for each applied pressure by calculating the lost mass of the Tempe Cell. The SWCC is obtained from the water content versus matric suction relationship. Typically, a minimum of 6 to 8 readings of different matric suction values will be used for obtaining the SWCC.

Two pressure gauges (one with a range of 0 to 10 kPa and another with a range of 0 to 200 kPa) were used for determining the SWCC. The 10 kPa range pressure gauge was used for determining the SWCC of coarse-grained soils (i.e., Filtration sand and Quarry sand). This narrow range pressure gauge is useful to precisely apply small pressures to carefully determine the air-entry value and residual suction value from the SWCC of the coarse-grained soils. The various zones of the SWCC for the coarse-grained soils are typically in the range of 0 to 10 kPa. However, for fine-grained soils, both the pressure gauges were used. The pressure gauge with the 10 kPa range was used for obtaining the SWCC in the low matric suction range (i.e., 0 to 10 kPa); and the 200 kPa pressure gauge was replaced measuring the SWCC in the matric suction range of 10 to 200 kPa. For suction values greater than 200 kPa, WP4-T is used.

3.8 WP4-T

The SWCC range for fine-grained soils (i.e., Sil-co-sil 106 and Min-u-sil 30) typically extends over a large suction range from 0 to 10,000 kPa. However, as described earlier, the pressure range for Tempe Cell is from 0 to 200 kPa. The WP4-T (Figure 3.8) measures water potential from 0 to -300 MPa and uses an internal fan that speeds up equilibration to reduce measurement times to less than 5 minutes. Therefore, for large suction values (i.e. larger than 200 kPa) of Sil-co-sil 106 and Min-u-sil 30, the WP4-T was used to determine the water content versus matric suction relationship.

The WP4-T works on the principle of chilled mirror technique according to ASTM D6836-02. The WP4-T consists of a sealed block chamber in which the soil sample can be placed in a 15 ml polyurethane sampling cup. The block chamber consists of a mirror and an optical sensor for detecting condensation on the mirror. At equilibrium of the sample with the chamber environment, the WP4-T measures water potential of the air in the chamber which is the same as water potential of the soil sample. With the help of the built in software, the total suction of the soil sample is displayed on the LCD panel. The matric suction is approximately equal to total suction assuming that osmotic suction is negligible as the soils do not have salt concentrations. The corresponding water content of the soil sample was then determined using oven following the procedures described in ASTM D2216.

Figure 3.8 WP4-T

Table 3.1 summarizes the specifications of WP4-T which are from Decagon Devices, Inc. website.

Table 3.1 Specifications of WP4-T

Accuracy:	±0.1 MPa from 0 to -10 MPa 1% from -10 to -300 MPa
Range:	0 to -300 MPa
Measurement Time:	~5 minutes for most soil samples ~20 minutes for plant tissue samples
Temperature Control:	15 to 50°C (± 0.2°C)
Sensor Type:	1) Chilled-mirror dewpoint sensor 2) Infrared temperature sensor
Operating Environment:	5 to 43°C (41 to 110°F)
Universal Power:	110 V to 220 V AC, 50/60 Hz
Warranty:	1 years, parts and labor
Sample Dish Capacity:	7 ml recommended (15 ml full)
Weight:	3.2 kg (5.2 kg shipping weight)
Dimensions:	24.1 × 22.9 × 8.9 cm (9.5 × 9.0 × 3.5 in)
Case Material:	Powder-painted aluminum
Data Communications:	RS232 compatible 8-data bit ASCII code 9600 baud no parity 1 stop bit
Display:	20 × 2 alphanumeric dot-matrix LCD with backlighting
Interface Cable:	Standard RS232 serial cable (included)

3.9 Suction Profile Set

The suction profile set (Figure 3.9) designed by Li (2008) facilitates in the development of a pre-calibrated relationship between the capillary stresses (i.e., matric suction) and the soil depth varying the depth water table below the surface of any desired soil. The matric suction in the soil (i.e., above the water table) can be measured using tensiometers. Typically two tensiometers were installed in the soil which has the same density as the soil in the bearing capacity cylinder (see Fig. 3.1, item 3) at 50 mm and 100 mm below

the soil surface to measure the matric suction. Equilibrium conditions with respect to matric suction values were typically achieved in a period of 12 to 24 hours.

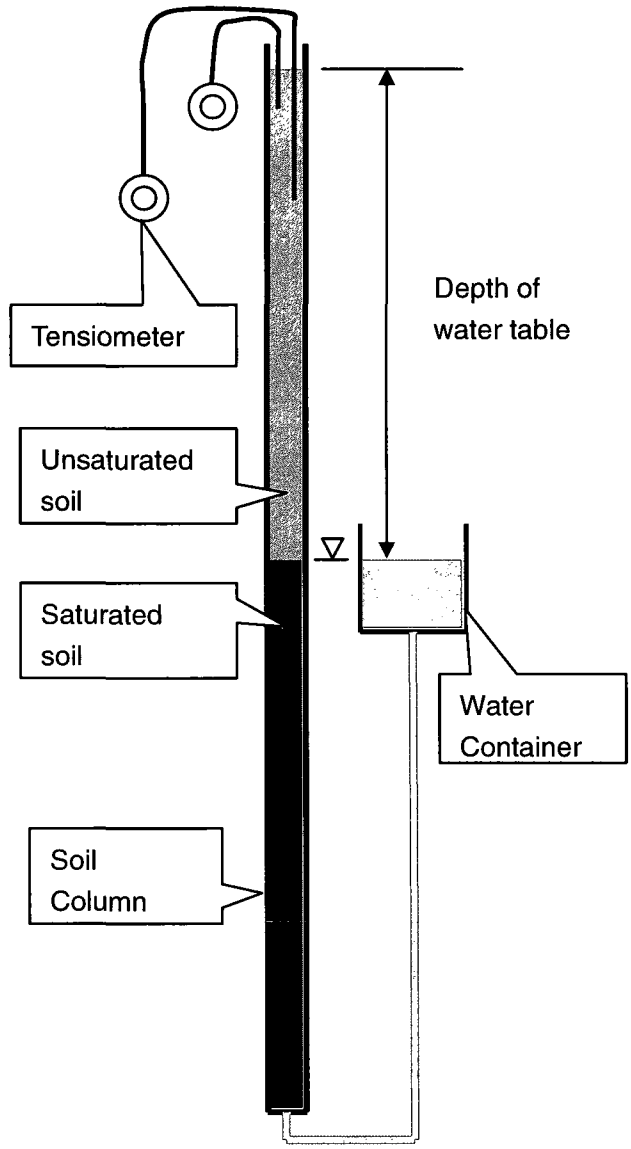

Figure 3.9 Schematic diagram of suction profile set (Li 2008)

The set consists of a long transparent acrylic soil column (50 mm in diameter and 1500 mm in height), a water container, thin plastic drain tube, valves and a pulley block. Suction profile set is fixed on the left side of the bearing capacity frame (see Figure 3.1, item 10). The pre-calibrated relationship measured between matric suction and depth of water table can be used to achieve expected matric suction values in the soil container of

bearing capacity test system quickly by adjusting the water table depth. This relationship was verified using tensiometers measuring the suction values in the soil container of bearing capacity test system.

This technique discussed above can eliminate the soil fabric disturbance that may contribute to unreliable measurement of matric suction using tensiometers. The matric suction should be reliably measured as its range is narrow (i.e., from 0 to 10 kPa) for coarse-grained soils. The tensiometer ceramic tip also can easily get ruptured and will become dysfunctional when they are inserted into coarse-grained soils with angular or sub-angular grains. This technique was first used by Li (2008) for determining the bearing capacity tests for Unimin 2075 sand and was found to be useful and hence extended in the presented study.

More details with respect to tensiometers are described in the next section.

3.10 Tensiometers

Tensiometer (Figure 3.10) is conventionally used for the direct measurement of matric suction in unsaturated soils in a range of 0 to 100 kPa. The details of tensiometer structure, principle, calibration and installation are discussed in the following sections.

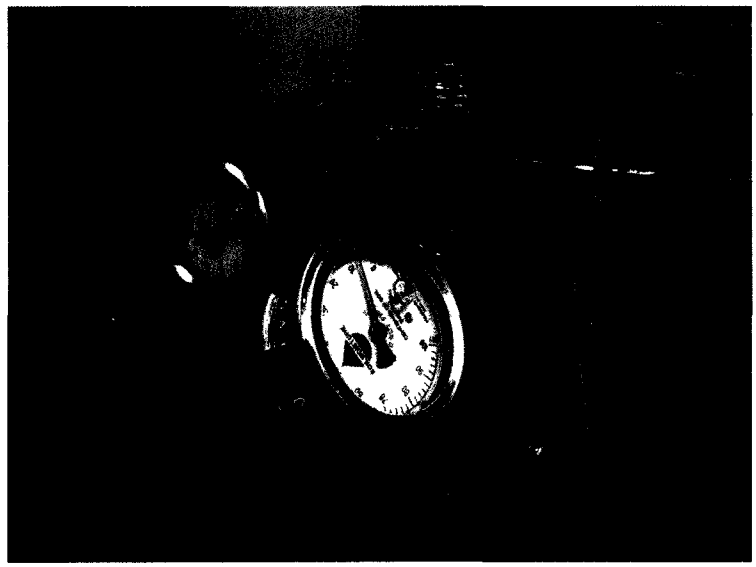

Figure 3.10 Tensiometers of Model 2100 with a plastic holder

3.10.1 Tensiometer Structure

The commercial tensiometers used in the present research program were manufactured by Soilmoisture Equipment Corp. in California, USA. The unit used is model 2100 which consists of a plastic body tube, a porous ceramic cup sensor with a 1 bar (100 kPa) air-entry value, and a vacuum dial gauge. A thin neoprene tube is also used to connect body tube and ceramic cup to transfer suction from sensor to gauge.

The ceramic cup is typically an inverted cup or small probe that can be filled with water. This tip is used to create a saturated hydraulic connection between the unsaturated soil and the water in the tensiometer body through the use of a pressure sensor. A typical setup of laboratory commercial tensiometer is shown in Figure 3.11.

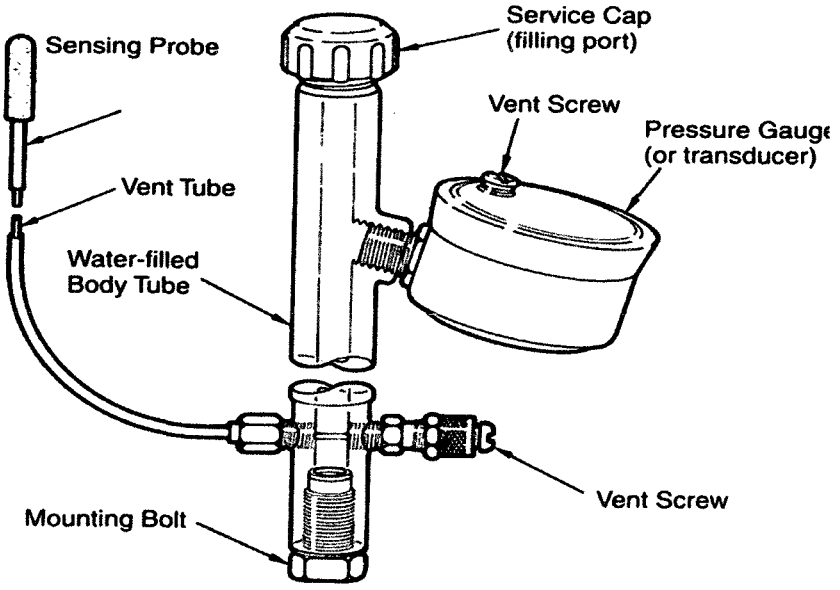

Figure 3.11 Schematic of the small-tip laboratory tensiometer (Fredlund and Rahardjo 1993)

3.10.2 Principle and Methodology

The technique for measuring the matric suction in soils using the tensiometer relies on the properties of the high-air entry (HAE) materials typically prepared using ceramic materials such as kaolinite. The HAE materials are characterized by microscopic pores of

relatively uniform size and size distribution. The surface tension forces maintain the gas-liquid interfaces formed in the material's pores of the saturated HAE material (ceramic disk). In other words, surface tension acts as a membrane for separating the air and water phases.

The maximum sustainable difference between the air pressure, u_a, above the disk and the water pressure, u_w, within and below the disk is inversely proportional to the maximum pore size of the material and mathematically expressed using Young-Laplace Equation 3.1. Figure 3.12 explains the operating principle of HAE ceramic cup (Lu and Likos, 2004).

$$(u_a - u_w)_b = \frac{2T_s}{R_s} \qquad [3.1]$$

where, $(u_a - u_w)_b$ = air-entry value, kPa

T_s = the surface tension of the air water interface, kPa

R_s = the effective radius of the maximum pore size of the HAE material

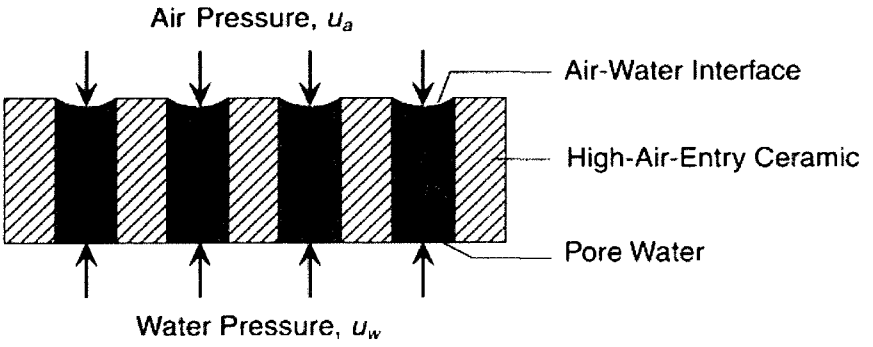

Figure 3.12 Operating principle of HAE ceramic cup (Lu and Likos 2004)

3.10.3 Calibration of Tensiometer

The ceramic cup should be immersed in water for at least one hour or more to fill the pores with water. The tensiometer system is then filled with de-aired water. A small suction is applied at the filler end for removing air from the bourdon tube in the vacuum dial gauge. Also, the tube can be tapped to release the air bubbles. A small vacuum

pressure should be applied again to flush the air-free water through the system to remove the air. After the process is done, the service cap is replaced and the water vent screw is tightened. The tensiometer after these preparation techniques is ready for laboratory or field installation.

Evaporation can significantly influence the matric suction value measurement. Long-term evaporation from the ceramic cup should be avoided, since it reduces the sensitivity of the instrument.

3.10.4 Tensiometer Installation

In order to install the tensiometer in the soil, a good contact is required between the ceramic cup and the soil to maintain continues link between the pore water and the measurement system. A thin wall 6 mm tube can be used to core a hole in the soil to place the ceramic cup. The plastic tube should be handled carefully and not to be bent. The ceramic cup must be mounted in the region where matric suction values are required (Fredlund and Rahardjo 1993). Furthermore, the ceramic cup and pressure gauge should be placed at the same elevation.

After installation is completed, the unit will come to equilibrium condition with the soil and the matric suction value can be read directly on the dial gauge in kPa.

3.11 Load Cell

A lightweight "S"-Beam load cell 20210 (Figure 3.13) was used to measure the load. The unit can function both in tension or compression. The output can be received and recorded with Data Acquisition System (DAQ).

The load cell has 0.11 to 177.93 kN capacities. It is made of Nickel/Chrome Plated Alloy Steel and can work under -17.78 – 65.56 deg. C.

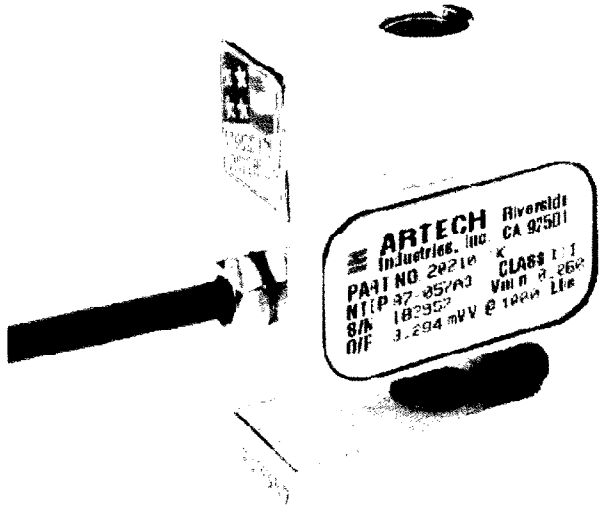

Figure 3.13 "S"-Beam load cell 20210

3.12 Displacement Transducer

The displacement of the footing was measured using Linear Strain Transducer (LSCT), HS50/5732 (Figure 3.14).

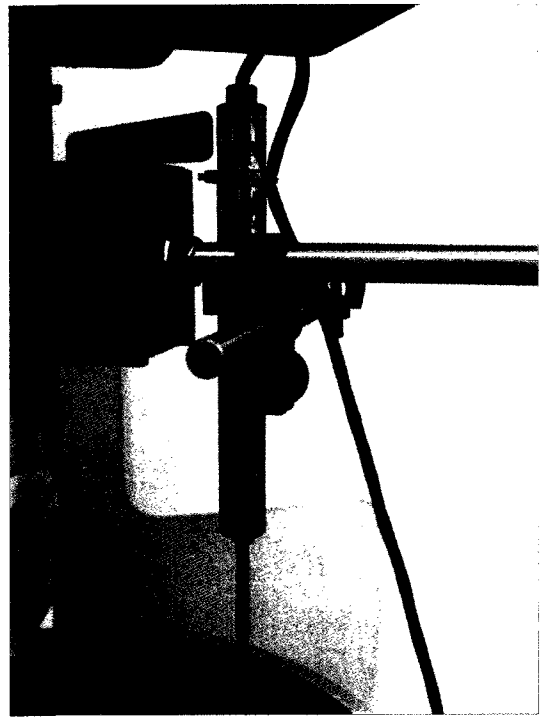

Figure 3.14 Linear Strain Transducer with a magnetic holder

The weight of LSCT is less than 250 g and can be fixed on a magnetic holder. The maximum displacement of this model is 51 mm. The hysteresis-compensated with linearity is better than ± 0.1% of full scale in both directions. It requires input of 10V DC with an output up to 6.5 mV per volt.

3.13 Data Acquisition System

The data acquisition system used in the present research program was NI USB-6210 (Figure 3.15) from National Instruments Corporation to collect data of measured parameters. The NI USB-6210 is a bus-powered M Series multifunction data acquisition (DAQ) module for USB that is optimized for superior accuracy at fast sampling rates. It offers 16 analog inputs; a 250 kS/s single-channel sampling rate; four digital input lines; four digital output lines; four programmable input ranges (±0.2 to ±10 V) per channel; digital triggering; and two counter/timers.

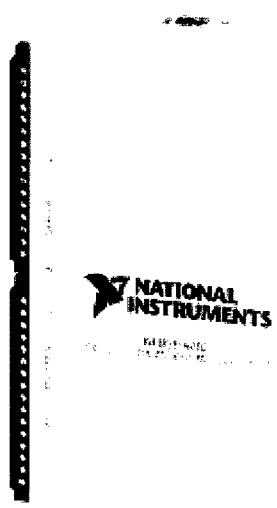

Figure 3.15 NI USB-6210

3.14 Summary

This chapter briefly summarizes details of the equipments used in the research program presented in the thesis. The bearing capacity test system was used to conduct model footing tests in a specially designed unit. The triaxial shear apparatus was used to determine the effective shear strength parameters. The Tempe Cell and WP4-T were used to measure the Soil-Water Characteristic Curve (SWCC). The suction profile set was used for developing pre-calibrated relationship between the matric suction and the soil depth from surface (i.e., depth of water table). The details of additional tools used (i.e., tensiometers, load cell, settlement transducer and data acquisition system) were also presented.

CHAPTER 4

SOIL PROPERTIES

4.1 Introduction

This chapter summarizes the properties of four different soils used in the research program; namely, Filtration sand, Quarry sand, Sil-co-sil 106 and Min-u-sil 30. Two of the four soils were coarse-grained sands and the remainder two soils were fine-grained silica. The conventional properties which include the grain size analysis and the effective shear strength parameters were determined in the Geotechnical laboratory of the University of Ottawa. Unsaturated soil properties of the four soils were also determined. Tempe cell was used for determining the Soil-Water Characteristic Curve (SWCC) of the two coarse-grained soils. The SWCC for the two fine-grained soils (i.e., Sil-co-sil 106 and Mil-u-sil 30) were determined using both the Tempe cell and the WP4-T. The suction profile (i.e., the relationship of matric suction with respect to depth above the water table in the soil container used for measuring the bearing capacity of model footings) was determined using a specially designed apparatus which is referred as suction profile set. Equipment details and methodologies for conducting the tests were discussed in Chapter 3.

4.2 Soil Type

The grain size distribution of Filtration sand and Quarry sand are determined by conducting sieve analysis using 1000g dry sand following ASTM D422 (1994b). The data of grain size distribution of these two soils are in Table A.1 and Table A.2 of Appendix. The sieve analysis results of Sil-co-sil 106 and Min-u-sil 30 are supplied by the

manufacture. Figure 4.1 summarizes the results.

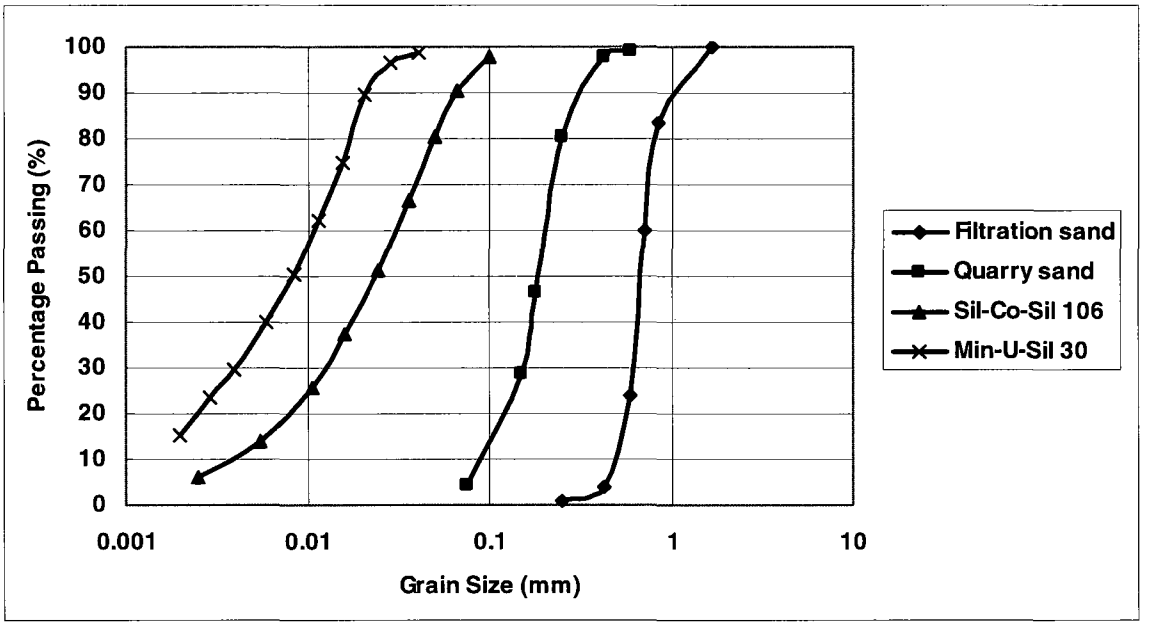

Figure 4.1 Summary of grain size distribution

The median grain size, D_{50} of Filtration sand and Quarry sand are 0.68 mm and 0.19 mm, respectively. The coefficient of uniformity, C_u (i.e., D_{60}/D_{10}) of both soils are less than 6 and the coefficient of curvature, C_c (i.e., $(D_{30})^2/(D_{10}\times D_{60})$ of Filtration sand and Quarry sand are 0.88 and 1.44, respectively. Both soils were classified as poorly graded sand (SP) according to the Unified Soil Classification System (USCS).

For Sil-co-sil 106 and Min-u-sil 30, the median grain size, D_{50} is 0.024 mm and 0.0083 mm, respectively. 50 % or more passes the No. 200 sieve (opening diameter: 75 um). As both soils are non-plastic and inorganic silt which are primarily composed of SiO_2 (99.7%), they were classified as silt (ML) according to USCS.

4.3 Filtration sand

The Filtration sand used in the present study is obtained from FILTERSIL Inc. in Mauricetown, New Jersey. This commercial industrial quartz sand is selected for use in the research program because it is dense, durable sand and is resistant to degradation during handling and backwashing.

4.3.1 Chemical Analysis

The data of chemical composition supplied by manufacture is summarized in Table A.3 of Appendix.

4.3.2 Suction Profile

Suction profile of Filtration sand was measured using the suction profile set described in Chapter 3. The results obtained from this set were used to control the depth of the water table to achieve pre-decided matric suction profile below the model footings prior to conducting the bearing capacity tests. The Filtration sand was initially saturated in the suction profile set by raising the water level from bottom of the soil column. The water table is then lowered to various depths and the capillary suction is measured using tensiometers to obtain the suction profile.

Figure 4.2 shows the relationship between the water table and matric suction for the Filtration sand using the suction profile set for two depths 50 mm and 100 mm (see Fig. 3.1, item 10). The stresses associated with the model footing loading are typically distributed in the depth from 0 to 1.5B and these two depths fall in this range (Poulos and Davis 1974, Agarwal and Rana 1987). The contribution of matric suction towards the bearing capacity and resistance to settlement due to the loading of the footing also comes from this depth of 0 to 1.5 B (Oh and Vanapalli 2008, Oh et al. 2009). Therefore, the

average matric suction value from the matric suction profile under the model footing is necessary for interpreting the results. The depth 50 mm and 100 mm correspond to values of B and 2B for the maximum size footing used in the present research program (i.e., 50 mm).

The water table was first lowered to 50 mm below the soil surface for a period of 24 hrs to attain equilibrium conditions with respect to capillary stresses (i.e. matric suction). The matric suction readings were measured at two different levels of depth using tensiometers. This procedure was repeated by varying the depth of water table below the soil surface to different levels (i.e., 150 mm, 250 mm, 350 mm, 450 mm, 550 mm, 650 mm, and 750 mm, 850 mm) while measuring matric suction values after 24 hrs. A maximum depth of 850 mm was chosen because the maximum height of the soil container (see Fig.3.1, item 3) is 700 mm. The data of suction profile is summarized in Table A.4 of Appendix.

The measured dry unit weight of the specimen was equal to 16.72 kN/m^3.

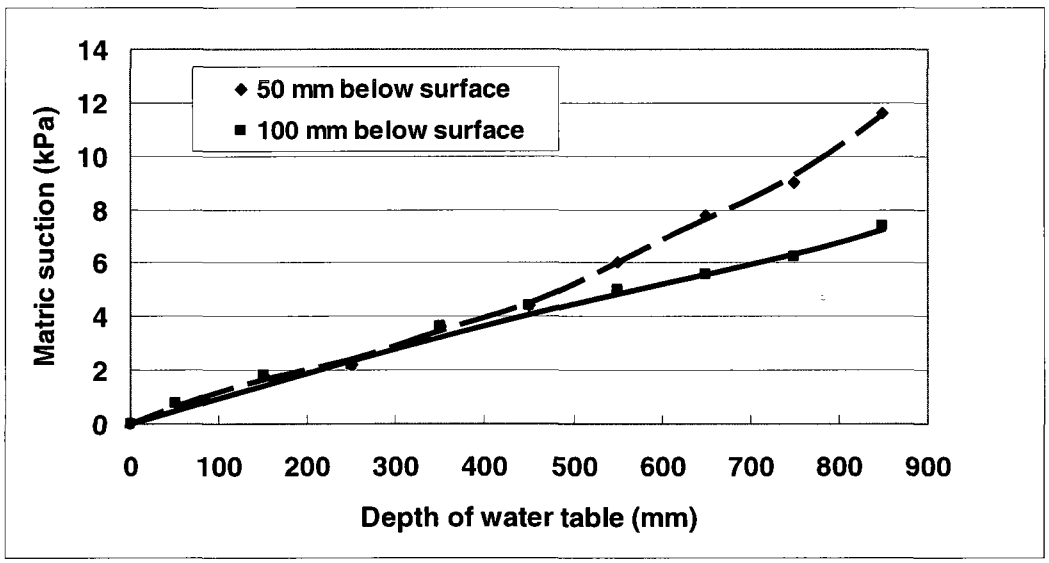

Figure 4.2 Suction profile of Filtration sand

The matric suction in the Filtration sand increases linearly for the depth of 100 mm after lowering depth of water table. However, for the depth of 50 mm, the matric suction increase linearly up to 450 mm and then increases nonlinearly at a faster rate. Such a behavior was attributed to the evaporation of water from the soil column at the surface. These results suggest that the matric suction close to surface of the footing should be reliably determined as matric suction is sensitive to environmental conditions and it significantly influences the bearing capacity and settlement behavior of unsaturated soils.

4.3.3 Shear Strength

The effective shear strength parameters (i.e., c' and ϕ') of Filtration sand were measured using triaxial shear apparatus under consolidated drained conditions (i.e., CD tests). The amount of soil required for achieving dry unit weight equal to16.25 kN/m^3 for a specimen with the dimensions of 50 mm in diameter and 108 mm in height was determined. A saturated porous stone and filter paper were placed on the pedestal of the triaxial cell and a rubber membrane of 50 mm in diameter was secured with an O-ring. The pre-calculated amount of sand was placed in the rubber membrane using a small spoon and intermittently compacting the sand with a little mallet. After the soil was filled in the rubber membrane a filter paper and porous stone were placed on the top of the specimen. Filter paper was used for preventing the migration of soil particles into the porous stone. The rubber membrane at the specimen base and the top cap were secured with rubber "O" rings. Once the above operations were done, the triaxial cell was assembled, filled with water, and placed on the apparatus in the testing frame. The triaxial cell and the sample lines were connected to the appropriate valves before applying cell pressure and back pressure sequentially to conduct the test following the ASTM D4767-04.

The rate of shear used of 1.14 mm/min was used for determining the shear strength parameters; the same rate was used for loading the model footings for determining the

bearing capacity. Similar rates of shear were used by earlier investigators for determining the effective shear strength parameters using direct shear apparatus and also for loading the model footings on coarse-grained sands (Mohamed and Vanapalli 2006, Li 2008, Vanapalli et al. 2010).

The stress versus strain curves under different normal stresses (i.e., 50 kPa, 100 kPa and 150 kPa) is shown in Figure 4.3. The modulus of elasticity under normal stress of 50 kPa was slightly higher in comparison to data tested with a normal stress of 100 kPa. This may be attributed to some differences in initial properties of the specimen or due to experimental errors. The stress-strain relationship is nonlinear which is similar to the model footing test results (described in Chapter 5). The failure occurs typically at an axial strain in the range of 1-4%. These results are consistent with the results of other investigators on coarse-grained soils (Salgado et al. 2000).

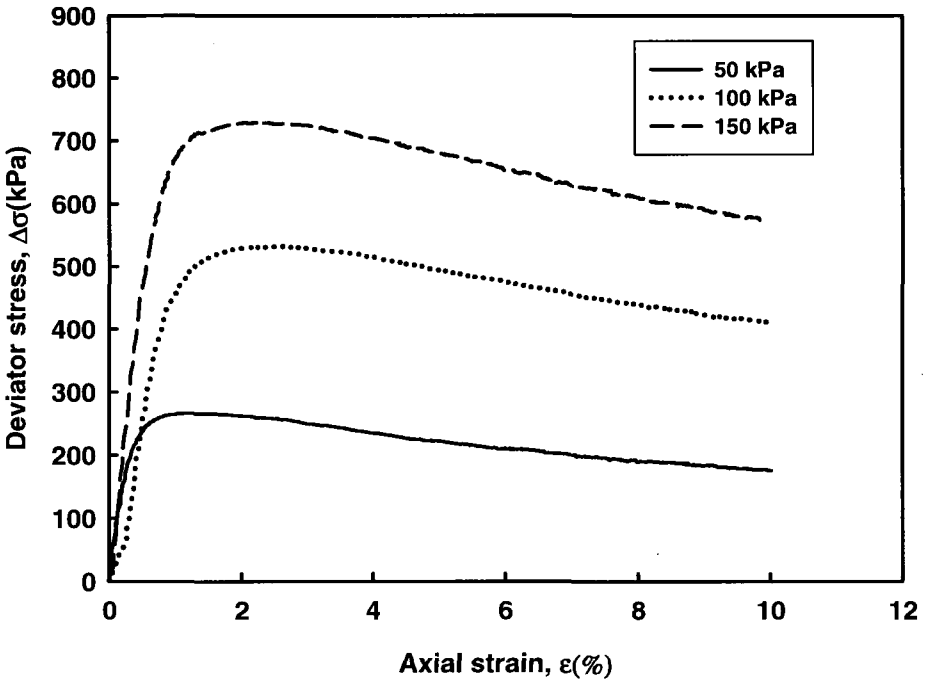

Figure 4.3 Stress versus strain response of triaxial specimens under different normal stresses for the Filtration sand

In Figure 4.4, both Mohr's envelopes and stress point form relations (i.e., q – p plots) are summarized. The shear strength parameters effective cohesion, c' and internal friction angle, ϕ' were equal to zero and 45.7° respectively from both these relationships.

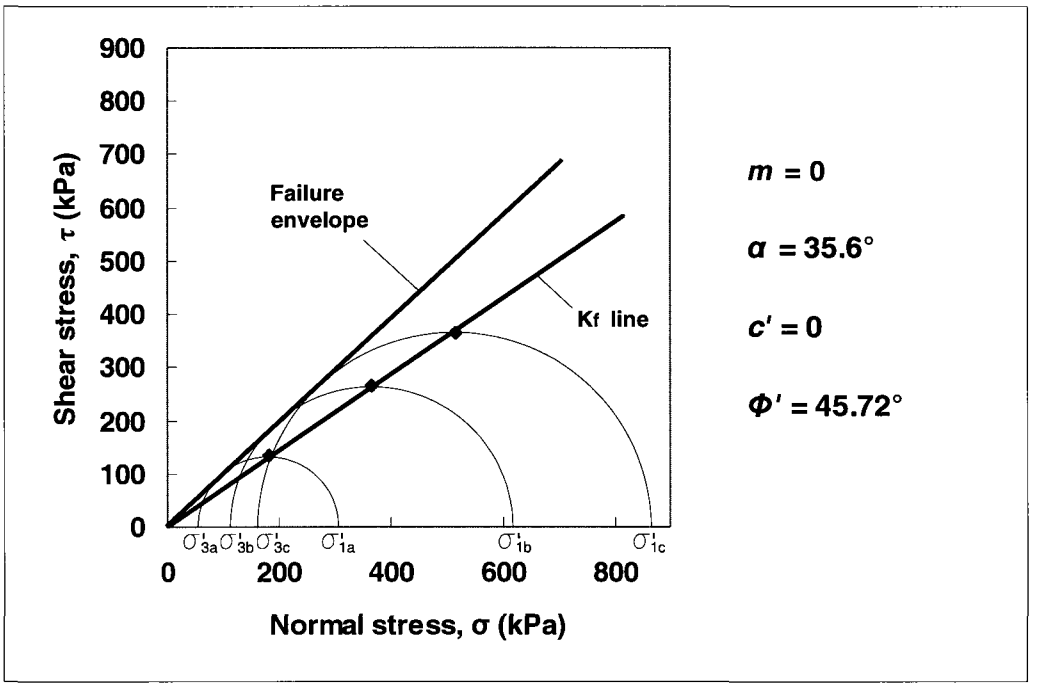

Figure 4.4 Triaxial shear test result of Filtration sand

The bearing capacity factors increase significantly for large ϕ' values, which are typical for coarse-grained soils. Also, bearing capacity of unsaturated soils is significantly influenced even for small values of matric suction for coarse-grained soils (Steensen-Bach et al. 1987, Vanapalli and Mohamed, 2007, Vanapalli 2009). Therefore, ϕ' should be determined carefully for reliable determination of the bearing capacity of soils under different values of matric suction. However, there are several other parameters such as the dilatancy and applied normal stress also can influence the internal friction angle, ϕ'. Bolton (1986) studies on sands show that the effective stress and soil density

affect the rate of dilatancy of soils and thereby influence the internal friction angle, ϕ' value.

4.3.4 Soil Water Characteristic Curve (SWCC)

Information related to the water storage characteristics of unsaturated soils can be derived from the soil water characteristic curve (SWCC). A typical SWCC exhibits three identifiable stages of desaturation (Vanapalli et al. 1996): the boundary effect stage or capillary saturation zone, the transition stage or desaturation zone (i.e., primary and secondary transition stage), and the residual stage. The air-entry value (AEV) of the tested soil was determined by the intersection of the two linear slope segments in the boundary effect and transition stages of the SWCC (see Fig. 4.5). Similarly, the residual suction was determined by the intersection of the two linear slope segments in the transition and residual stages of the SWCC (Vanapalli et al. 1999).

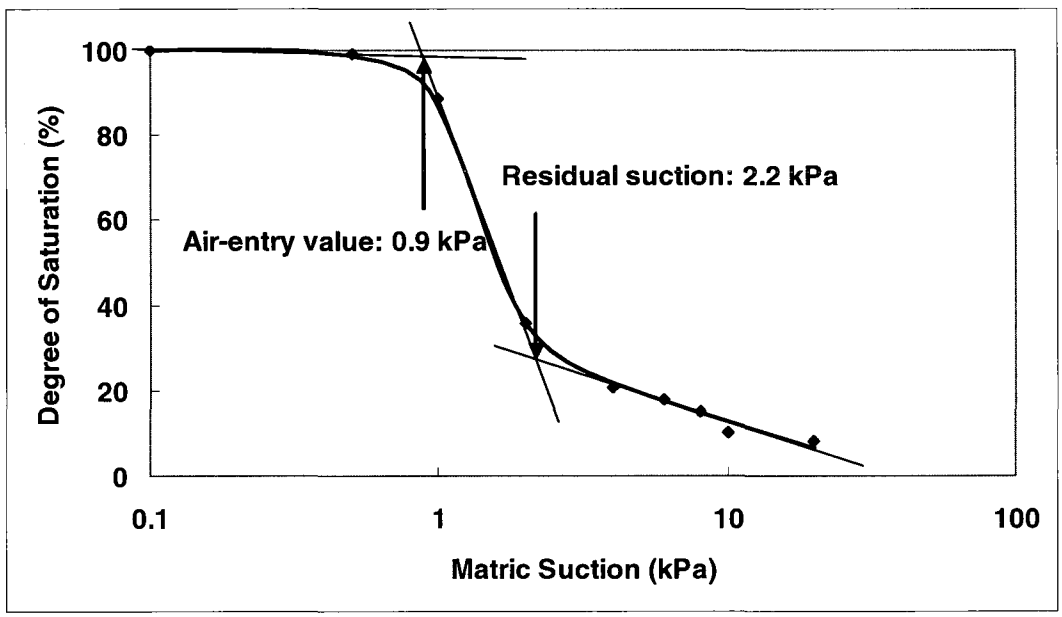

Figure 4.5 SWCC of Filtration sand in the suction range of 0 to 20 kPa

The SWCC of Filtration sand was measured on a specimen (which is 63.9 mm in

diameter and 31.9 mm in height) with dry unit weight equal to 16.19 kN/m^3. The initial conditions of the test specimen used for measuring the SWCC are similar to that of specimens used for measuring shear strength and bearing capacity tests. The water content at saturated condition of specimen was 22.87%. Figure 4.5 shows the measured SWCC of Filtration sand.

The air-entry value (i.e. the matric suction value at which air recedes into the soil pores) of Filtration sand is 0.9 kPa and the residual suction is 2.2 kPa. The shape of the SWCC depends on the pore size distribution and volume change of the soil and the air-entry value and the residual suction value are affected by the initial water content, soil structure, mineralogy, and the stress history (Vanapalli et al. 1999). Filtration sand desaturates at a fast rate as the soil particles are relatively coarse-grained in nature and the pore size distribution is more uniform. More than 90% of the water was drained when the matric suction in the tested specimen reached a value of 20 kPa. These results are consistent with the results of other coarse-grained soils reported in the literature (Reinson et al. 2005, Mohamed and Vanapalli, 2006, Alim et al. 2009).

4.4 Quarry sand

Quarry sand is natural sand from Burnside Quarry on March road in Ottawa.

4.4.1 Suction Profile

The same procedures described in section 4.2.3 were used for determining suction profile of Quarry sand. Figure 4.6 shows the relationship between the water table and matric suction for two depths 50 mm and 100 mm. The data of suction profile is provided in Table A.5 of Appendix. The measured dry unit weight of the specimen was equal to 16.19 kN/m^3.

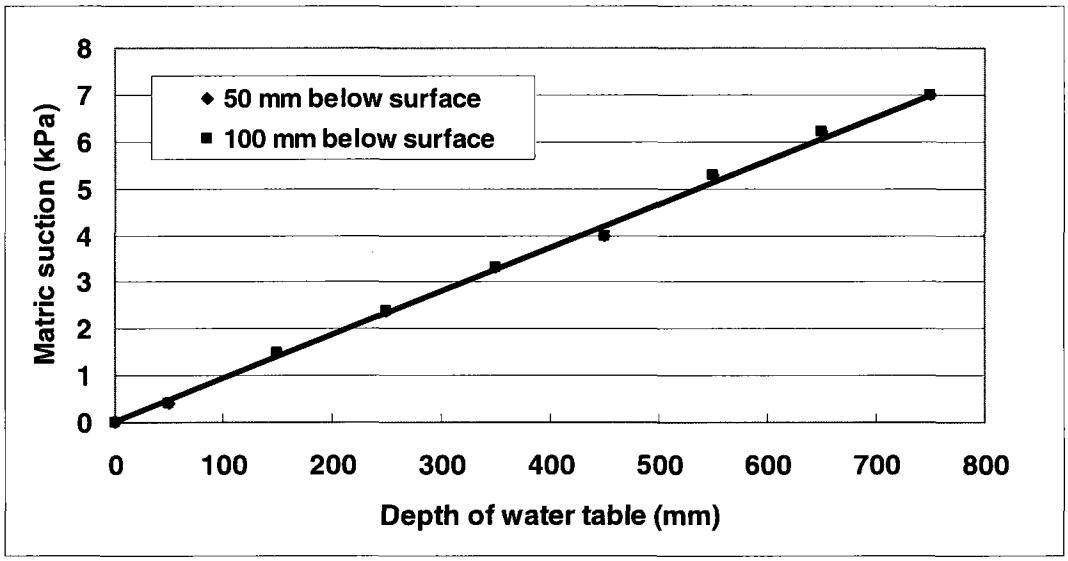

Figure 4.6 Suction profile of Quarry sand

Suction profile of Quarry sand shows that the matric suction increases as the depth of water table increases. Both tensiometers show the same increment of matric suction value after lowering the water table. Because Quarry sand is relatively finer than Filtration sand, the evaporation of water from the soil column close to surface does not play as much as an important role for Quarry sand. However, matric suction values are still sensitive to environment conditions.

4.4.2 Shear Strength

Similar procedures described in section 4.2.4 were used for measuring the effective shear strength parameters (i.e., c' and ϕ') of Quarry sand. The dry unit weight of the specimen was equal to 16.24 kN/m^3. Figure 4.7 shows the stress versus strain curves under different normal stresses (i.e., 50 kPa, 100 kPa and 150 kPa). The failure occurs at an axial strain in the range of 1-4%. In Figure 4.8, both Mohr's envelopes and q – p form provide the same results for the shear strength parameters, which effective cohesion, c' was equal to zero and internal friction angle, $\phi' = 43.73°$.

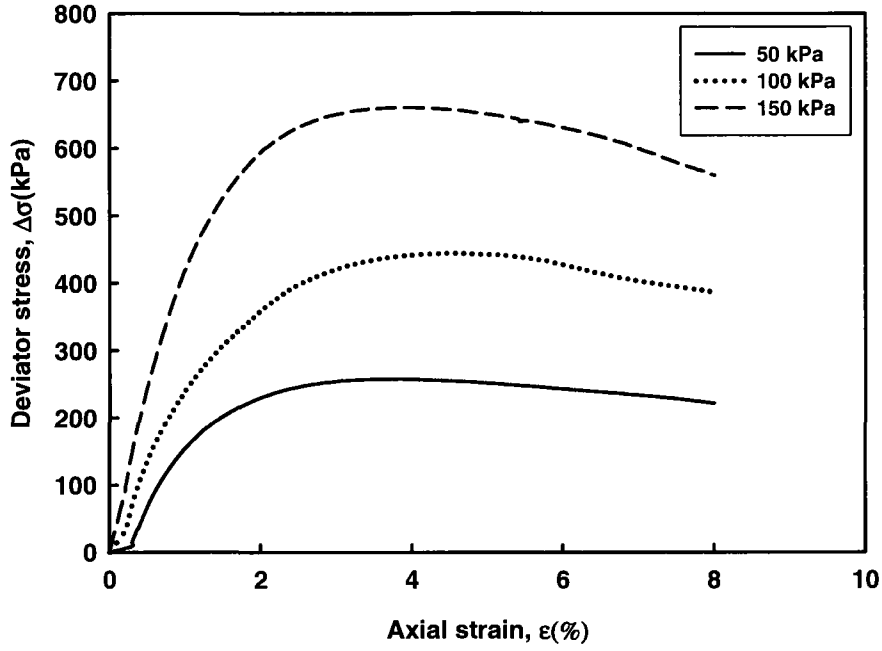

Figure 4.7 Stress versus strain response of triaxial specimens under different normal stresses for the Quarry sand

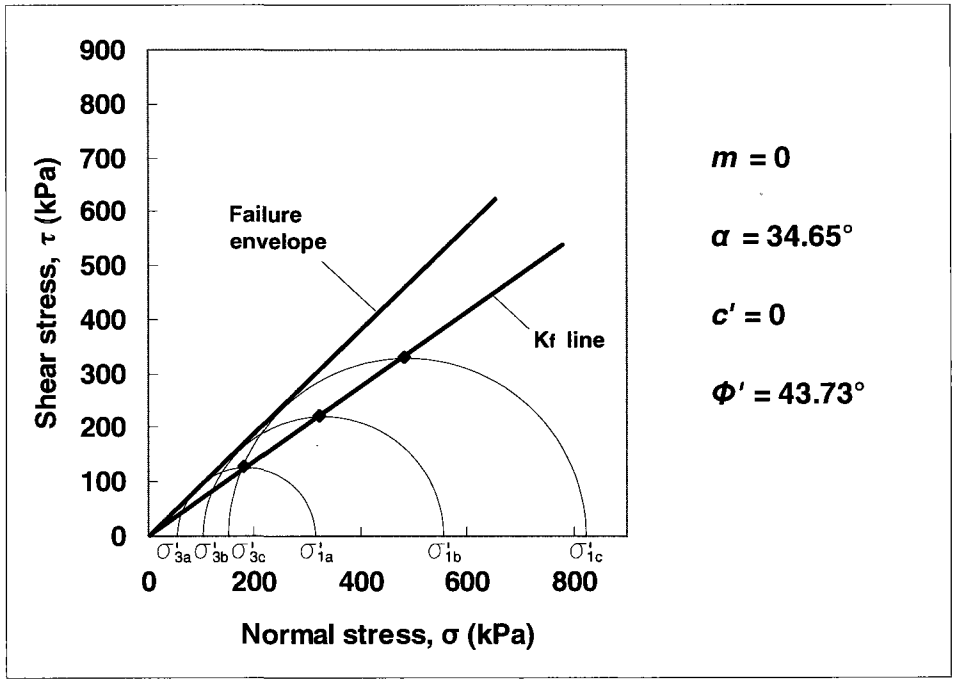

Figure 4.8 Triaxial shear test result of Quarry sand

4.4.3 Soil Water Characteristic Curve (SWCC)

The measured SWCC of Quarry sand for two different suction ranges are shown in Figure 4.9. From Figure 4.9a, the air-entry value and residual suction of Quarry sand were found to be 3.2 kPa and 9 kPa, respectively.

The SWCC was measured on a specimen (which is 63.9 mm in diameter and 31.9 mm in height) with a dry unit weight equal to 16.19 kN/m^3. The water content at saturated condition was 24.25%. Reinson et al. (2005) stated that the air-entry value is a function of the size of the largest pores, which are larger for coarse-grained soils and smaller for fine-grained soils. Quarry sand is relatively finer compared to Filtration sand and hence it has a higher air-entry value and desaturates at a relatively low rate.

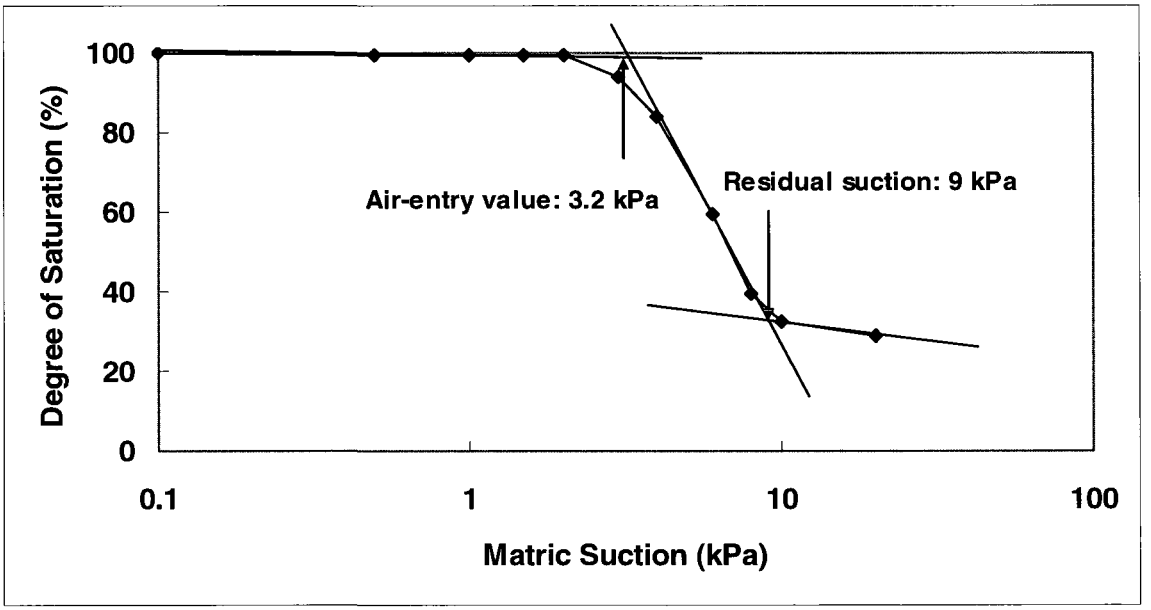

(a) SWCC of Quarry sand in the suction range of 0 to 20 kPa

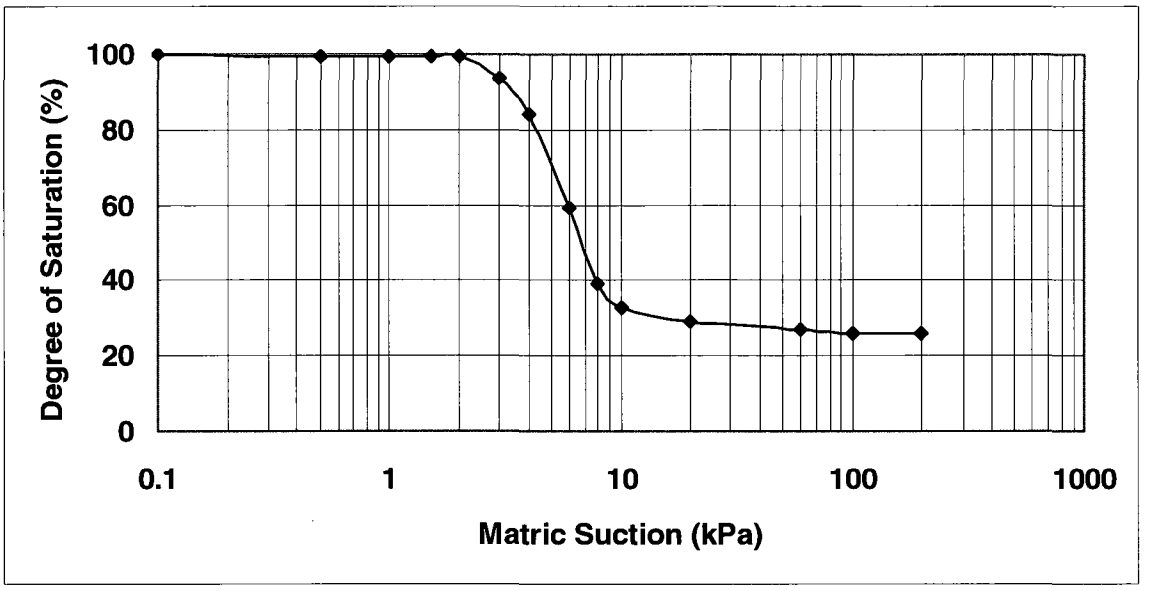

(b) SWCC of Quarry sand in the suction range of 0 to 200 kPa

Figure 4.9 SWCC of Quarry sand

4.5 Sil-co-sil 106

Sil-co-sil 106 (Barco 290) is fine-grained commercial silt obtained from Opta Minerals Inc. in Waterdown, Ontario.

4.5.1 Chemical Analysis and Physical Properties

The data of chemical and physical properties of Sil-co-sil 106 supplied by manufacture are summarized in Table A.6 and Table A.7 of Appendix.

4.5.2 Suction Profile

The relationship between matric suction and depth of water table for Sil-co-sil 106 is summarized in Figure 4.10. The data of suction profile is provided in Table A.8 of Appendix. The measured dry unit weight of the specimen was equal to 15.76 kN/m^3.

Suction profile of Sil-co-sil 106 shows that the matric suction increases after 50 mm

depth of water table. Such a behavior implies that the capillary height of Sil-co-sil 106 was equal to 50 mm. Adhesion of water to the walls of a vessel will cause an upward force on the water at the edges. The surface tension acts to hold the surface intact, so instead of just moving the edges upward, the whole water surface is dragged upward. Therefore, the water table was still on the soil surface until it was lowered to 50 mm. Both tensiometers show the same increment of matric suction value after lowering the water table, similar to the Quarry sand results discussed earlier.

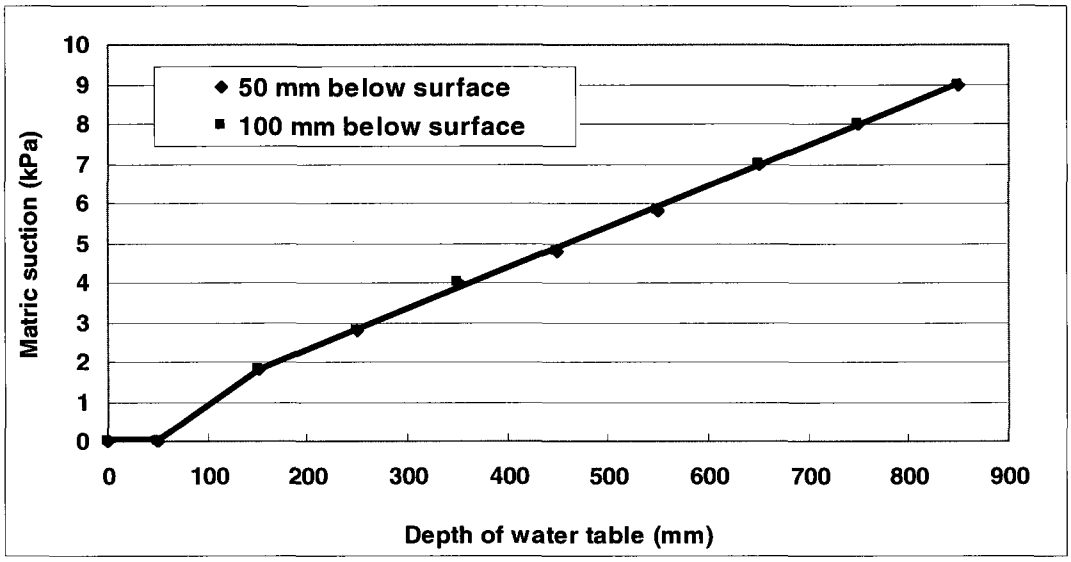

Figure 4.10 Suction profile of Sil-co-sil 106

4.5.3 Shear Strength

The effective shear strength parameters (i.e., c' and ϕ') of Sil-co-sil 106 were measured using triaxial shear apparatus under consolidated drained conditions. The dry unit weight of the test specimens used in the study were equal to 14.61 kN/m^3. A shear rate of 1.14 mm/min was used similar to other soils used in this study. The stress versus strain curves under different normal stresses (i.e., 50 kPa, 100 kPa and 150 kPa) is shown in Figure 4.11. The stress-strain relationship is nonlinear and leveled off at an axial strain of 10%.

Figure 4.12 shows the result of the triaxial shear tests using Mohr's envelopes and q – p form. The effective cohesion, c' was equal to zero and the internal friction angle ϕ' = 38.96°.

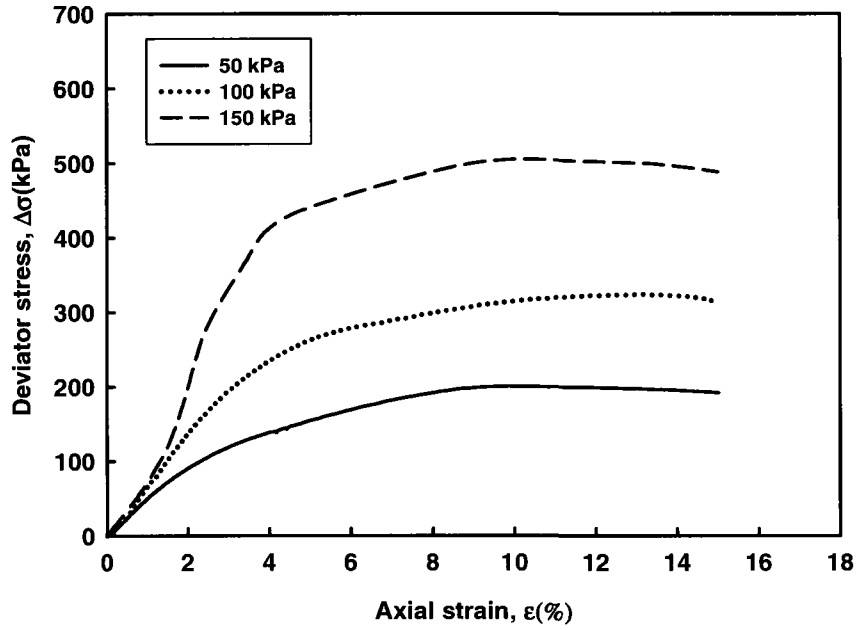

Figure 4.11 Stress versus strain response of triaxial specimens under different normal stresses for the Sil-co-sil 106

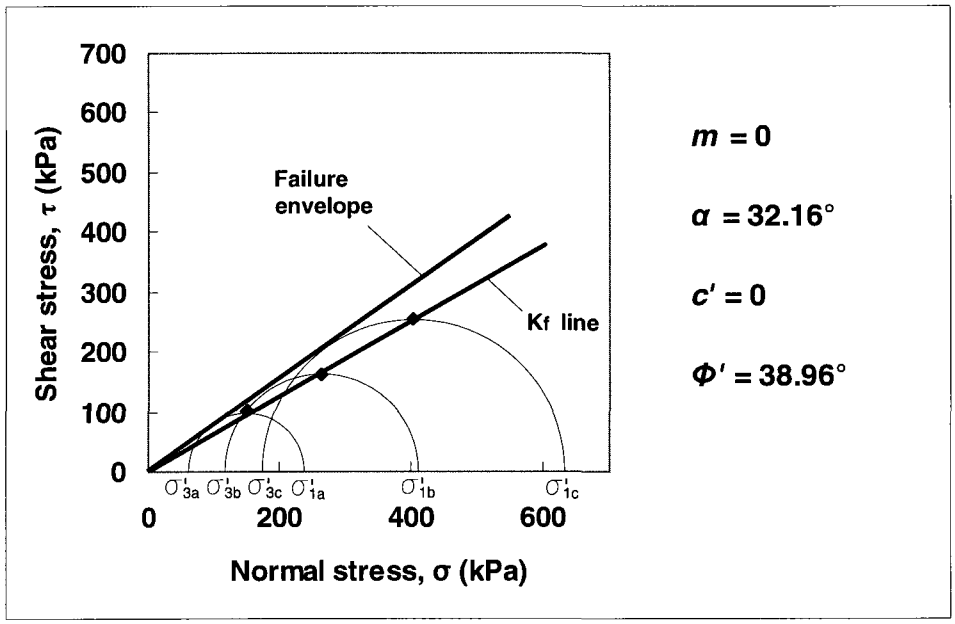

Figure 4.12 Triaxial shear test result of Sil-co-sil 106

4.5.4 Soil Water Characteristic Curve (SWCC)

Figure 4.13 shows the measured SWCC of Sil-co-sil 106. The air-entry value of Sil-co-sil 106 is 30 kPa which is relatively high compared to the coarse-grained soils (i.e., Filtration sand and Quarry sand).

The SWCC was measured on a specimen (which is 63.9 mm in diameter and 31.9 mm in height) with dry unit weight equal to 14.22 kN/m^3. The water content at saturated condition was 31.25%. Fredlund et al. (2002) studies show that a material's SWCC is closely related to its grain size distribution. Fine-grained soils typically have non-uniform pore size distributions. Consequently, the SWCC of Sil-co-sil 106 exhibit relatively flatter slope in comparison to coarse-grained soils (i.e., Filtration sand and Quarry sand).

Rowlett (2000) measured the SWCC for Sil-co-sil 90 which is a little bit finer than Sil-co-sil 106 used in the present study. The air-entry value for Sil-co-sil 90 was between 20 kPa and 30 kPa. There is a good comparison between the SWCC measured from both these studies.

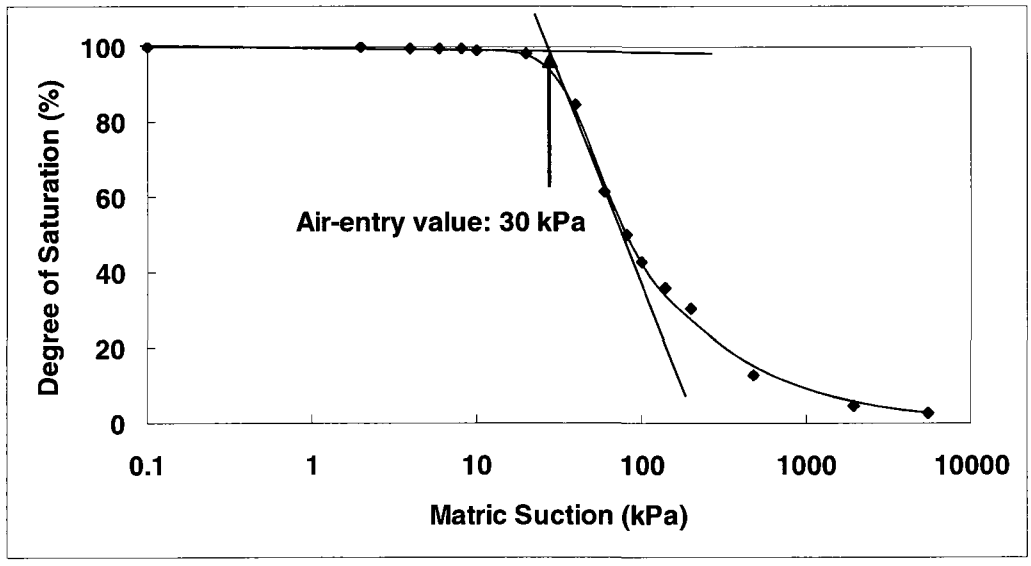

Figure 4.13 SWCC of Sil-co-sil 106

4.6 Min-u-sil 30

Min-u-sil 30 is fine-grained industrial silt obtained from the Plant of Berkeley Springs in West Virginia under U.S. Silica Company in Atlanta, USA.

4.6.1 Chemical Analysis and Physical Properties

The data of chemical and physical properties of Min-u-sil 30 supplied by manufacture are summarized in Table A.9 and Table A.10 of Appendix.

4.6.2 Suction Profile

Figure 4.14 shows the relationship between matric suction and depth of water table for Min-u-sil 30. The data of suction profile is provided in Table A.11 of Appendix. The measured dry unit weight of the specimen was equal to 13.11 kN/m^3.

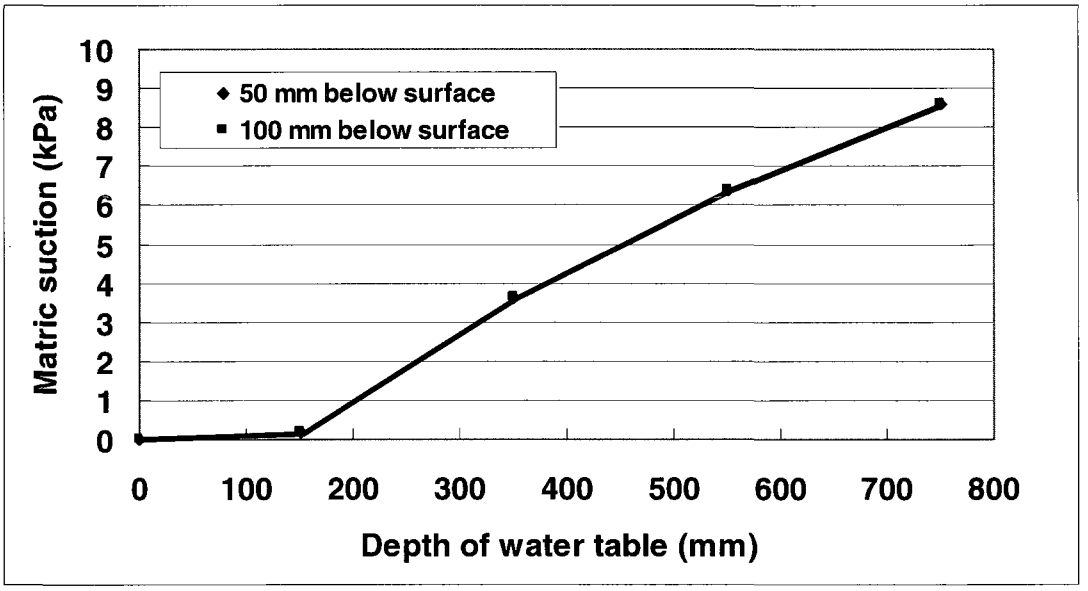

Figure 4.14 Suction profile of Min-u-sil 30

Suction profile of Min-u-sil 30 shows that the matric suction starts increasing after 150

mm depth of water table. Similar to Quarry sand and Sil-co-sil 106, the increment of matric suction value on both tensiometers for Min-u-sil 30 was found the same after lowering the water table.

4.6.3 Shear Strength

Similar procedures described in section 4.2.4 were used for measuring the effective shear strength parameters of Min-u-sil 30. The dry unit weight of the specimen was equal to 13.03 kN/m^3.

The stress versus strain curves under different normal stresses (i.e., 50 kPa, 100 kPa and 150 kPa) is shown in Figure 4.15. The stress-strain relationship is nonlinear and leveled off at an axial strain of 10%. Similar behavior was observed from the model footing test results of Min-u-sil 30 (described in Chapter 5).

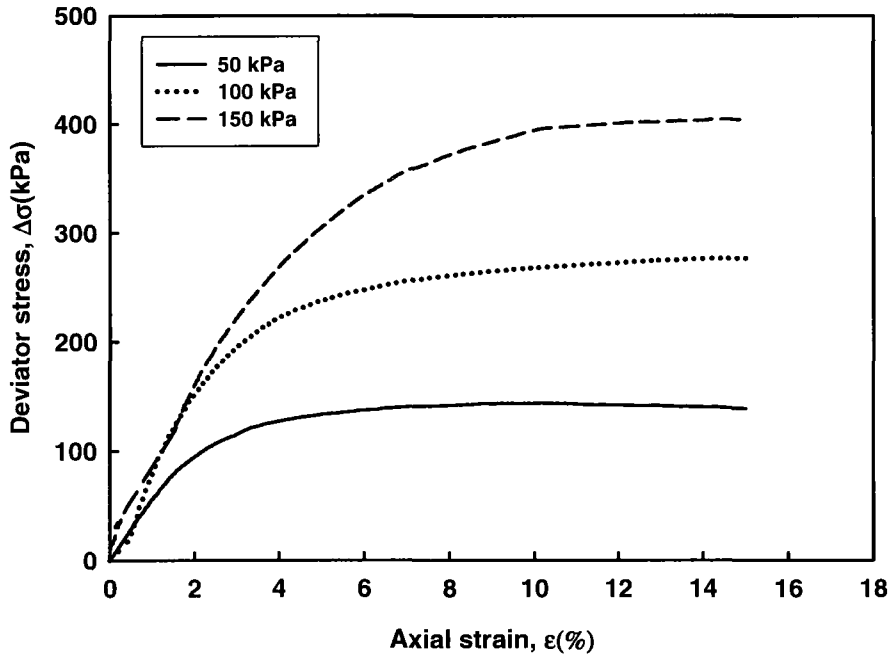

Figure 4.15 Stress versus strain response of triaxial specimens under different normal stresses for the Min-u-sil 30

Figure 4.16 shows the result of the triaxial shear test in terms of Mohr's envelopes and q – p form. The effective cohesion, c' was equal to zero and the internal friction angle ϕ' = 35.33°.

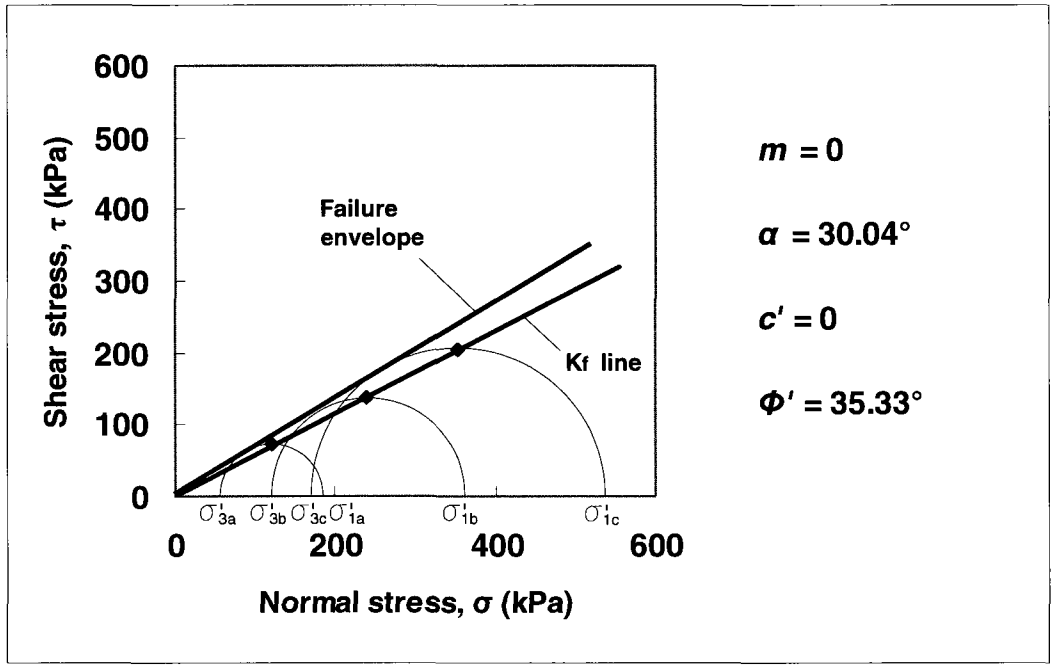

Figure 4.16 Triaxial shear test result of Min-u-sil 30

4.6.4 Soil Water Characteristic Curve (SWCC)

Figure 4.17 shows the measured SWCC of Min-u-sil 30. The air entry value of Min-u-sil 30 is 100 kPa.

The SWCC was measured on a specimen (which is 63.9 mm in diameter and 31.9 mm in height) with dry unit weight equal to 12.43 kN/m^3. The water content at saturated condition was 41.21%. The SWCC of Min-u-sil 30 is similar to Sil-co-sil 106 as the characteristics of both these soils were approximately the same.

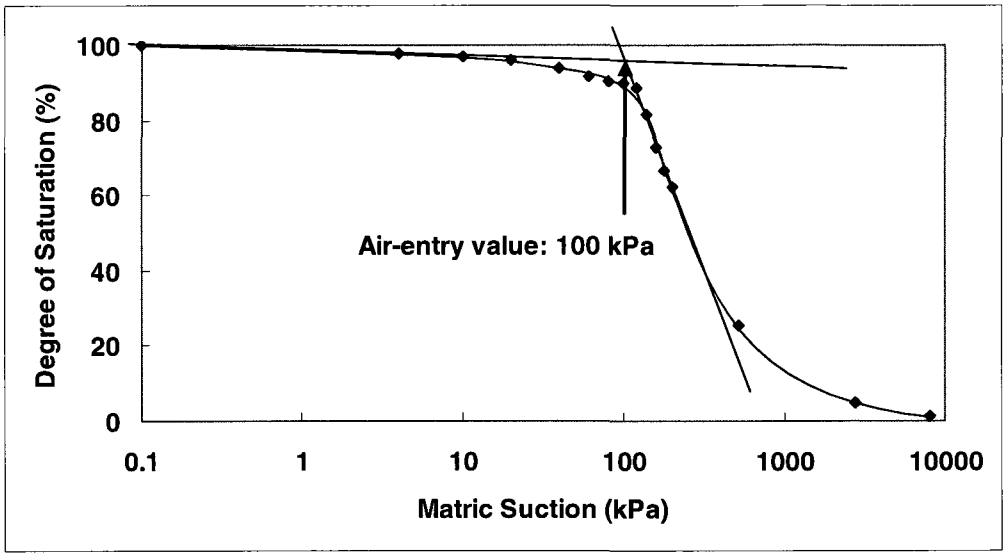

Figure 4.17 SWCC of Min-u-sil 30

4.7 Summary

The properties of four different soils which include the grain size distribution, suction profile, the shear strength parameters, and the SWCC have been determined. The finer soils have relatively lower internal friction angle and higher air-entry values (Table 4.1). The effective cohesion values for all the soils were equal to zero as they are all non-plastic soils. The soil properties summarized in this chapter are used in the analysis of bearing capacity and settlement behavior test results which are presented in Chapter 5.

Table 4.1 Summary of soil properties

Soil	D_{50} (mm)	Shear strength parameters		Air-entry value (kPa)
		c'	ϕ'	
Filtration sand	0.68	0	45.72°	0.9
Quarry sand	0.19	0	43.73°	3.2
Sil-co-sil 106	0.024	0	38.96°	30
Min-u-sil 30	0.0083	0	35.33°	100

CHAPTER 5

RESULTS AND DISCUSSIONS

5.1 Introduction

Model footing tests were conducted on four different soils; namely, Filtration sand, Quarry sand, Sil-co-sil 106 and Min-u-sil 30 under both saturated and unsaturated conditions using the bearing capacity test system described in Chapter 3. The bearing capacity and settlement were determined over a matric suction range of 0 to 8 kPa for all these soils. The experimental set up was limited to achieving matric suction values of 8 kPa as the height of the soil container was limited (i.e. 700 mm). The range of suction studied extends over the boundary effect, transition and residual stages for two of the coarse-grained soils studied (Vanapalli et al. 1996). However, for the other two relatively fine-grained soils, the matric suction range of 0 to 8 kPa falls in the boundary effect zone. Both these soils are still in a state of saturated condition for this matric suction range.

Four model footings of different sizes (i.e., 20 mm × 20 mm; 37 mm × 37 mm; 41.75 mm in diameter; and 50 mm × 50 mm) were used in the present research program to study the influence of footing size on the bearing capacity and also settlement behavior of different unsaturated soils. The focus of the study presented in this chapter is to provide comparisons between the measured and predicted bearing capacity and settlement behavior of different unsaturated soils. The bearing capacity of the unsaturated soils is predicted using the approach presented by Vanapalli and Mohamed (2007) and the settlement was estimated using the approach by Oh et al. 2009.

Some key details with respect to testing techniques used are also summarized in this Chapter. The testing techniques are succinctly provided where necessary to assist in the discussion of the results.

5.2 Soil and Test Preparation

The procedure for the preparation of soil before conducting model footing tests is summarized below:

1. Prepare the soil container: The base of the soil container with slots (see Figure 3.4b) was cleaned to ensure free flow of water. A lid with perforations was placed on the base of the soil container to cover the slots. A geotextile of the same diameter as the base of the soil container was placed on top of the lid. Lastly, a filter paper of the same diameter as the geotextile was placed on the geotextile, to allow the free flow of water but block the soil particles migration. The base plate and soil container were then fastened with screws tightly to prevent any leakage of water.
2. The soil was placed into the container in several layers. Each soil layer thickness was equal to 100 mm was evenly compacted using a 2 kg weight manually. This procedure was useful in achieving a relatively higher value of density index, D_r, which is the ratio of the difference between the void ratios of a cohesionless soil in its loosest state and existing natural state to the difference between its void ratio in the loosest and densest states. The densest density of the soil was obtained by filling the mould with the soil by tapping it sharply on the sides with a rubber mallet. The loosest density of the soil was obtained by filling the mould with the soil without subjecting it to any vibrations.
3. A valve connected to the base of the soil container provides access of water to the compacted soil in the container under a controlled head of water. Water flows through slots in the container base and rises up from bottom slowly until the soil is saturated (i.e., the water table reaches the soil surface in the container). This technique facilitates escape of air from bottom of the soil container to the soil surface gradually to ensure saturated condition.
4. Two Tensiometers were installed for the measurement of matric suction. One was placed at 10 mm under the soil surface and the other was inserted to a depth of 1.5 B (B is the footing width) beneath the soil surface. The information of matric suction at two points (i.e., close to surface and at 1.5 B depth) was used in the calculation of the

measurement of average matric suction. The procedure used is consistent with the methods followed in Vanapalli and Mohamed (2007) and Oh et al. 2009.

5. The load cell and displacement transducer were calibrated before conducting tests to collect reliable and reproducible data.
6. Different values of matric suction (i.e., 2 kPa, 4 kPa, 6 kPa and 8 kPa) were achieved by adjusting the water head following the suction profile method and confirmed by Tensiometers. The procedure followed is summarized in greater detail in section 3.9. The model footing was loaded to failure after reaching equilibrium conditions with respect to the pre-decided matric suction value. More details of how the equilibrium conditions were achieved are discussed in a later section of this chapter.
7. After completion of each test, the soil in the top layer was sliced into grid and re-compacted using 2 kg weight to achieve similar initial conditions as other tests. The tank was saturated again using the procedures described earlier. This procedure was used as sand fabric is not significantly influenced in comparison to fine-grained soils. This technique facilitated in conducting a large number of tests in the research program. Several trial tests were conducted by earlier investigators at the University of Ottawa Geotechnical laboratory using this procedure for sandy soils (Li 2008, Vanapalli et al. 2010). The tests were then conducted with a different value of matric suction. Sufficient care was taken to ensure identical initial conditions for all the tests conducted.

5.3 Bearing Capacity Test Programme

A total of 80 tests were conducted at a strain rate of 1.143 mm/min to study the bearing capacity and settlement behaviour of four sands using four different sizes of footings. The strain rate was kept constant for all the tests. This strain rate was chosen because earlier investigators used the same value for determining the bearing capacity and settlement behavior of coarse-grained unsaturated sands (Mohamed and Vanapalli 2006, Li 2008, Oh and Vanapalli 2008). The results of these studies also show reasonably good comparisons can be obtained between the measured and predicted bearing capacity and settlement values using this strain rate. The details of the various tests conducted for the present research program are summarized in Table 5.1.

Table 5.1 Summary of the various tests conducted at different matric suction values using different model footing sizes

Soil	Footing size	Matric suction (kPa)				
Filtration sand	20 mm × 20 mm	0	2	4	6	8
Quarry sand	37 mm × 37 mm	0	2	4	6	8
Sil-co-sil 106	Dia = 41.75 mm	0	2	4	6	8
Min-u-sil 30	50 mm × 50 mm	0	2	4	6	8

The compacted soil specimen in the container was first saturated by controlling the water head until the water table reaches the soil surface. The tests in saturated condition were conducted when the two Tensiometers indicated zero matric suction reading. The model footing was placed on the surface of the compacted soil specimen and loaded to failure.

As discussed in the earlier Chapter (see 3.9), the water table was lowered to various levels of depth to achieve different matric suction values after the soil specimen was fully saturated. The matric suction values in the soil container that were achieved by adjusting the water head were also confirmed using two Tensiometers readings placed at different depths. The value at the centroid of the matric suction distribution diagram from 0 to 1.5B depth region was used as the representative matric suction value for the analysis of the experimental results. The procedures used for testing were consistent with earlier studies conducted at the University of Ottawa (Mohamed and Vanapalli 2006; Vanapalli et al. 2007). Several earlier studies also discuss these procedures (Mohamed and Vanapalli 2006, Oh and Vanapalli 2008, Vanapalli 2009).

Various representative matric suction values within the stress bulb can be achieved by varying the depths of water table using the suction profile method. As summarized in Table 5.1, average matric suction values of 2 kPa, 4 kPa, 6 kPa and 8 kPa in the stress bulb zone (i.e., from 0 to 1.5B depth region) were achieved using the suction profile method. Equilibrium conditions with respect to matric suction values of 2 kPa, 4 kPa, 6 kPa and 8 kPa in the stress bulb zone (i.e., from 0 to 1.5B depth region) were typically

achieved in a time period of 24 hours. The model footing was loaded to failure after achieving equilibrium conditions with respect to each desired value of matric suction.

5.4 Results of Bearing Capacity and Settlement

5.4.1 Filtration sand

The measured dry unit weight of Filtration sand after compaction was equal to 16.21 kN/m^3. This value corresponds to 98.23% of the density index value. Figure 5.1 to 5.4 show the applied pressure versus settlement behavior from bearing capacity tests conducted on four different sizes of footings, respectively. The footing was loaded to a settlement value which is equal to 25% of the footing size.

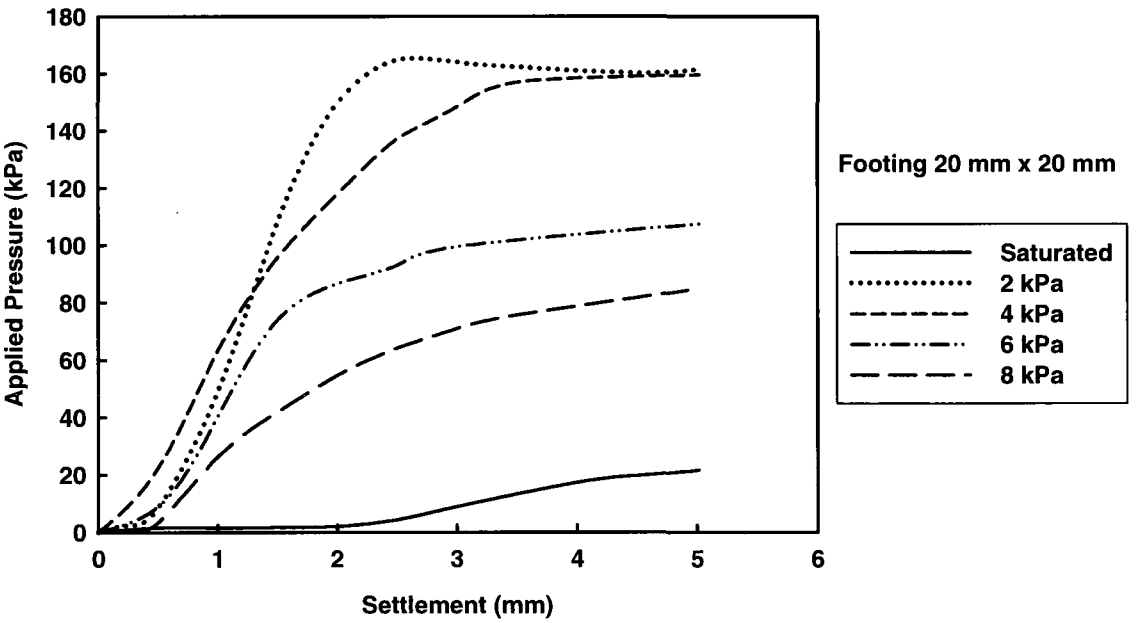

Figure 5.1 Applied pressure versus settlement of Filtration sand under the footing of 20 mm × 20 mm

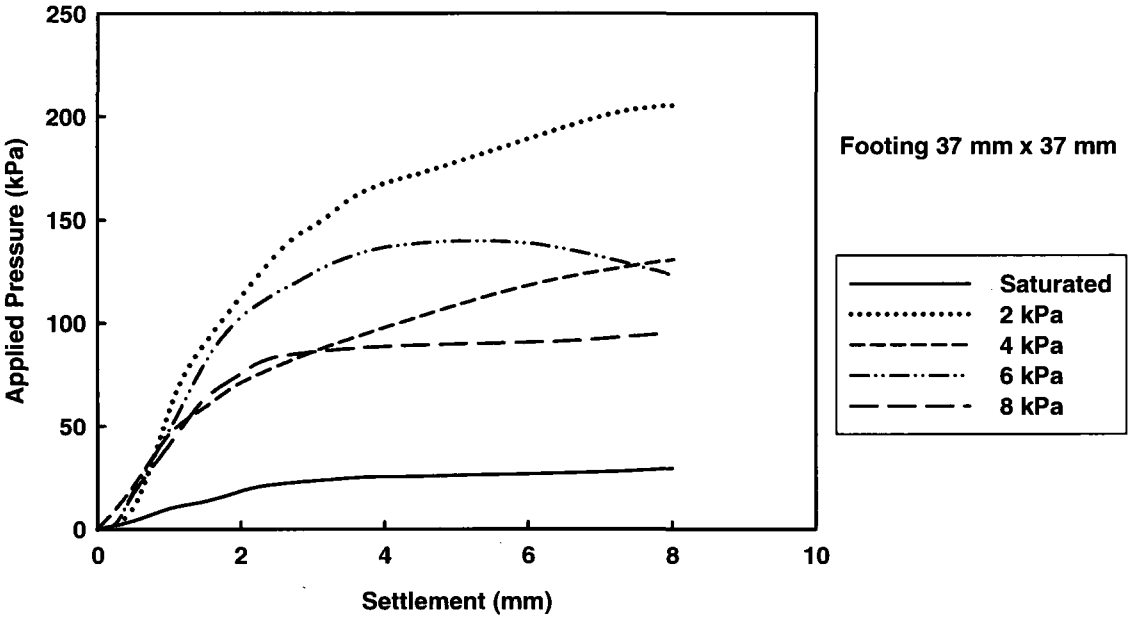

Figure 5.2 Applied pressure versus settlement of Filtration sand under the footing of 37 mm × 37 mm

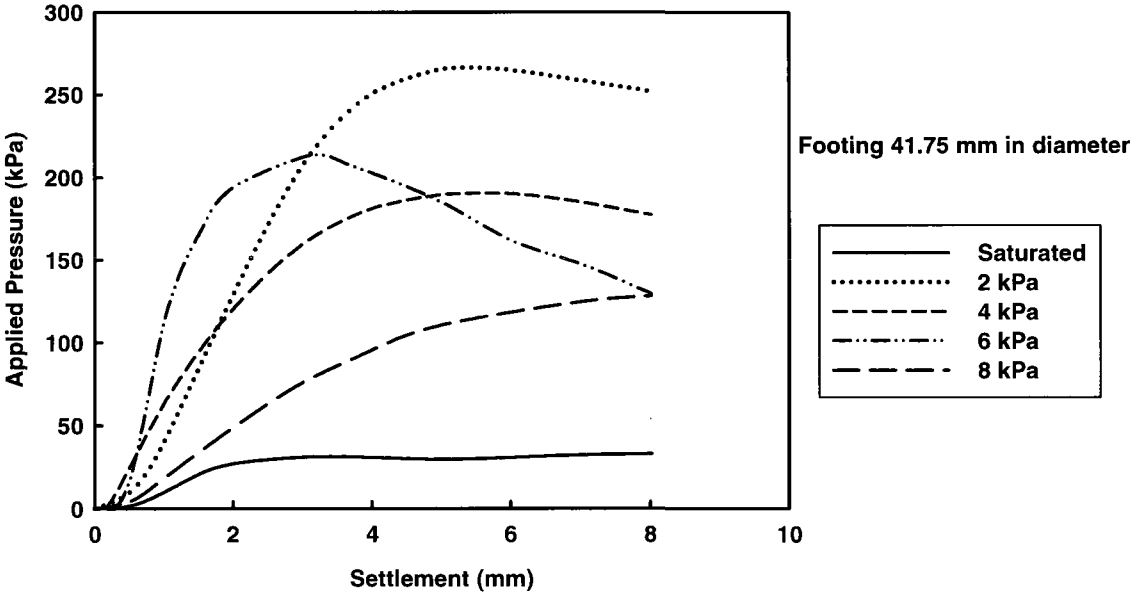

Figure 5.3 Applied pressure versus settlement of Filtration sand under the footing of 41.75 mm in diameter

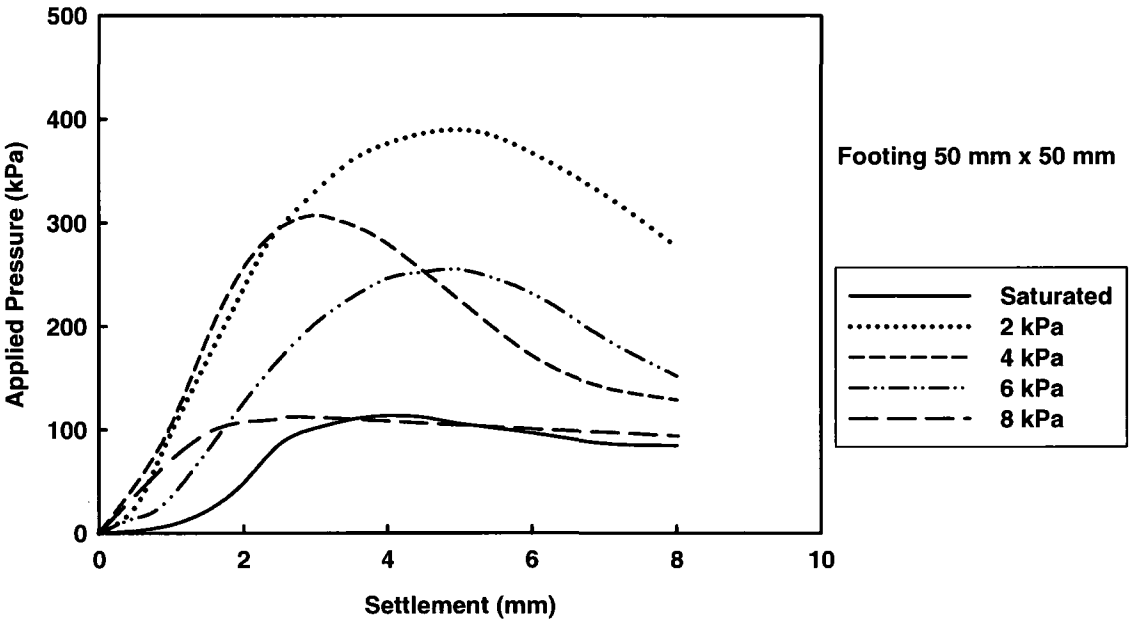

Figure 5.4 Applied pressure versus settlement of Filtration sand under the footing of 50 mm × 50 mm

From the test results (Figure 5.1 to 5.4), two different modes of failure, namely; general shear failure and local shear failure were observed. For instance, the footing 41.75 mm in diameter demonstrated two different failure modes for 2 kPa and 8 kPa matric suction values (Figure 5.5). General shear mode of failure was observed for 2 kPa matric suction and local shear mode of failure was observed for 8 kPa matric suction value (see Figure 5.6(c)).

The soil in an unsaturated condition with matric suction 2 kPa was effective in pulling the particles together and offering more resistance to the applied load and hence there is limited settlement with well defined failure load (Figure 5.7). In other words, the mode of the failure represents general shear failure conditions (see Fig. 5.5(a)). However, at 8 kPa matric suction value, most of the water drained from the sand (i.e., the degree of saturation is low at 15.05% and the specimen behavior was more like a dry sand) offering little resistance. Due to this reason, the load carrying capacity of the footing was relatively high at 2 kPa matric suction value in comparison to 8 kPa matric suction values (see Figure 5.6). More discussions are offered on this topic analyzing the results in later section of the Chapter.

(a) 2 kPa $S = 35.67\%$ (b) 8 kPa $S = 15.05\%$

Figure 5.5 Failure surface of Filtration sand under the footing of 41.75 mm in diameter

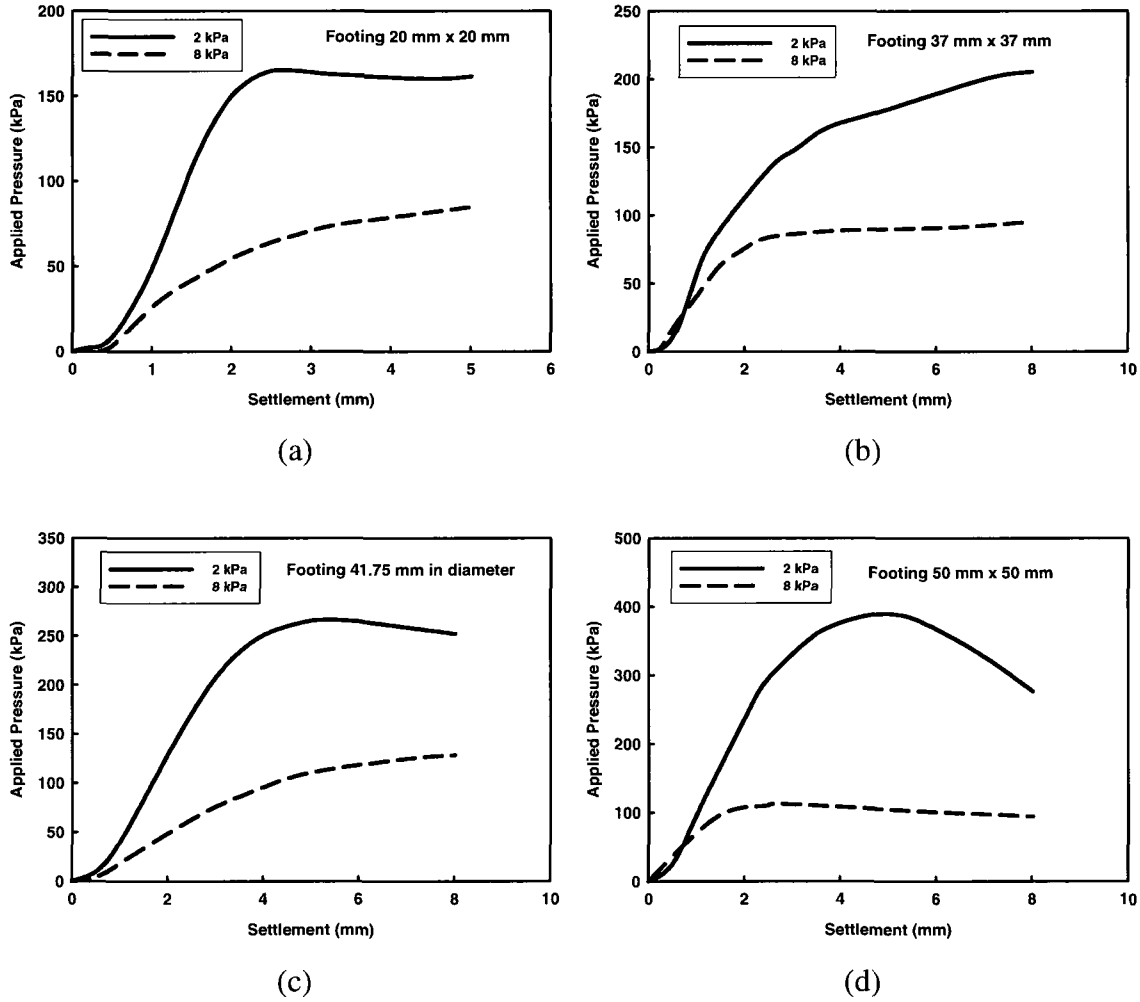

Figure 5.6 Applied pressure versus settlement of Filtration sand for 2 kPa and 8 kPa under four footings

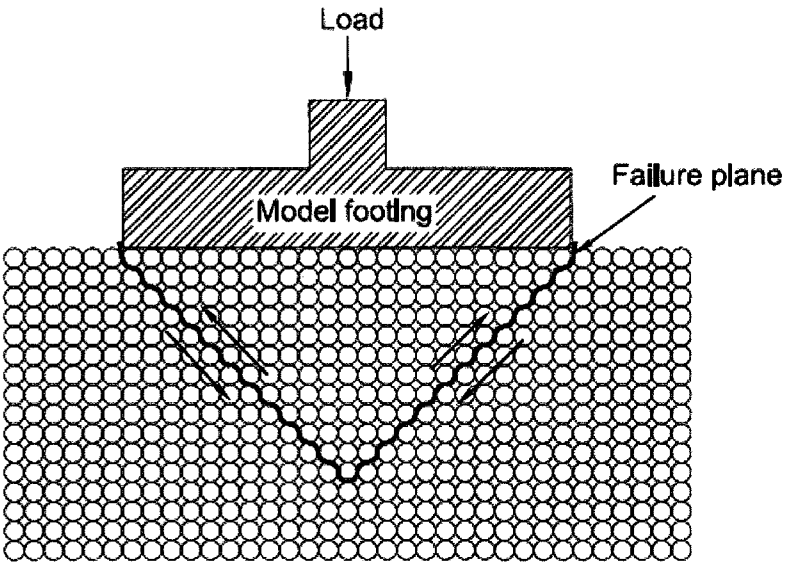

Figure 5.7 Well defined failure plane under model footing (Oh et al. 2009)

The difference in the failure mode (i.e., general shear or local shear) can also be attributed to the size of the model footing. When a footing size is relatively large (i.e., 50 mm × 50 mm) compared with the soil particle sizes, the general shear failure conditions are predominant because the soil matric suction offers more resistance. However, when a footing size is relatively small, the load applied on the model footing is mostly carried by the individual soil particles and there is significantly less contribution to the frictional resistance arising between the soil particles (Oh et al. 2009). In other words, at the same matric suction value the failure mode can be different depending on the size of the footing for the same soil.

Figure 5.8 shows the failure surfaces of different unsaturated conditions under the footing of 50 mm × 50 mm. The diameter of bulged zone was approximately 200 mm which is less than the diameter of the soil container (i.e., 300 mm) (Fig. 5.8(a)). This behaviour implies that there is no boundary effect influence on the model footing test results. These results are consistent with the numerical modeling studies (Figure 2.15) undertaken by Oh and Vanapalli (2008). Both the numerical modelling studies and the experimental

results show the bearing capacity of model footings of 50 mm width or lower can be conducted using relatively smaller size tanks such as 300 mm diameter.

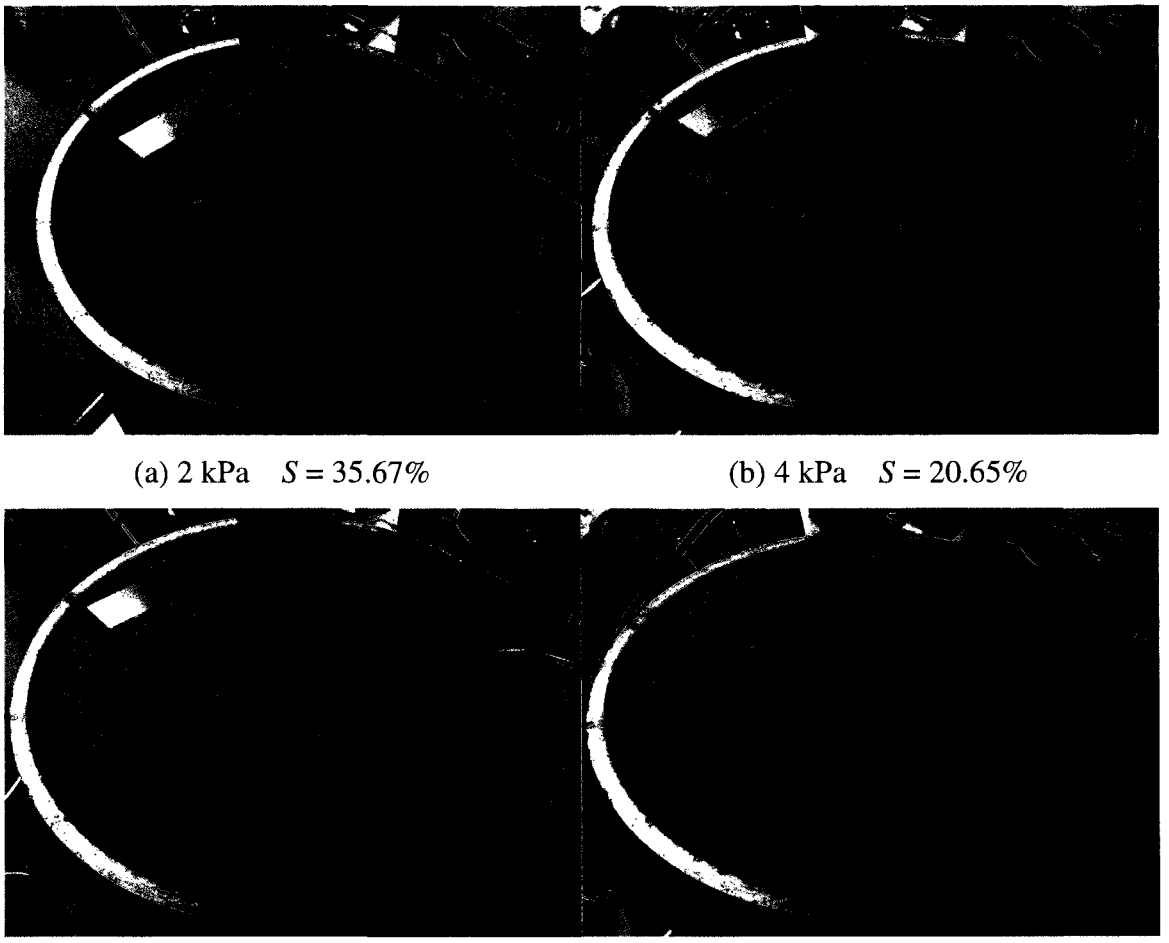

(a) 2 kPa $S = 35.67\%$ (b) 4 kPa $S = 20.65\%$

(c) 6 kPa $S = 17.9\%$ (d) 8 kPa $S = 15.05\%$

Figure 5.8 Failure surface of Filtration sand under the footing of 50 mm × 50 mm

The variation of bearing capacity and settlement behavior with respect to different matric suction values for four model footings are shown in Figure 5.9 along with the Soil-Water Characteristic Curve (SWCC). The results demonstrate that matric suction plays an important role in the contribution of increasing bearing capacity and reducing settlement in the boundary effect and transition zones. The settlements estimated for an applied stress of 20 kPa are used in this figure. This stress is chosen as settlement behavior is in elastic range for the applied stress of 20 kPa. Also, in many practical scenarios, typical stresses on the foundation are of the order of 20 kPa.

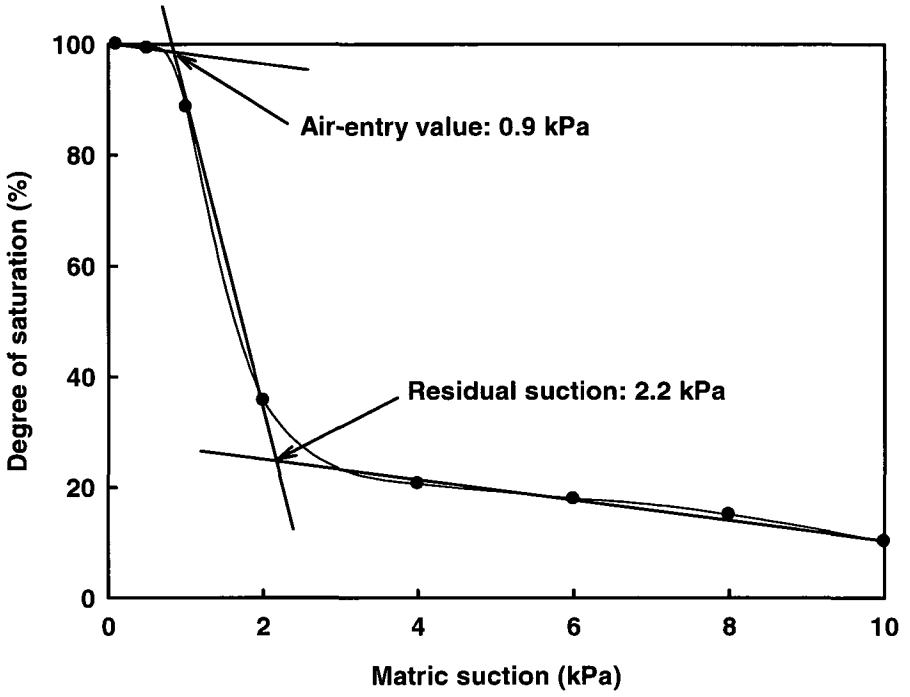
Air-entry value: 0.9 kPa
Residual suction: 2.2 kPa
Degree of saturation (%)
Matric suction (kPa)
100
80
60
40
20
0
0
2
4
6
8
10

(a)

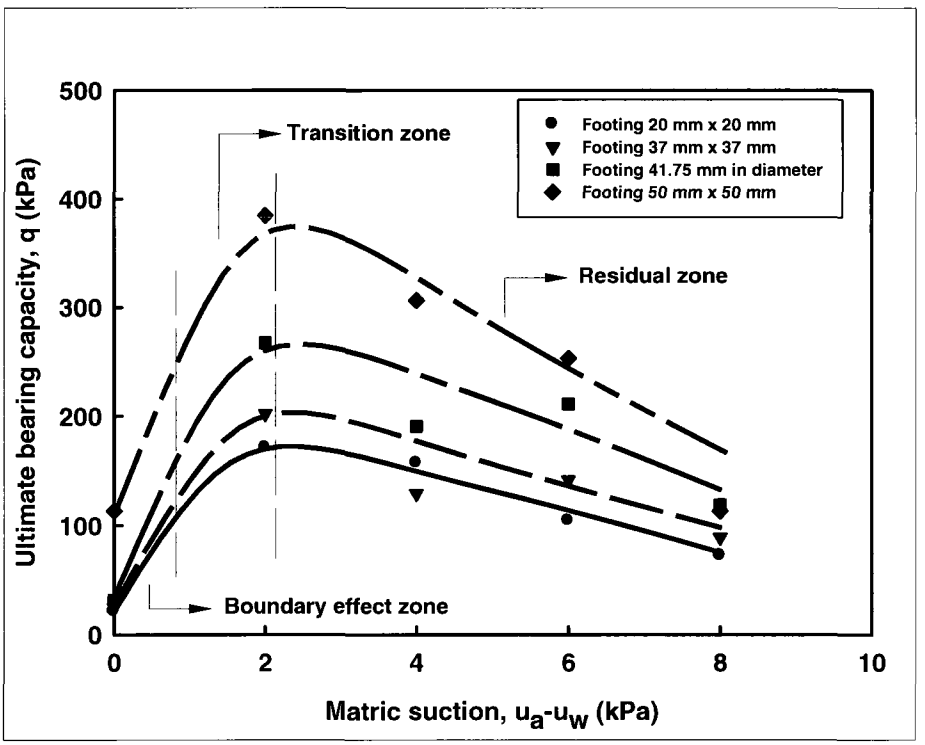
Transition zone
Residual zone
Boundary effect zone
Footing 20 mm x 20 mm
Footing 37 mm x 37 mm
Footing 41.75 mm in diameter
Footing 50 mm x 50 mm
Ultimate bearing capacity, q (kPa)
Matric suction, u_a-u_w (kPa)
500
400
300
200
100
0
0
2
4
6
8
10

(b)

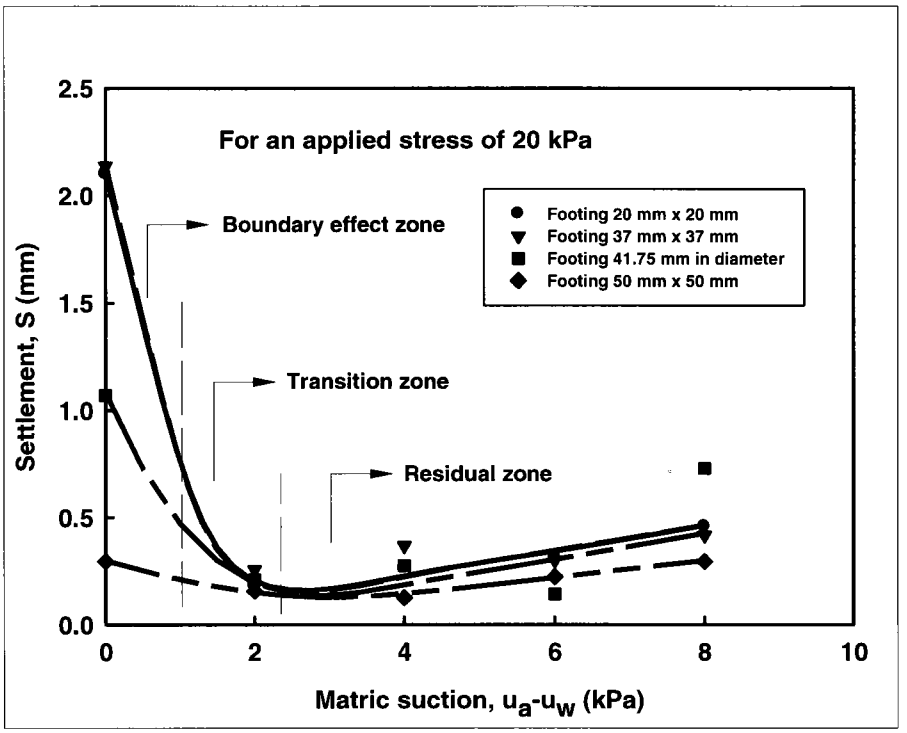

(c)

Figure 5.9 The variation of bearing capacity and settlement behavior with respect to matric suction for Filtration sand along with the SWCC

5.4.1.1 Bearing capacity

Figure 5.9(b) shows the bearing capacity increases up to residual suction value (i.e., 2.2 kPa) and then decreases with further increase in matric suction values for all the four model footings. There is a significant increase in the bearing capacity due to the contribution of matric suction in the boundary effect and transition zones. For the matric suction values higher than residual suction, the degree of saturation S becomes low and the contribution of matric suction towards bearing capacity (i.e. $(u_a - u_w)_{AVR}S^{\psi}$ in Equation [2.32]) is small and also the corresponding density, γ value decreases as water content reduces due to desaturation. Therefore, the bearing capacity decreases for higher matric suction values in the residual zone. Similar behavior was observed from the studies of Steensen-Bach et al. (1987), Vanapalli and Mohamed (2007), Li (2008) and Vanapalli et al. (2010).

$$q_{ult} = [c' + (u_a - u_w)_b (1 - S^{\psi}) \tan \phi' + (u_a - u_w)_{AVR} S^{\psi} \tan \phi'] \times N_c \xi_c + 0.5 B \gamma N_\gamma \xi_\gamma \quad [2.32]$$

The bearing capacity value also increases with an increase in the footing size under various matric suction values. For example, the size of footing 50 mm × 50 mm is 2.5 times larger than footing 20 mm × 20 mm, and the ultimate bearing capacity of footing 50 mm × 50 mm is approximately around two times greater than footing 20 mm × 20 mm. It is of interest to note that the bearing capacity of the circular footing (i.e. 41.75 mm in diameter) was higher than the equivalent square footing (37 mm × 37 mm) by a mean value of 1.38 times (Figure 5.8(b)). Such a behavior can be attributed to the B value in Equation [2.32], which is the width or diameter of the footing. As the values of shape factors ξ_c and ξ_γ are the same for square or circular footings, the increase in the bearing capacity of a circular footing can be attributed to its larger B value in comparison to the square footings. Gourvenec et al. (2006) showed that the bearing capacity of a circular footing is more than that of an equivalent square footing by 3% based on the finite element analysis (FEA) studies.

5.4.1.2 Settlement behavior

Table 5.2 summarizes the moduli of elasticity values derived from the experimental results. The modulus of elasticity values increase with an increase in matric suction value in the boundary effect and transition zones. Due to this reason, elastic settlements of four model footings are relatively low up to residual suction value (Figure 5.9(c)). However, the settlements increase when the matric suction values are higher as there is a gradual decrease in the modulus of elasticity value in this zone (i.e. residual zone). After residual suction, the degree of saturation S becomes low and the contribution of matric suction towards modulus of elasticity (i.e., $\frac{(u_a - u_w)}{(P_a/100)}(S^{\beta})$ in Equation [2.37]) is small. Therefore, modulus of elasticity decreases and thus settlement increases after residual suction.

$$E_{unsat} = E_{sat}\left[1 + \alpha \frac{(u_a - u_w)}{(P_a/100)}(S^{\beta})\right] \quad [2.37]$$

$$E = \frac{1-\nu^2}{\Delta\delta / \Delta q_p} B_p I_w \qquad [2.24]$$

Table 5.2 Moduli of elasticity under four model footings of Filtration sand

Matric suction (kPa)	Footing size (mm)			
	20 x 20	37 x 37	D = 41.75	50 x 50
0	152	277	561	2706
2	1759	2301	2871	5128
4	1218	1609	2182	6349
6	1009	1980	4209	3578
8	700	1423	823	2720

Figure 5.9(c) shows that the footings (i.e., 20 mm x 20 mm and 37 mm x 37 mm) approximately have the same elastic settlements under various matric suction values because the sizes of both model footings are relatively close to each other and also they are smaller size footings. The settlement in a larger size model footing (i.e., 50 mm x 50 mm) is lower than the settlement in a smaller size footing (i.e., 20 mm x 20 mm). Such a behavior can be attributed to higher value of modulus to elasticity for larger size footings in comparison to smaller size footings. Equation [2.24] can be used as a tool to explain this behavior. These results demonstrate that even low values of matric suction can significantly increase the modulus of elasticity of coarse-grained soils.

5.4.1.3 Comparisons between the measured and predicted bearing capacity values and elastic settlements

Figure 5.10 shows the comparisons between the measured and predicted bearing capacity values and elastic settlements for the model footing of 37 mm x 37 mm using Equations [2.32], [2.37] and [2.24]. The local shear failure criterion was used in the prediction of the bearing capacity. A value of $\tan\phi^* = 2/3\tan\phi'$ was used to determine the modified internal friction angle. For the calculation of settlement, Poisson's ratio, ν value equal to 0.3 was used in the study, assuming drained loading conditions for the tested soils. The

fitting parameters ψ, β and α were equal to 1, 1 and 2.5 respectively based on the criteria discussed in Oh et al. 2009.

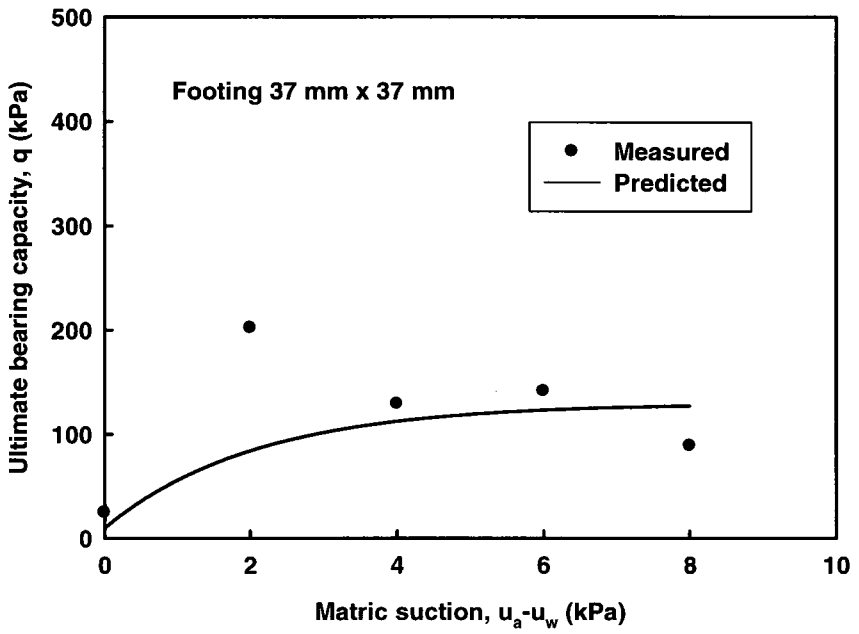

(a)

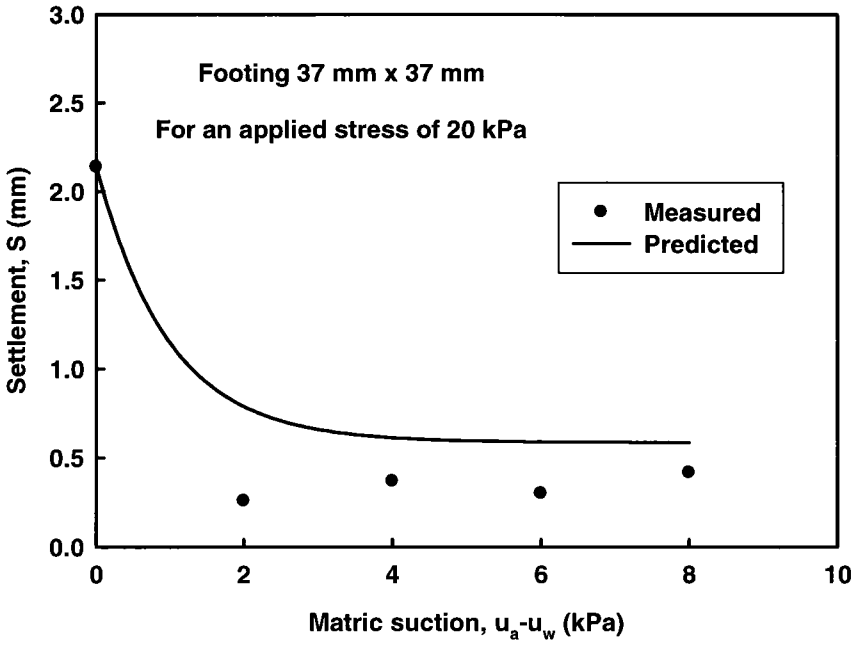

(b)

Figure 5.10 Comparisons of measured and predicted bearing capacity, and settlement of Filtration sand

There is reasonably good agreement between the measured and predicted bearing capacity values and settlements. The measured bearing capacity value for 2 kPa is higher than the predicted value. No attempts are made to explain this behavior as it was unexpected result; however, all the remained of the experiments were conducted carefully. The measured settlements are slightly lower than the predicted ones; however, the difference is less than 0.5 mm. If a smaller value of α (i.e., 2, 1.5, 1 or 0.5) was used, according to Equations [2.37] and [2.24], the modulus of elasticity would be smaller and the elastic settlement would be larger. In other words, the results would show more conservative estimates (Figure 5.11).

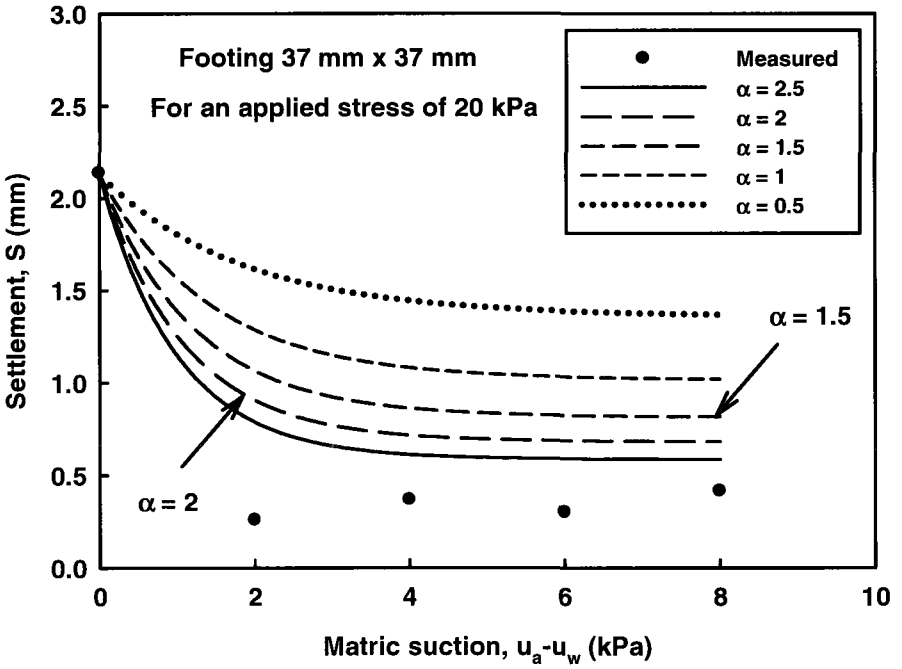

Figure 5.11 Variation of settlement with the parameter, α, for the footing 37 mm × 37 mm in Filtration sand

5.4.2 Quarry sand

The bearing capacity and settlement behavior of Quarry sand was determined at dry unit weight of 16.28 kN/m^3. The relative density index, D_r value should be approximately 70% for a surface footing to fail under general shear failure mode (Vesić, 1973). The relative density index, D_r value for Quarry sand corresponds to 77.58% which should

translate to achieving general shear failure conditions. However, such a behavior was not observed from Quarry sand. This may in part be attributed to the presence of fines (4% of silt). Figure 5.12 to Figure 5.15 show the applied pressure versus settlement obtained from bearing capacity tests under four different sizes of footings, respectively. More defined failure characteristics were observed for the larger size model footings which were explained in the earlier section.

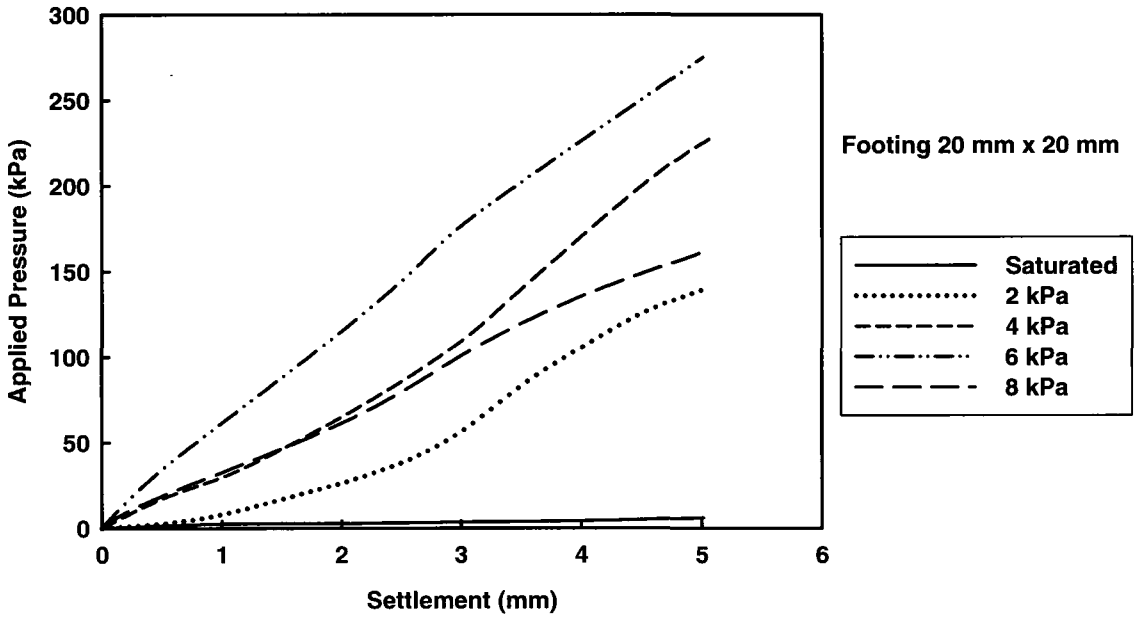

Figure 5.12 Applied pressure versus settlement of Quarry sand under the footing of 20 mm x 20 mm

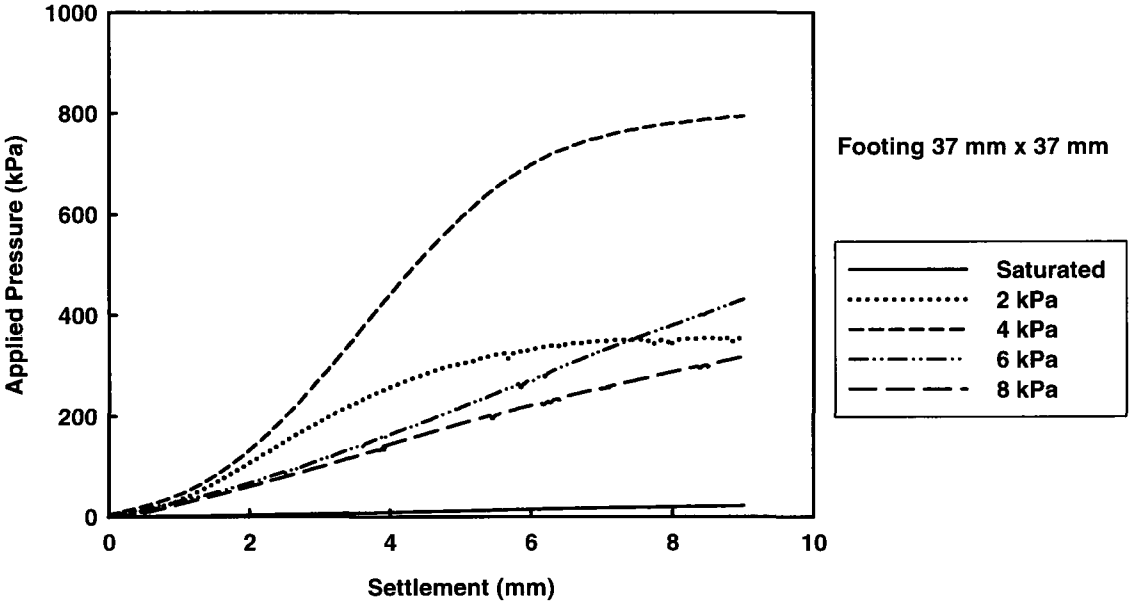

Figure 5.13 Applied pressure versus settlement of Quarry sand under the footing of 37 mm × 37 mm

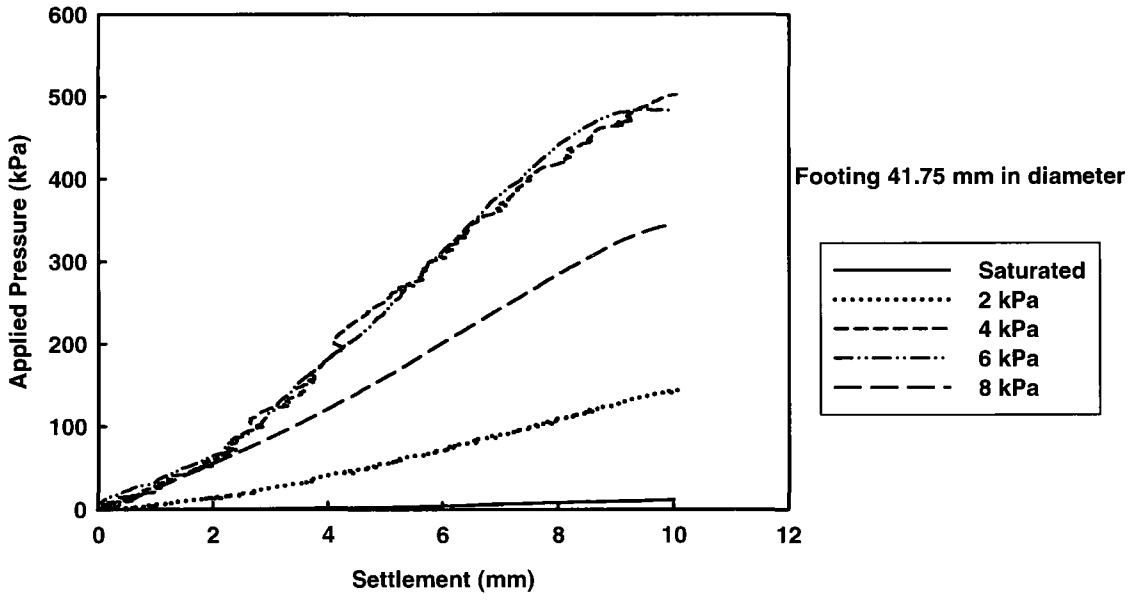

Figure 5.14 Applied pressure versus settlement of Quarry sand under the footing of 41.75 mm in diameter

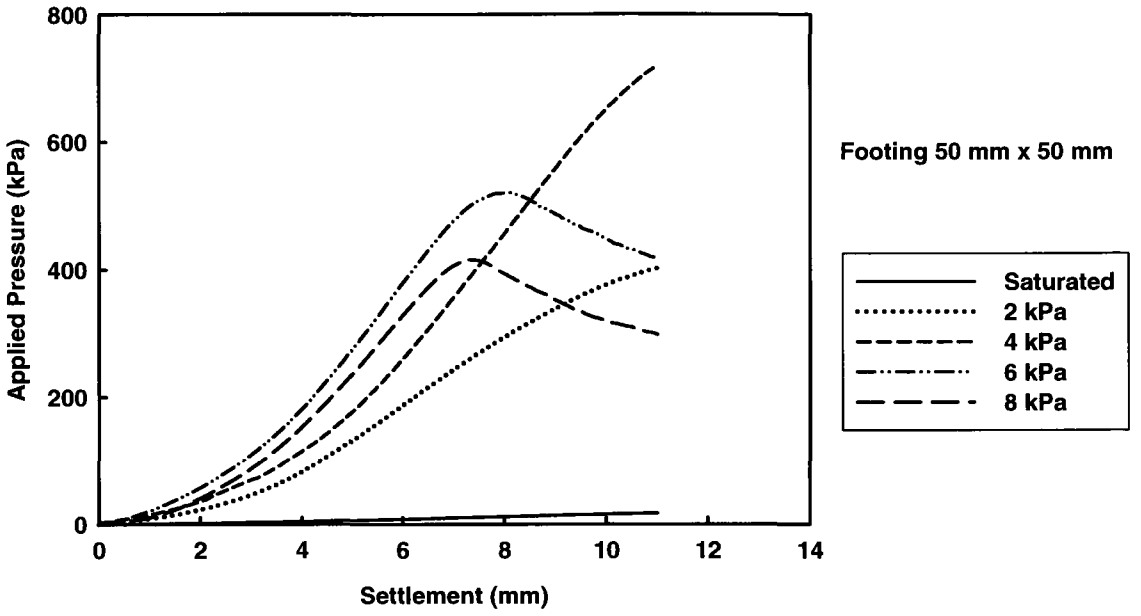

Figure 5.15 Applied pressure versus settlement of Quarry sand under the footing of 50 mm × 50 mm

The mode of failure is close to punching shear failure conditions from the test results. The ultimate bearing capacity was therefore assumed to be a value equal to 20% of the footing size in the present research according to ASTM D1194-94. Figure 5.16 shows the failure surfaces of footing 41.75 mm in diameter under different matric suction values. For the condition of 2 kPa (Figure 5.16(a)), the failure surface did not extend up to the soil surface, while for the conditions (i.e., 4 kPa, 6 kPa and 8 kPa), the failure surface extended up to the soil surface. However, there was no visible bulging on the soil surface.

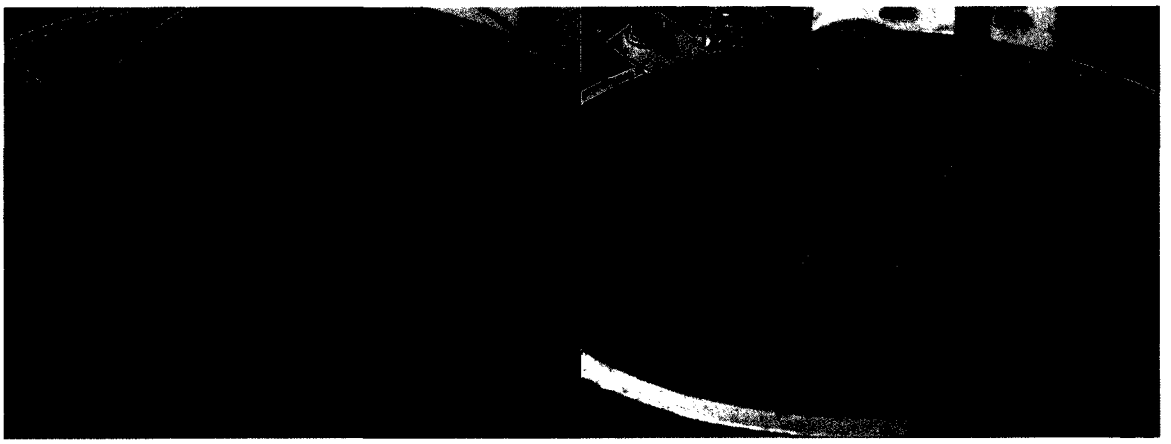

(a) 2 kPa $S = 99.60\%$ (b) 4 kPa $S = 84.04\%$

(c) 6 kPa $S = 59.52\%$ (d) 8 kPa $S = 39.35\%$

Figure 5.16 Failure surface of Quarry sand under the footing of 41.75 mm in diameter

Figure 5.17 shows the variation of bearing capacity and settlement behaviour with respect to different matric suction values for three model footings (i.e., footing 20 mm × 20, footing 41.75 mm in diameter and footing 50 mm × 50 mm) along with the SWCC. Unreasonable results were obtained using footing 37 mm × 37 mm; these results may be attributed to errors in the collection of data. Therefore, the results of 37 mm × 37 mm were not shown.

For discussing the settlement behavior, measured elastic settlements at an applied stress of 40 kPa were used. This stress is chosen as settlement behaviour is in elastic range for the applied stress of 40 kPa.

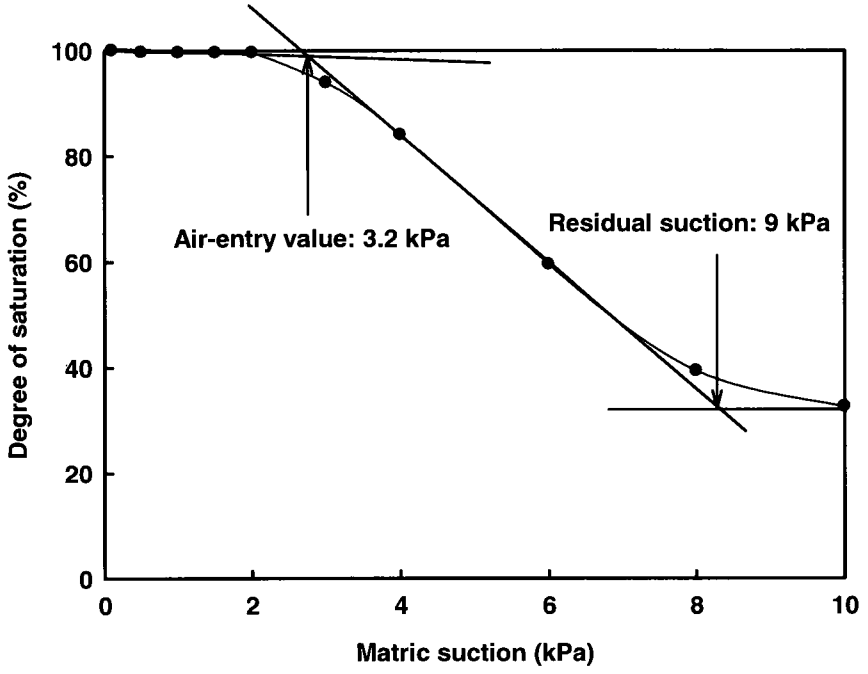
Degree of saturation (%)
100
80
60
40
20
0
0
2
4
6
8
10
Matric suction (kPa)
Air-entry value: 3.2 kPa
Residual suction: 9 kPa

(a)

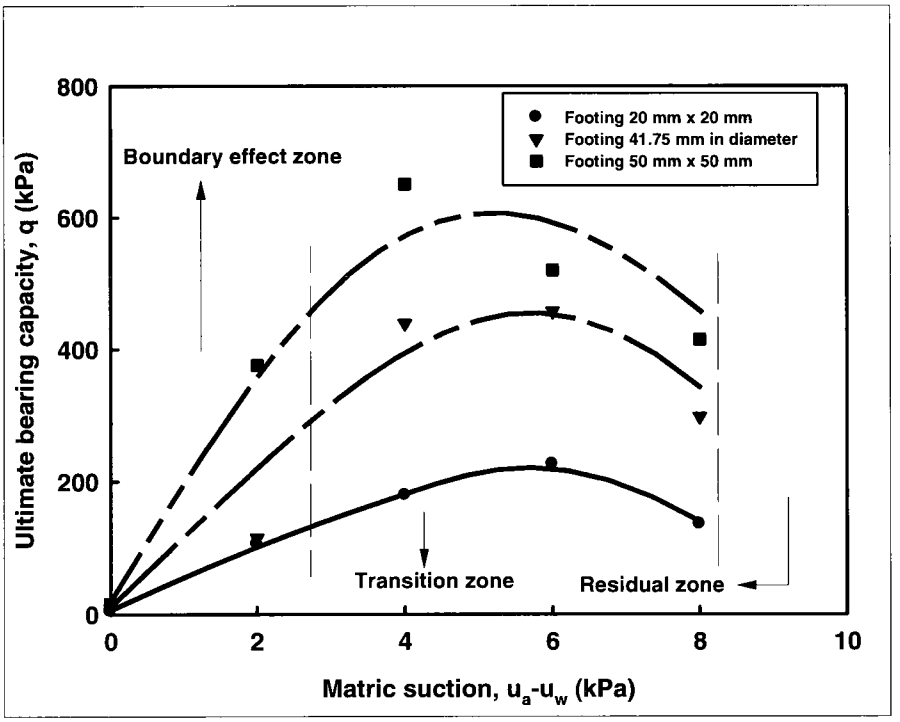
Ultimate bearing capacity, q (kPa)
800
600
400
200
0
0
2
4
6
8
10
Matric suction, u_a-u_w (kPa)
Footing 20 mm x 20 mm
Footing 41.75 mm in diameter
Footing 50 mm x 50 mm
Boundary effect zone
Transition zone
Residual zone

(b)

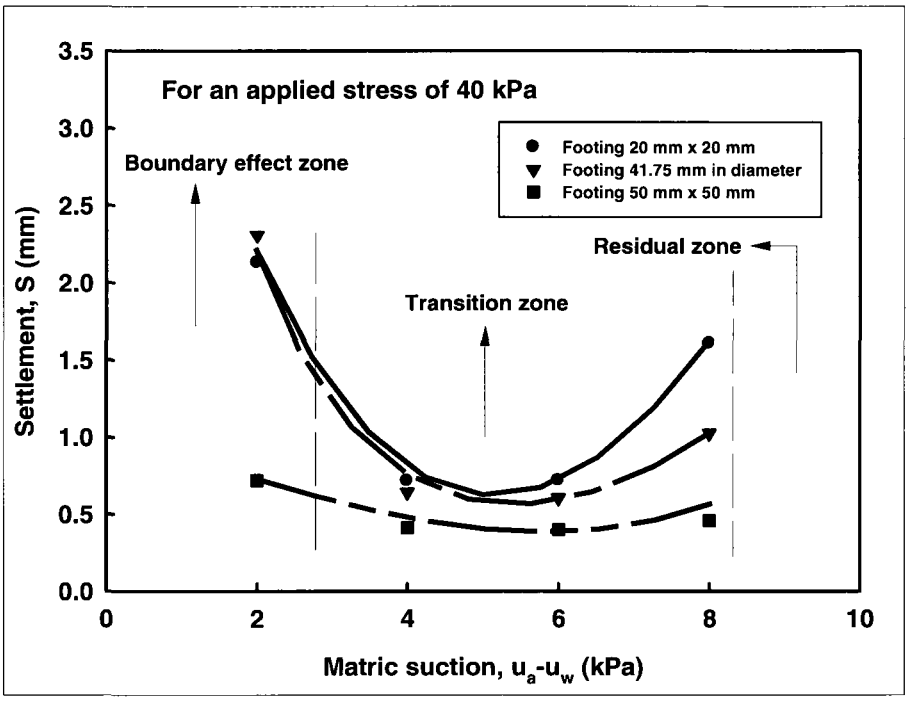

(c)

Figure 5.17 The variation of bearing capacity and settlement behavior with respect to matric suction for Quarry sand along with the SWCC

5.4.2.1 Bearing capacity

Figure 5.17(b) shows the bearing capacity increases as matric suction increases in the boundary effect zone. In the transition zone, the bearing capacity increases first in the lower matric suction region and then decreases with further increase in matric suction. For the matric suction values higher than air-entry value (i.e., 3.2 kPa), the degree of saturation S reduces dramatically and the contribution of matric suction towards bearing capacity (i.e. $(u_a - u_w)_{AVR}S^{\psi}$ in Equation [2.32]) significantly decreases and also the corresponding density, γ value decreases as water content reduces due to desaturation. Therefore, the bearing capacity increases nonlinearly until a certain value of matric suction when $(u_a - u_w)_{AVR}S^{\psi}$ and γ become relatively small.

$$q_{ult} = [c' + (u_a - u_w)_b(1 - S^{\psi})\tan\phi' + (u_a - u_w)_{AVR}S^{\psi}\tan\phi'] \times N_c\xi_c + 0.5B\gamma N_\gamma\xi_\gamma \qquad [2.32]$$

However, there were experimental limitations with respect to the measurement of matric suction. The matric suction value on the soil surface was sensitive to the surrounding environment and was having a significant influence on the calculation of the matric suction value (i.e. $(u_a - u_w)_{AVR}$) as the waiting period increased. In some experiments, the actual representative matric suction value might be higher than the measured value.

The bearing capacity of a larger footing is higher than the bearing capacity of a smaller size footing at any given matric suction value (Fig. 5.17(b)). Reasons associated with this behavior were discussed in an earlier section.

5.4.2.2 Settlement behavior

Figure 5.17(c) shows the elastic settlement decreases with an increase in modulus of elasticity as matric suction increases in the boundary effect zone. In the transition zone, decreasing trend of elastic settlement can be observed in the lower matric suction region. However, the elastic settlement gradually starts increasing as the matric suction approaches the residual zone which is attributed to the gradual decrease of modulus of elasticity. Because the degree of saturation S becomes low and the contribution of matric suction towards modulus of elasticity (i.e. $\frac{(u_a - u_w)}{(P_a/100)}(S^\beta)$ in Equation [2.37]) is small.

Table 5.3 shows the moduli of elasticity under three model footings. Similar trends in behaviour were also reported by Oh et al. (2009) (see Figure 2.25). Besides, the result (Fig. 5.17(c)) also shows that larger footing can reduce more settlement under various matric suction values.

$$E_{unsat} = E_{sat}\left[1+\alpha\frac{(u_a - u_w)}{(P_a/100)}(S^\beta)\right] \quad [2.37]$$

$$E = \frac{1-\nu^2}{\Delta\delta/\Delta q_p} B_p I_w \quad [2.24]$$

Table 5.3 Moduli of elasticity under four model footings of Quarry sand

Matric suction (kPa)	Footing size (mm)		
	20 x 20	D = 41.75	50 x 50
2	301	520	2230
4	895	1870	3879
6	892	1986	4019
8	399	1172	3498

5.4.2.3 Comparisons between the measured and predicted bearing capacity values and elastic settlements

Figure 5.18 shows the comparisons between the measured and predicted bearing capacity values and elastic settlements for the model footing of 41.75 mm in diameter using Equations [2.32], [2.37] and [2.24]. The parameters are the same as Filtration sand (i.e., $\tan\phi^* = 2/3\tan\phi'$, $\nu = 0.3$, $\psi = 1$, $\beta = 1$ and $\alpha = 2.5$).

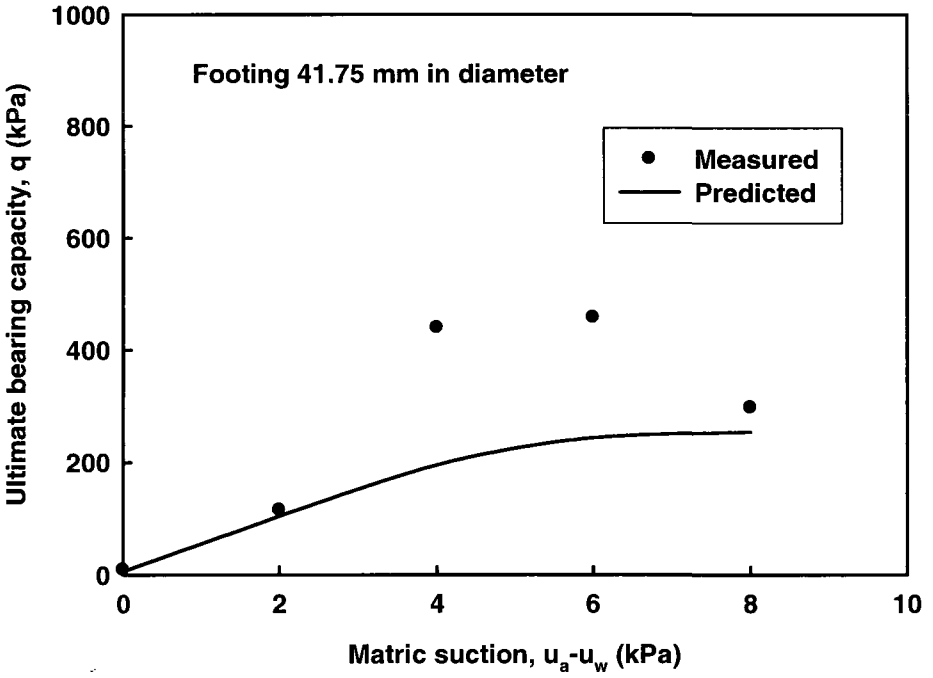

(a)

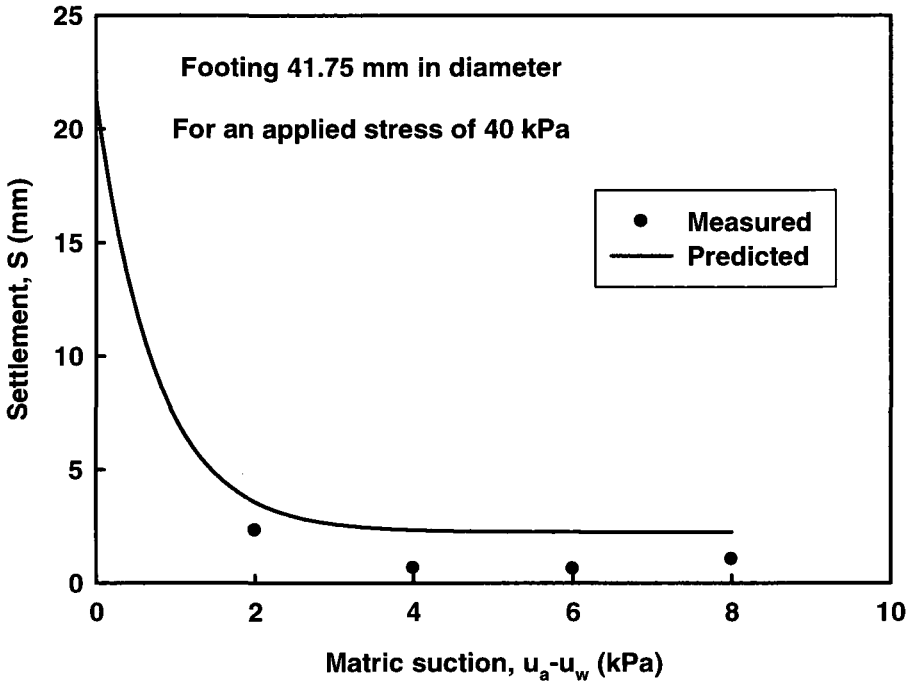

(b)

Figure 5.18 Comparisons of measured and predicted bearing capacity, and settlement of Quarry sand

There is also reasonable agreement between the measured and predicted bearing capacity values and settlements. Several of the salient features for Filtration sand discussed in the earlier sections can also be observed for Quarry sand. However, there were some discrepancies between the measured and predicted values which may be attributed to the different modes of failure.

The measured bearing capacity values are higher than the predicted values and the measured settlements are slightly lower than the predicted ones. Such a behavior is conservative; however, more investigations are required on different types of sands to fully characterize the behavior.

Different values of parameter α (i.e., 2, 1.5, 1 or 0.5) were used to understand the sensitivity with respect to settlement. Figure 5.19 summarizes these results. If a smaller value of α (i.e., 2, 1.5, 1 or 0.5) was used, according to Equations [2.37] and [2.24], the

modulus of elasticity would be smaller and the elastic settlement would be larger. In other words, the results would show more conservative estimates.

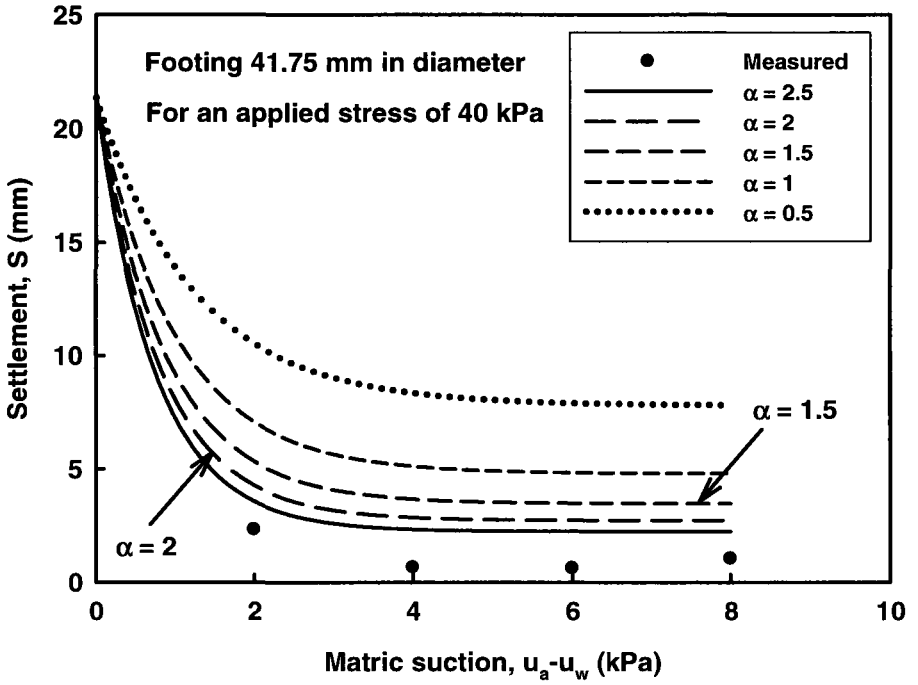

Figure 5.19 Variation of settlement with the parameter, α, for the footing 41.75 mm in diameter in Quarry sand

5.4.3 Sil-co-sil 106

The Sil-co-sil 106 used in the present research is manufactured from quartz that has a high percentage of silt sizes content (92.8%). Several studies have shown that this soil is highly sensitive to water content changes (Fall et al. 2004, Nasir and Fall 2009). This soil is stable at low water contents and offer high resistance to static loads. However, it is unstable under impact or dynamic loading conditions. Once collapse initiates in some pockets of the silt size particle aggregations with high degree of saturation and low suction, water gradually squeezes out and carries soil along with it under impact of vibration (Li 2008).

This soil is studied in this research program because of its wide applications in mining industry. It is chosen as a candidate material to understand the bearing capacity and

settlement behavior and to check whether semi-empirical equations proposed for unsaturated soils can be extended for this soil.

The experimental procedures described for determining the variation of bearing capacity and settlement behavior of model footings in earlier sections were used for the Sil-co-sil 106. Typical punching shear failure conditions were observed when the model footings were loaded in this soil.

After the completion of each test, the soil container was subjected to vibration (i.e., using a rubber hammer and knocking on the side of bearing capacity tank container). It was interesting to note that even under the impact of low intensity rubber hammer knock; a smooth surface was achieved due to the movement of soil and water. In other words, the density and water content conditions were similar to initial conditions prior to conducting the test. Several precautions were taken to check that identical initial testing conditions prevail prior to conducting the next series of bearing capacity tests. This was ascertained by checking the dry unit weight of Sil-co-sil 106, which was equal to 15.05 kN/m^3.

Figure 5.20 to Figure 5.23 show the applied pressure versus settlement obtained from bearing capacity tests under four different sizes of footings, respectively. The footing was loaded to a settlement value which is equal to 30% of the footing size.

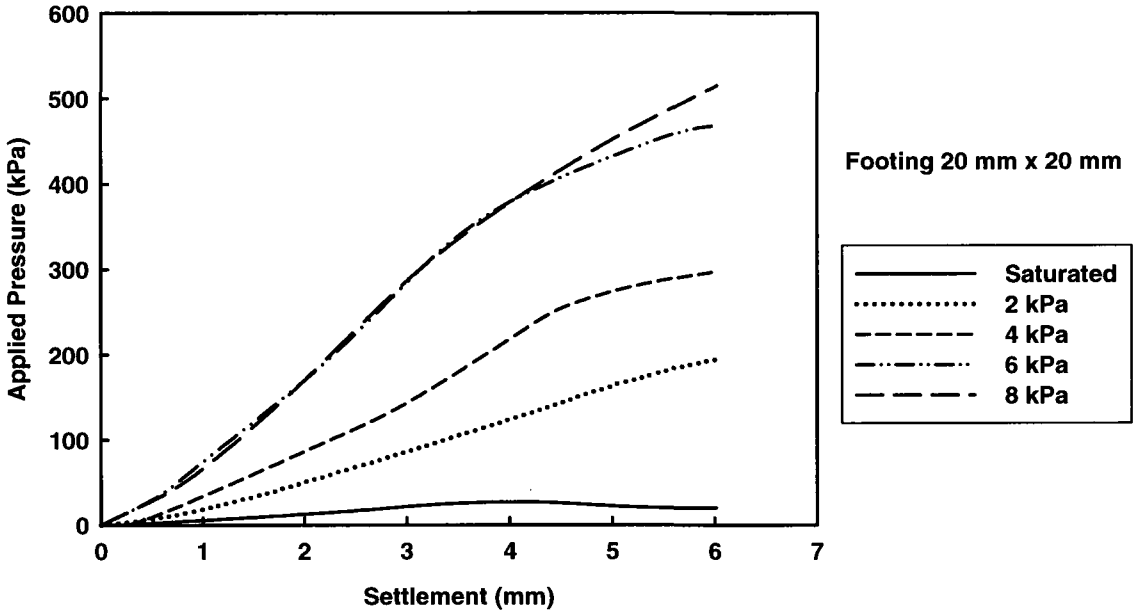

Figure 5.20 Applied pressure versus settlement of Sil-co-sil 106 under the footing of 20 mm × 20 mm

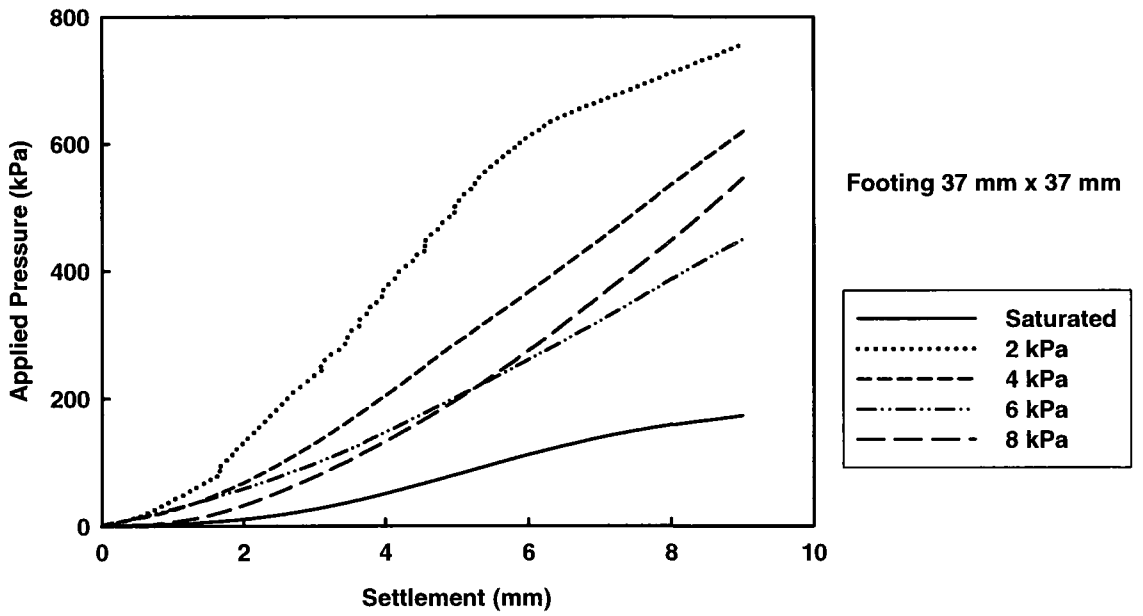

Figure 5.21 Applied pressure versus settlement of Sil-co-sil 106 under the footing of 37 mm × 37 mm

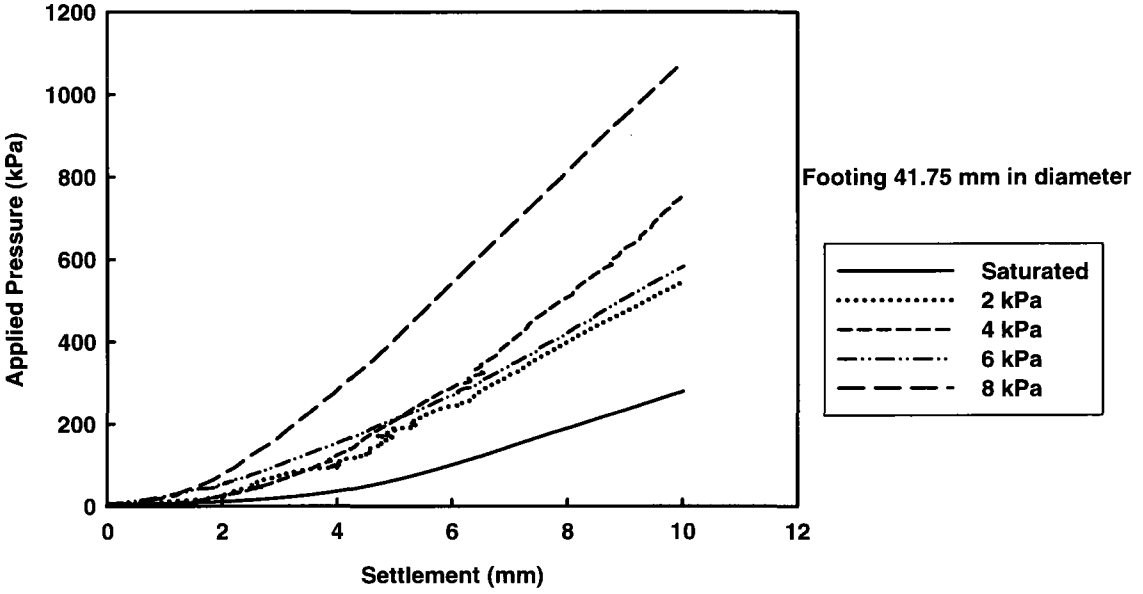

Figure 5.22 Applied pressure versus settlement of Sil-co-sil 106 under the footing of 41.75 mm in diameter

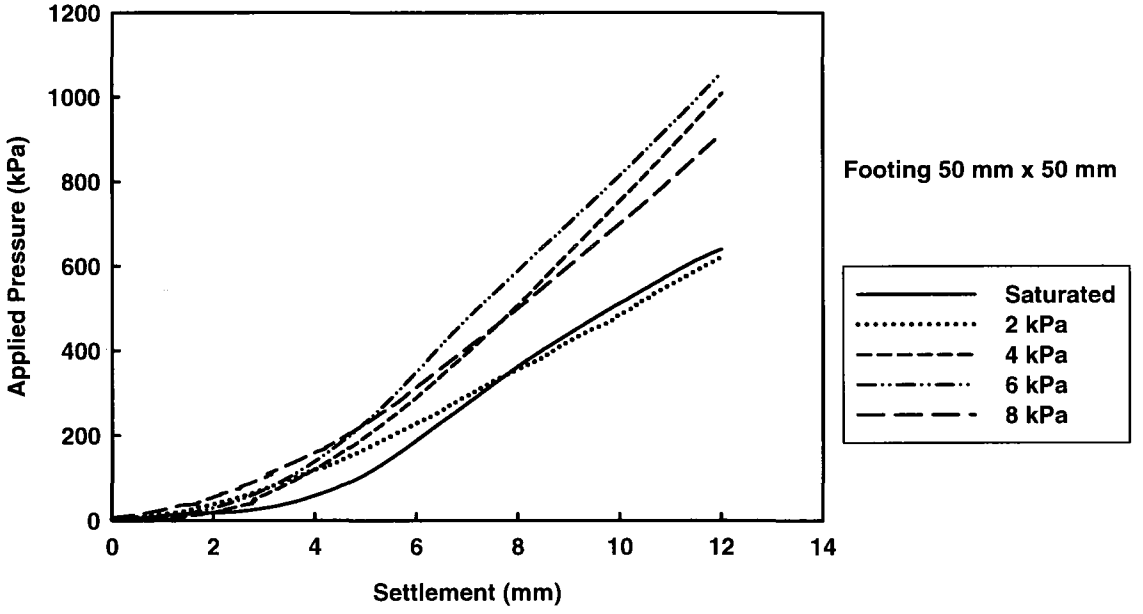

Figure 5.23 Applied pressure versus settlement of Sil-co-sil 106 under the footing of 50 mm × 50 mm

The results from Figure 5.20 to 5.23 demonstrate that the applied pressure increases with an increase in the settlement. No defined peak failure conditions were observed for most

of the results as the resistance to the applied static load was increasing with settlement. In other words, the nature of this soil is stiff under static loading conditions.

Figure 5.24 shows the soil surfaces after test under the condition of 2 kPa (i.e., the degree of saturation is 99.83%) for the four footings. Typical punching shear behaviour was observed from all the different footings. Due to this reason, the ultimate bearing capacity was defined when the settlement reached 20% of the footing size according to ASTM D1194-94.

(a) Footing 20 mm × 20 mm (b) Footing 37 mm × 37 mm

(c) Footing 41.75 mm in diameter (d) Footing 50 mm × 50 mm

Figure 5.24 Surface of Sil-co-sil 106 after test under the condition of 2 kPa for different footings

The variation of bearing capacity and settlement with respect to different matric suction values for four model footings are shown in Figure 5.25 and Figure 5.26, respectively.

For the measured values of elastic settlement, an applied stress of 80 kPa was used. This stress is chosen as settlement behavior was still in the elastic range for the applied stress of 80 kPa.

5.4.3.1 Bearing capacity

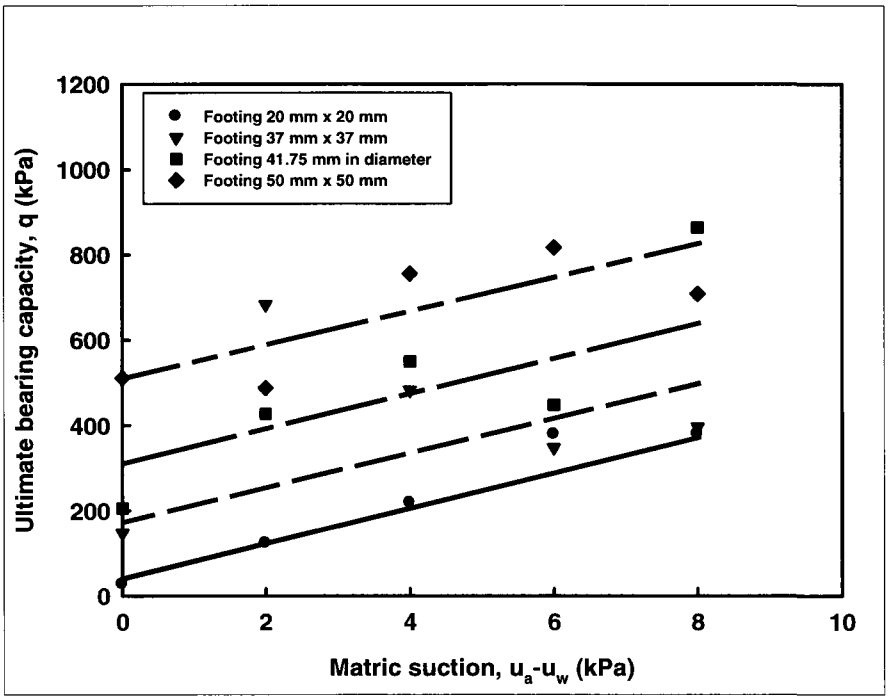

Figure 5.25 Relationship of bearing capacity versus matric suction of Sil-co-sil 106

The results demonstrate that Sil-co-sil 106 can carry high static load compared to the other two sands discussed earlier. Such a behavior can be attributed to temporary cementation that develops at the interparticle contact of the silt size fraction (Lee et al. 2007). The soil behaves more like a composite material rather than particulate material and contributes to the bearing capacity and offers resistance to the settlement. In addition to the contribution of cementation, the bearing capacity also increases due to the contribution of matric suction (Fig. 5.25). The matric suction range (i.e., 0 to 8 kPa) tested is lower than the air-entry value of the Sil-co-sil 106 which is 30 kPa. In other words, the matric suction range (i.e., 0 to 8 kPa) is still in the boundary effect zone and the increase in bearing capacity is linear.

The bearing capacity of the model footings also increases with an increase in the footing size under various matric suction values. The circular footing of 41.75 mm in diameter has higher bearing capacity than the equivalent square footing of 37 mm × 37 mm. The reasons associated with this behavior have been explained in an earlier section.

Some scatter in the data (i.e., 2 kPa under the footing of 37 mm × 37 mm, 6 kPa and 8 kPa under the footing of 41.75 mm in diameter) can be attributed to the measured matric suction readings in stress bulb by Tensiometers. The matric suction readings were sensitive and were changing during the test. These results clearly demonstrate that the stress state (i.e., matric suction is changing) without any change in water content. The change in matric suction may be attributed to the temporary cementation forces that are developing at the interparticle contact points. Such a behavior may also be attributed to non-uniform water contents within the soil. More studies are necessary to study the soil structural changes and also the micro fissures and cracks that may have developed and contributed to the non-uniform water contents to provide more rigorous and valid justifications.

5.4.3.2 Settlement behavior

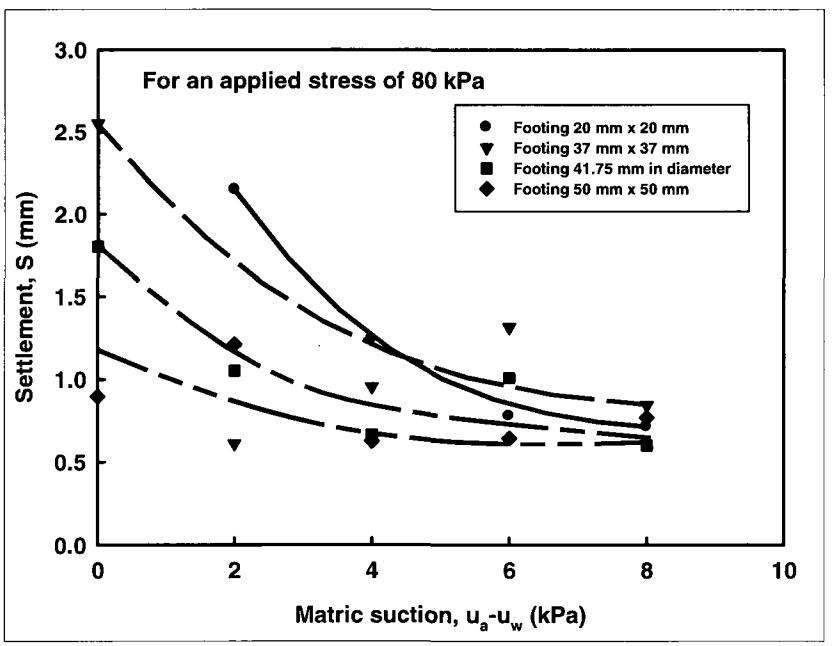

Figure 5.26 Relationship of settlement versus matric suction of Sil-co-sil 106

The trends of the results in Figure 5.26 show that the elastic settlement decreases with an increase in the modulus of elasticity due to the contribution of matric suction. The erratic results may be attributed to the non-uniform properties of the soil and changing matric suction values during the test. However, the results are consistent with general trends observed in the settlement behavior of footings; larger size footing settlements are lower than a smaller size footing. More details with respect to this behavior were discussed in an earlier section.

5.4.4 Min-u-sil 30

Min-u-sil 30 is the soil that has maximum percentage of fines (99.5%) in comparison to other soils used in present research program. The measured dry unit weight of Min-u-sil 30 was 13.17 kN/m^3. Figure 5.27 to Figure 5.30 show the results of the applied pressure versus settlement obtained from bearing capacity tests under four different sizes of footings, respectively. The footing was loaded to a settlement value which is equal to 30% of the footing size.

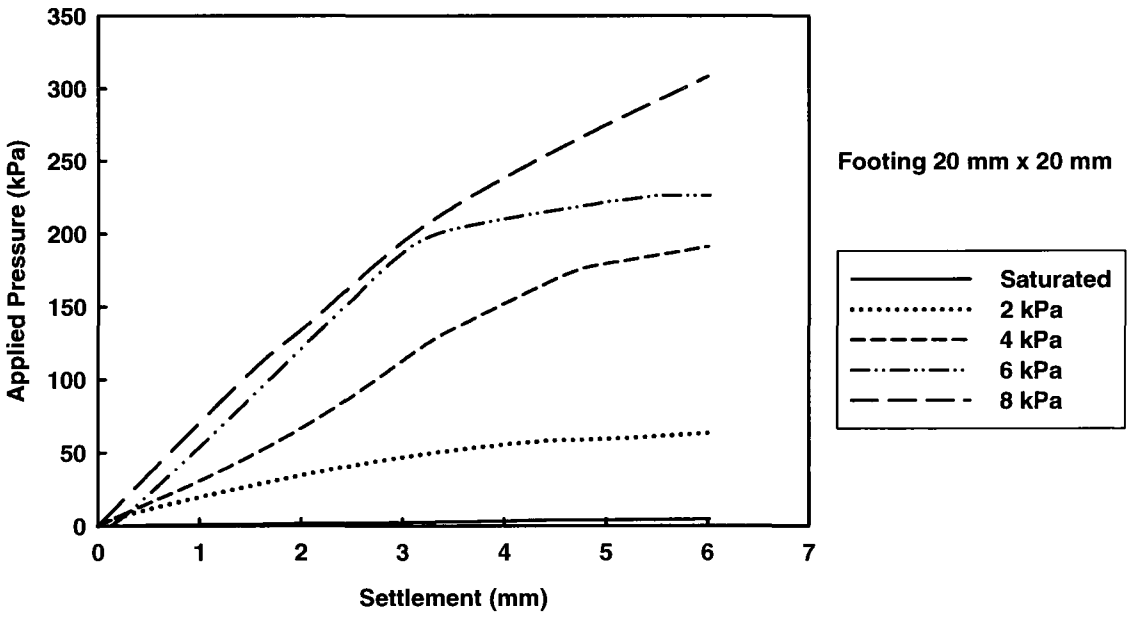

Figure 5.27 Applied pressure versus settlement of Min-u-sil 30 under the footing of 20 mm × 20 mm

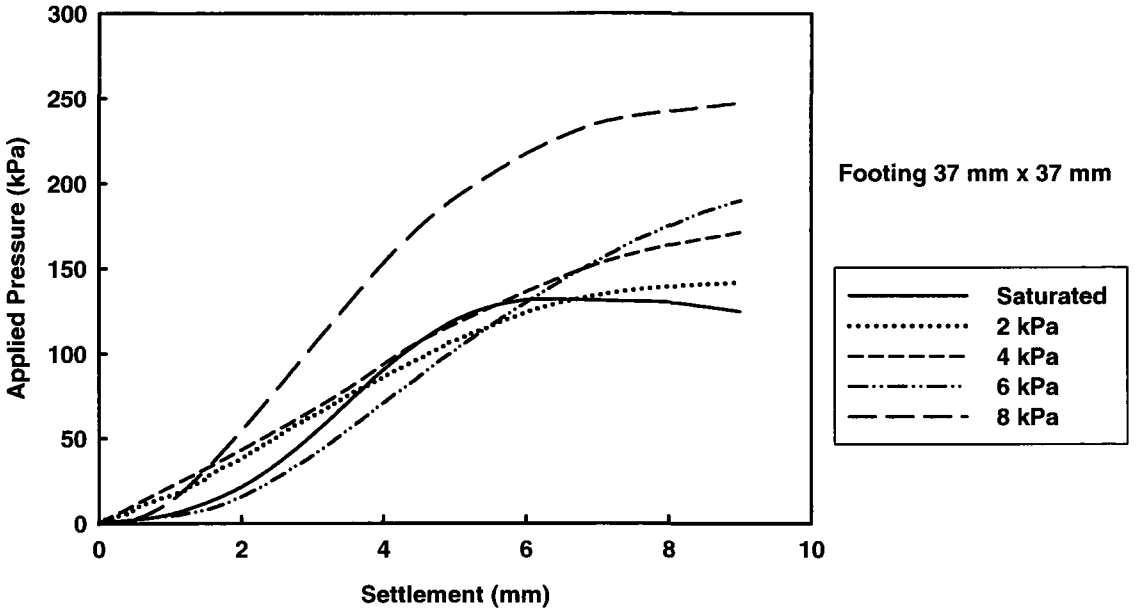

Figure 5.28 Applied pressure versus settlement of Min-u-sil 30 under the footing of 37 mm × 37 mm

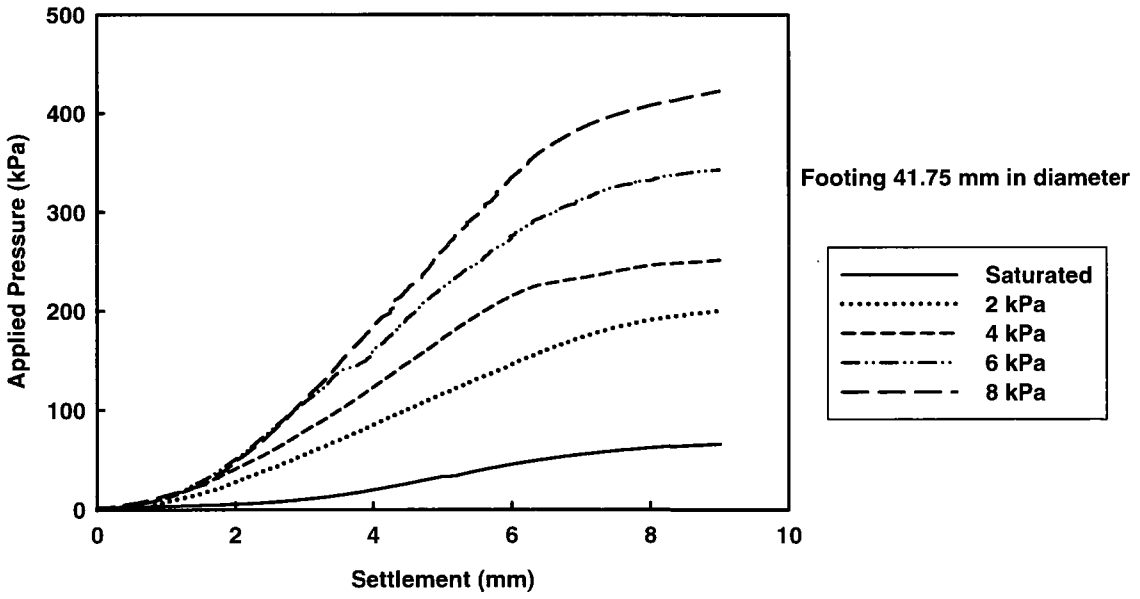

Figure 5.29 Applied pressure versus settlement of Min-u-sil 30 under the footing of 41.75 mm in diameter

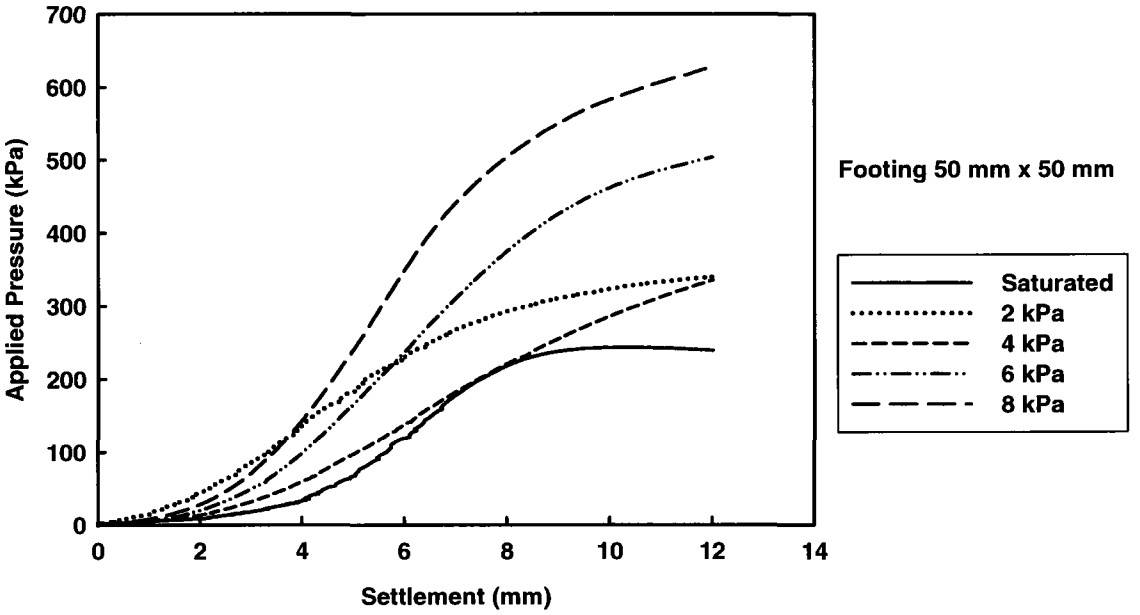

Figure 5.30 Applied pressure versus settlement of Min-u-sil 30 under the footing of 50 mm × 50 mm

Most of the results showed local shear failure behavior under different footings (Figure 5.27 to 5.30). Therefore, the ultimate bearing capacity was defined as the inflexion pressure according to ASTM D1194-94. For the specimens showing punching shear failure mode, the bearing capacity value was estimated at the settlement which is 20% of the footing size (ASTM D1194-94). The variation of bearing capacity and settlement with respect to different matric suction values for three model footings (i.e., footing 20 mm × 20 mm, footing 41.75 mm in diameter and footing 50 mm × 50 mm) are shown in Figure 5.31 and Figure 5.32, respectively.

The results of 37 mm × 37 mm footing are not consistent with the expected behavior. Such a behavior may be attributed to the influence of micro fissures or cracks or due to differences in cementation activity in this soil. As discussed earlier, more studies are necessary to further investigate this behavior.

For the measured values of elastic settlement, an applied stress of 40 kPa was used. This stress is chosen as settlement behaviour is in elastic range for the applied stress of 40 kPa.

5.4.4.1 Bearing capacity

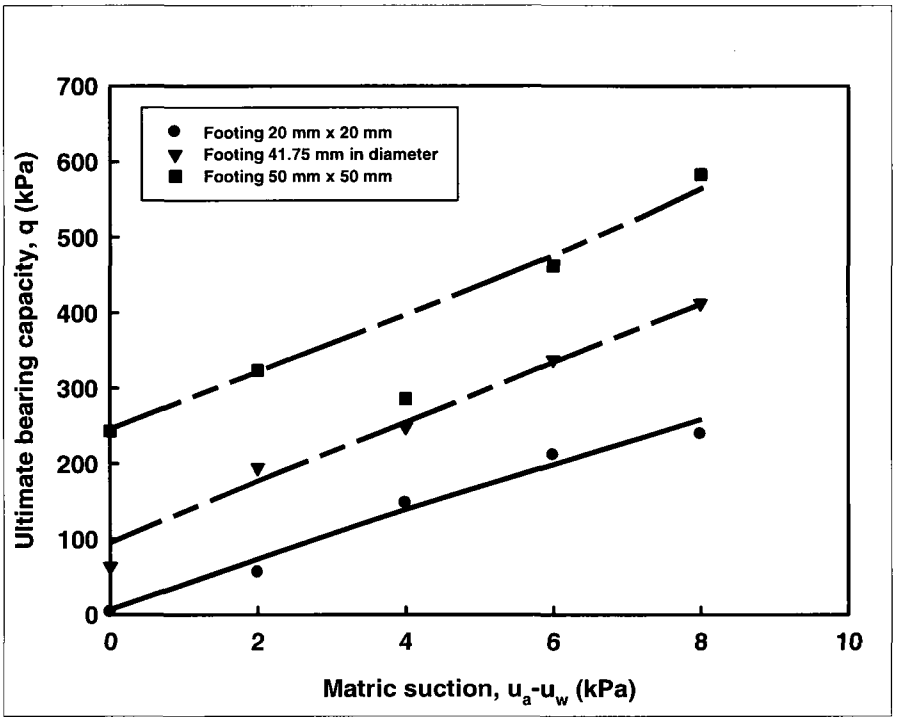

Figure 5.31 Relationship of bearing capacity versus matric suction of Min-u-sil 30

The trends from the results of three model footings (Figure 5.31) demonstrate that the bearing capacity increases linearly with increase in matric suction. This behavior is consistent with the behavior of Sil-co-sil 106, discussed in the earlier sections. As this soil has high air-entry value of 100 kPa, the range of matric suction from 0 to 8 kPa is in the boundary effect zone. In this range of matric suction, the relationship between bearing capacity and matric suction is linear. This behavior can be observed from the tests results.

For the suction range (i.e. 0 to 8 kPa), the degree of saturation S is equal to 1 so the part (i.e. $(u_a - u_w)_{AVR}$) in Equation [2.32] is proportional to the bearing capacity. Therefore, the bearing capacity increases with increase in matric suction.

$$q_{ult} = [c' + (u_a - u_w)_b(1 - S^{\psi}) \tan\phi' + (u_a - u_w)_{AVR} S^{\psi} \tan\phi'] \times N_c \xi_c + 0.5 B \gamma N_{\gamma} \xi_{\gamma} \qquad [2.32]$$

The bearing capacity value increases with an increase in the footing size under various matric suction values. Such a behavior can be attributed to the *B* value in Equation [2.32], which is the width or diameter of the footing. In addition, the change in matric suction due to the temporary cementation forces was also observed as Sil-co-sil 106. More research is necessary to understand the influence of cementation forces on the matric suction readings.

5.4.4.2 Settlement behavior

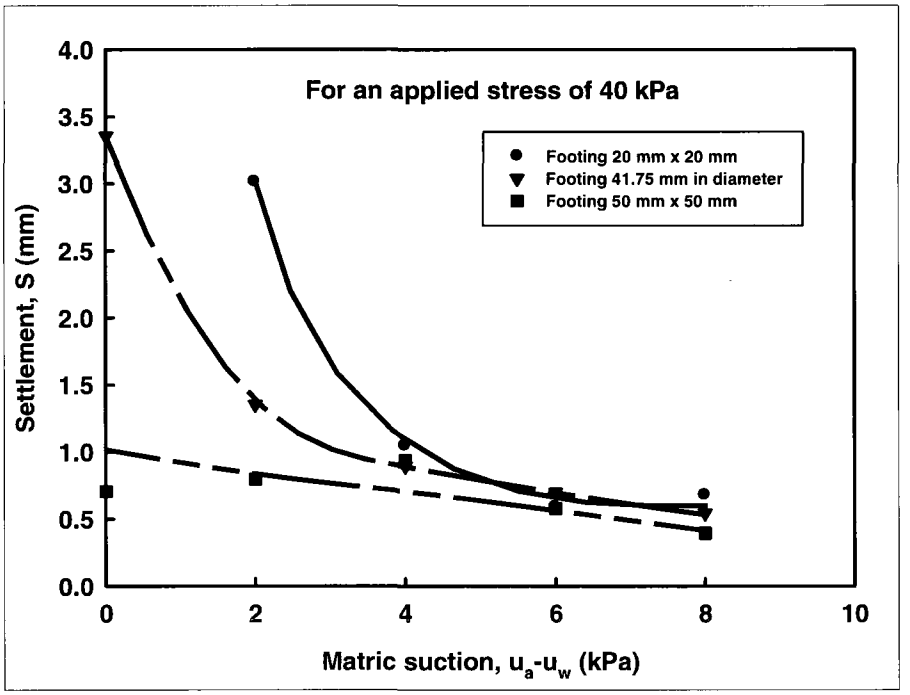

Figure 5.32 Relationship of settlement versus matric suction of Min-u-sil 30

Similar to Sil-co-sil 106, Min-u-sil 30 showed similar trends in the settlement behaviour. Elastic settlement decreases with increase in matric suction since both soils have relatively high air-entry values which are higher than the suction range (i.e., 0 to 8 kPa). The modulus of elasticity (i.e. Eq. [2.37]) can increase along with matric suction as the degree of saturation *S* is equal to 1 in the suction range. Therefore, the settlement decreases with an increase in matric suction. Furthermore, larger size footing settlements are lower than the smaller size footing for all the different matric suction values that were used in the testing program.

$$E_{unsat} = E_{sat}\left[1+\alpha\frac{(u_a-u_w)}{(P_a/100)}(S^{\beta})\right] \qquad [2.37]$$

$$E = \frac{1-\nu^2}{\Delta\delta/\Delta q_p} B_p I_w \qquad [2.24]$$

5.4.4.3 Comparisons between the measured and predicted bearing capacity values and elastic settlements

Figure 5.33 shows the comparisons between the measured and predicted bearing capacity values and elastic settlements of Min-u-sil 30 using Equations [2.32], [2.37] and [2.24]. The parameters are $\tan\phi^* = 2/3\tan\phi'$, $\nu = 0.3$, $\psi = 1$, $\beta = 1$ and $\alpha = 2.5$.

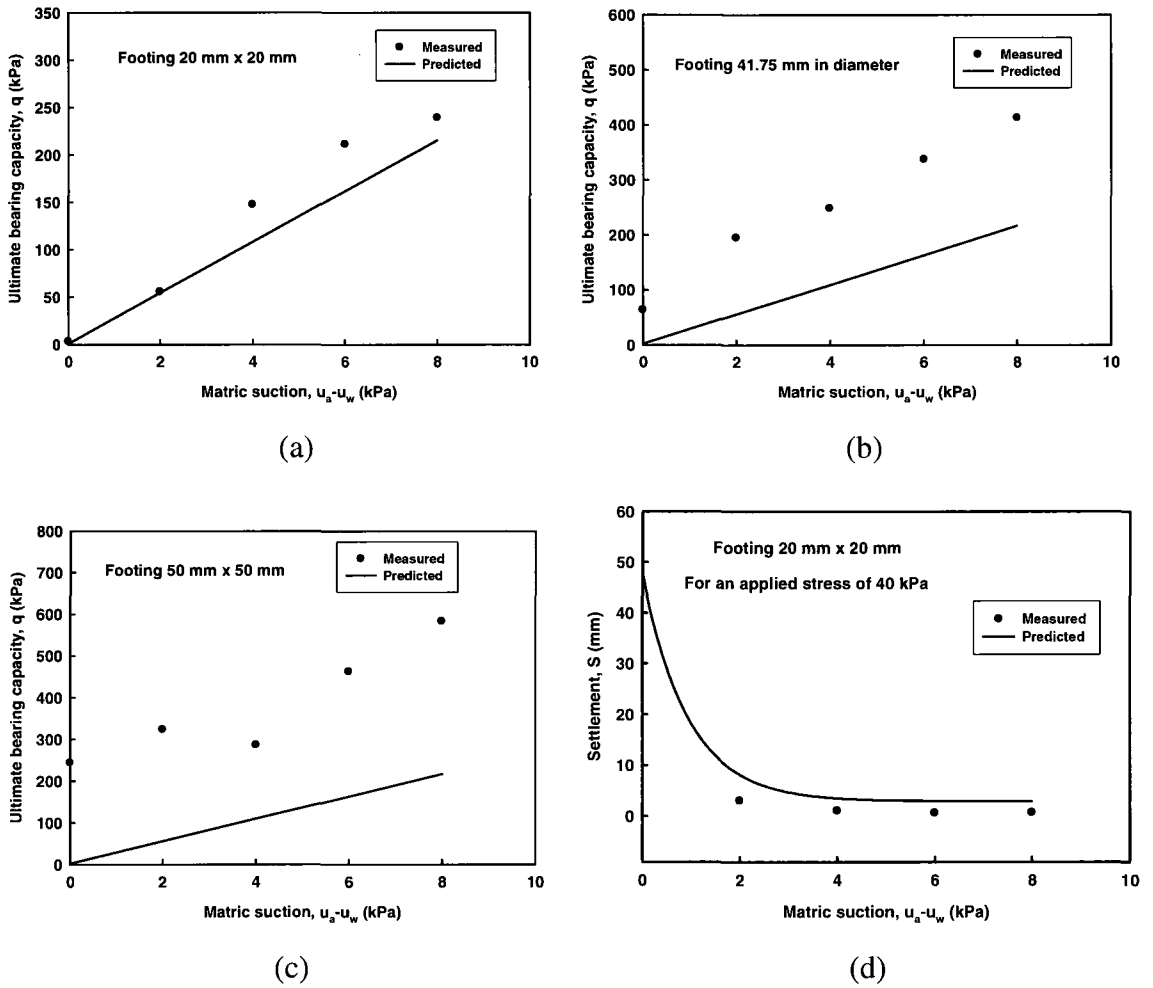

Figure 5.33 Comparisons of measured and predicted bearing capacity, and settlement of Min-u-sil 30

There is some agreement between the measured and predicted bearing capacity values and settlements for the model footing of 20 mm × 20 mm at lower matric suction values. However, as the model footing size increases, the measured bearing capacity values are relatively higher than the predicted values. The differences in the measured and predicted bearing capacity values can be attributed to the cementation forces. Rinaldi and Capdevila (2006) stated that matric suction and cementation together have significant influence on the stress-strain behaviour of many soils. However, the matric suction is still the main parameter that contributes to an increase in the bearing capacity and reducing settlement of soils that are in a state of unsaturated condition.

5.5 Summary

In this chapter, the results of bearing capacity and settlement behaviour for four different unsaturated soils were analyzed. The bearing capacity test system (described in Chapter 3) used was reliable and efficient for conducting the proposed research program using the model footing tests. For the coarse-grained soils (i.e., Filtration sand and Quarry sand), the bearing capacity increases up to the residual suction value and then decreases with further increase in matric suction value; however, the settlement decreases up to residual suction value and gradually starts increasing along with an increase in the matric suction. The proposed equations by Vanapalli and Mohamed (2007) and Oh et al. (2009) are respectively found to be useful for interpreting and predicting the bearing capacity and elastic settlement of unsaturated soils.

For the fine-grained soils (i.e. Sil-co-sil 106 and Min-u-sil 30), the bearing capacity increases and settlement decreases in the matric suction range of 0 to 8 kPa. The bearing capacity value increases with an increase in the footing size. There is a linear increase in the bearing capacity because the matric suction range (i.e., 0 to 8 kPa) falls in the boundary effect zone. However, there is an opposite trend with respect to settlement behaviour; which is again consistent expected behavior in unsaturated soils. The results clearly show that cementation forces influence the bearing capacity and settlement behavior of Sil-co-sil 106 and Min-u-sil 30. This is demonstrated from the measured results which show higher bearing capacity and lower settlement than the expected

contribution from matric suction. More investigations are however necessary to better understand the various parameters that influence these soils.

CHAPTER 6

CONCLUSIONS AND RECOMMENDATIONS

6.1 Summary

The key objective of the research presented in this thesis is to determine the bearing capacity and settlement behaviour of four different soils of which the first two were coarse-grained soils (i.e. Filtration sand and Quarry sand) and the remainder two were fine-grained soils (i.e. Sil-co-sil 106 and Mil-u-sil 30) using four different sizes of model footings (i.e., 20 mm × 20 mm, 37 mm × 37 mm, 41.75 mm in diameter, and 50 mm × 50 mm) over a suction range of 0 to 8 kPa. The two fine-grained soils (i.e., Sil-co-sil 106 and Mil-u-sil 30) studied are commonly used in mining industry. Sil-co-sil 106 is used for a variety of foundry products and Min-u-sil 30 is used as filler and extender for paints, inks and plastics and other industrial applications.

The range of matric suction 0 to 8 kPa extends over the boundary effect, transition and residual stages (Vanapalli et al. 1999) for the two coarse-grained soils studied in the present research program. Both the coarse-grained soils provided an excellent opportunity to understand the nonlinear nature of the bearing capacity and settlement behaviour over this matric suction range. In addition, these test results also provided an opportunity to verify the semi-empirical models proposed by Vanapalli and Mohamed (2007) and Oh et al. (2009) for predicting the bearing capacity and settlement behaviour of the two coarse-grained soils, respectively. The semi-empirical models for predicting the bearing capacity and settlement behaviour need the saturated soil properties and the Soil-Water Characteristic Curve (SWCC).

The matric suction in the stress bulb below the model footings of the two fine-grained soils (i.e. Sil-co-sil 106 and Mil-u-sil 30) was changing because of cementation properties

during the test. Due to this reason, the bearing capacity and settlement behaviour of Sil-co-sil 106 were not predicted. However, for both these soils, the bearing capacity and settlement behaviour were determined and the results were analyzed. An attempt was made to predict the bearing capacity and settlement behaviour of Min-u-sil 30.

The bearing capacity and settlement behaviour from model footing tests for all the four soils were conducted under a controlled laboratory environment using a strain rate of 1.143 mm/min. The same strain rate was also used for determining the saturated shear strength parameters of the coarse-grained soils using the triaxial shear apparatus. The modelling studies by Oh & Vanapalli (2008) show that the bearing capacity of model footings of 50 mm width or lower can be conducted using relatively smaller size tanks of 300 mm diameter. Li (2008) designed a special bearing capacity test system using 300 mm diameter cylinder to conduct to model tests using footing sizes lower than 50 mm using soil suction profile technique (described in Chapter 3). The equipment and the technique were used in the present research program; they worked well for conducting all the 80 tests described in the present research program. These many numbers of tests would not have been possible to be conducted with the specially designed equipment.

6.2 Conclusions

The following conclusions can be drawn from the studies undertaken through this research program.

(i) The variation of bearing capacity of coarse-grained soils (i.e., Filtration sand and Quarry sand) with respect to matric suction was nonlinear in nature. The bearing capacity increases up to the residual suction value and then decreases with further increase in matric suction values. All the footings showed similar behaviour. The trends for settlement are however opposite; the settlement decreases up to residual suction value and gradually start increasing along with an increase in the matric suction. These results are consistent with the bearing capacity results reported in the literature by Mohamed and Vanapalli (2006) and settlement behaviour reported by Oh et al. (2009).

(ii) For the unsaturated fine-grained soils (i.e. Sil-co-sil 106 and Min-u-sil 30), bearing capacity increases and settlement decreases as the matric suction increases because the suction range (i.e. 0 to 8 kPa) is in the boundary effect zone. In other words, the suction range in the boundary effect zone is lower than the air-entry value (i.e. saturation zone). These results are consistent with the theoretical formulations of the bearing capacity and settlement behaviour of unsaturated soils.

(iii) The footing size (from 20 mm to 50 mm) has significant influence on the measured bearing capacity and settlement behaviour of the unsaturated soils. The bearing capacity value increases with an increase in the footing size. However, there is an opposite trend with respect to settlement behaviour; which translates to lower settlement for footings when the footing sizes are larger.

(iv) Sil-co-sil 106 has shown significant resistance to the static loading conditions; however, it offers limited resistance to vibration or dynamic loading conditions. When a footing is loaded in this soil, there is a partial collapse and water squeezes out from the zone of loading into other regions of low initial water content. This tendency proliferates with further loading of the footing and contributes to total collapse.

(v) The proposed equations by Vanapalli and Mohamed (2007) and Oh et al. (2009) are respectively useful for predicting the bearing capacity and elastic settlement of unsaturated soils. There are good comparisons between the measured and predicted bearing capacity and settlement values for all sands with different model footings.

(vi) A value of fitting parameter α (which is influenced by footing size) controls the variation of the modulus of elasticity (see Equation [2.37]) between 0.5 and 2 provides conservative elastic settlements. It is recommended to use these values in engineering practice.

6.3 Recommendations

Some recommendations are provided for future research work.

(i) The matric suction values closer to the soil surface are highly sensitive to the humidity conditions of the testing environment. The matric suction can be relatively high in dry environments and low in humid environments. Due to this reason, the representative matric suction value (i.e., $(u_a - u_w)_{AVR}$) estimated may be erroneous if matric suction values are not determined close to the surface. Therefore, it is suggested to measure the water content value closer to the surface and back calculate the matric suction value from the measured SWCC data on the same soil. Such a technique will be useful in the reliable estimation of representative matric suction value (i.e., $(u_a - u_w)_{AVR}$).

(ii) More tests are necessary to be conducted at different strain rates to understand its influence to the bearing capacity and settlement behaviour.

(iii) The matric suction in the stress bulb below the footings of all the two fine-grained soils (i.e. Sil-co-sil 106 and Mil-u-sil 30) is significantly influenced due to the cementation forces. Small model footings may not provide reliable results. It is recommended to use larger size model footings and a larger size bearing capacity tank for obtaining reliable and reproducible results. More research is necessary to understand the influence of cementation forces on the matric suction readings.

References

Adams, M.T., and Collin, J.G. 1997. Large model spread footing load tests on geosynthetic reinforced soil foundations. Journal of Geotechnical and Geoenvironmental Engineering, ASCE, Vol. 123, No. 1.

Agarwal, K.B., and Rana, M.K. 1987. Effect of ground water on settlement of footings in sand. *In* proceedings of the 9th European Conference on Soil Mechanics and Foundation Engineering, pp. 751-754.

Alim, M.A., Nishigaki, M., Chegbeleh, L.P., Akudago, J.A. and Komatsu, M. 2009. Determination of soil-water characteristic curves of unsaturated sandy soils using membrane filter with stainless wire mesh. Journal of the Faculty of Environmental Science and Technology, Okayama University, **14**(1), pp. 13-16.

ASTM, D1194-94. 2003. Standard test method for bearing capacity of soil for static load and spread footings. American Society of Testing Material, Philadelphia.

ASTM, D2216. 1994. Laboratory determination of water (moisture) content of soil and rock by mass. American Society of Testing Material, Philadelphia.

ASTM, D422. 1994b. Standard test method for particle size analysis of soils. American Society of Testing Material, Philadelphia.

ASTM, D4767-04. 2004. Standard test method for consolidated undrained triaxial compression test for cohesive Soils. American Society of Testing Material, Philadelphia.

ASTM, D6836-02. 2008. Standard test methods for determination of the soil water characteristic curve for desorption using a hanging column, pressure extractor, chilled mirror hygrometer, and/or centrifuge. American Society of Testing Material, Philadelphia.

Bolton, M.D. 1986. The strength and dilatancy of sands. Géotechnique, **36**(1): 65-78.

Broms, B.B. 1964. The effect of degree of saturation on the bearing capacity of flexible

pavements. Highway Research Recoed, No. 71: 1-14.

Carter, J.P. 2006. Application of structured soil models to shallow footing problems. Soil and Rock Behavior and Modeling (GSP 150), ASCE, 194, 2.

Costa, Y.D., Cintra J.C., and Zornberg J.G. 2003. Influence of matric suction on the results of plate load tests performed on a lateritic soil deposit. Geotechnical Testing Journal, **26**(2): 219 – 226.

Das, Braja M. 1999. Shallow foundations: bearing capacity and settlement. CRC Press LLC, Florida.

Davis, A.G., and Poulos, H.G. 1968. The use of elastic theory for settlement prediction under three dimensional conditions. Géotechnique, **18**: 67-91.

Dregne, H.E. 1976. Soils in arid regions. New York: American Elsevier, 5 pp.

Fall, M., Benzaazoua, M., and Ouellet S. 2004. Effect of tailings properties on paste backfill performance. *In* Proceedings of 8th International Symposia on Mining with Backfill, Beijing, China, pp. 193-202.

Fredlund, D.G., and Morgenstern, N.R. 1977. Stess state variables for unsaturated soils. Journal of Geotechnical Engineering, **103**(GT5): 447-466.

Fredlund, D.G., and Rahardjo, H. 1993. Soil mechanics for unsaturated soils. John Wiley & Sons, INC., New York.

Fredlund, M.D., Wilson, G.W., and Fredlund, D.G. 2002. Use of the grain-size distribution for estimation of the soil-water characteristic curve. Canadian Geotechnical Journal, **39**: 1103-1117.

Kumbhojkar, A.S. 1993. Numerical evaluation of Terzaghi's N_γ. Journal of Geotechnical Engineering, ASCE, **119**(3): 598.

Lade, P.V. 1988. Model and parameters for the elastic behavior of soils. *In* proceedings of the International Conference on Numerical Methods in Geomechnics, Innsbruck, Austria. *Edited by* G. Swoboda. Balkema, Rotterdam, the Netherlands.

Lade, P.V., and Nelson, R.B. 1987. Modeling the elastic behavior of granular materials.

International Journal for Numerical and Analytical Methods in Geomechanics, **11**(5):521-542.

Lancelotta, R. 1995. Geotechnical engineering. Balkema, Rotterdam, the Netherlands.

Lee, C., Lee, J., Lee, W., Yoon, H., Cho, T., and Quang, T.H. 2007. Cementation effects on rigid-soft particle mixtures. Geo-Denver: New Peaks in Geotechnics.

Li, X.D. 2008. Laboratory studies on the bearing capacity of unsaturated sands. Master's thesis, University of Ottawa, Ottawa, Ont.

Lu, N., and Likos, W. 2004. Unsaturated soil mechanics. John Wiley and Sons, New York, NY, USA.

Mayne, P.W., and Poulos, H.G. 1999. Approximate displacement influence factors for elastic shallow foundations. Journal of Geotechnical and Geoenvironmental Engineering, ASCE, **125**(6): 453-460.

Meyerhof, G.G. 1951. The ultimate bearing capacity of foundations. Géotechnique, **2**: 301 – 332.

Miller, G.A., and Muraleetharan, K.K. 1998. In situ testing in unsaturated soil. *In* Proceedings of the 2nd International Conference on Unsaturated Soils, Beijing, China, **1**: 416– 421.

Mohamed, F.M.O., and Vanapalli, S.K. 2006. Laboratory investigations for the measurement of the bearing capacity of an unsaturated coarse-grained soil. *In* Proceedings of the 59th Canadian Geotechnical Conference. Vancouver, British Columbia, Canada.

Mohamed, F.M.O., and Vanapalli, S.K. 2009. An experimental investigation of the bearing capacity of unsaturated sand using cone penetration tests. *In* Proceedings of the 62nd Canadian Geotechnical Conference & 10th Joint CGS/IAH-CNC Groundwater Conference, Halifax, Canada.

Mohamed, F.M.O., Vanapalli, S.K., and Saatcioglu, M. 2010. Comparison of bearing capacity of unsaturated sand using the cone penetration tests (CPT) and the plate load

tests (PLT). *In* Proceedings of the 5th International Conference on Unsaturated Soils, Barcelona, Spain.

Nasir, O., and Fall, M. 2009. Modeling the heat development in hydrating CPB structures. Computers and Geotechnics, **36**: 1207-1218.

Oh, W.T., and Vanapalli, S.K. 2008. Modelling the stress versus settlement behavior of model footings in saturated and unsaturated sandy soils. *In* Proceedings of the 12th International Conference of International Association for Computer Methods and Advances in Geomechanics (IACMAG), Goa, India.

Oh, W.T., Vanapalli, S.K., and Puppala, A.J. 2009. Semi-empirical model for the prediction of modulus of elasticity for unsaturated soils. Canadian Geotechnical Journal, **46**: 903-914.

Oloo, S.Y. 1994. A bearing capacity approach to the design of low-volume traffic roads. PhD thesis, University of Saskatchewan, Saskatoon, SK, Canada.

Oloo, S.Y., Fredlund, D.G., and Gan, J.K-M. 1997. Bearing capacity of unpaved roads. Canadian Geotechnical Journal, **34**: 398 – 407.

Poulos, H.G., and Davis E.H. 1974. Elastic solutions for soil and rock mechanics. John Wiley and Sons, NY, USA.

Reinson, J.R., Fredlund, D.G., and Wilson, G.W. 2005. Unsaturated flow in coarse porous media. Canadian Geotechnical Journal, **42**: 252-262.

Rinaldi, V.A., and Capdevila, J.A. 2006. Effect of cement and saturation on the stress-strain behavior of a silty clay. Unsaturated Soils 2006 (GSP 147), ASCE, Vol. 189, No. 94.

Rowlett, D.K. 2000. Development of a stand-pipe lysimeter for unsaturated waste rock. Master's thesis, University of Saskatchewan, Saskatoon, Sask., Canada.

Salgado, R., Bandini, P., and Karim, A. 2000. Shear strength and stiffness of silty sand. Journal of Geotechnical and Geoenvironmental Engineering, ASCE, Vol. 126, No. 5.

Schnaid, F., Consoli, N.C., Cudmani, R.O., and Militistsky, J. 1995. Load-settlement

response of shallow foundations in structured unsaturated soils. *In* Proceedings of the 1st International Conference of Unsaturated Soils, Paris, France, pp. 999 – 1004.

Simons, N.E., and Som, N.N. 1970. Settlement of structures on clay with particular emphasis on London clay. Construction Industry Research and Information Association, London. Report 22.

Skempton, A.W. 1948. The $\phi_u = 0$ analysis for stability and its theoretical basis. *In* Proceedings of the 2nd International Conference of Soil Mechanics and Foundation Engineering, **1**: 72-77.

Steensen-Bach, J.O., Foged, N., and Steenfelt, J.S. 1987. Capillary induced stresses – fact or fiction?. 9th ECSMFE, Groundwater Effects in Geotechnical Engineering, Dublin: 83-89.

Terzaghi, K. 1943. Theoretical soil mechanics. John Wiley and Sons, INC., New York, NY, USA.

Timoshenko, S., and Goodier, J.N. 1951. Theory of elasticity. McGraw-Hill, New York.

Vanapalli, S.K. 2009. Shear strength of unsaturated soils and its applications in geotechinical engineering practice. UNSAT Asia-Pacific 2009, Australia, Keynote.

Vanapalli, S.K., Fredlund, D.G., Pufahl, D.E., and Clifton, A.W. 1996. Model for the prediction of shear strength with respect to soil suction. Canadian Geotechnical Journal, **33**(3):379-392.

Vanapalli, S.K., Fredlund, D.G., and Pufahl, D.E. 1999. The influence of soil structure and stress history on the soil-water characteristic curve of a compacted till. Géotechnique, **49**(2): 143-159.

Vanapalli, S.K., and Mohamed, F.M.O. 2007. Bearing capacity of model footings in unsaturated soils. *In* Experimental Unsaturated Soil Mechanics. Springer Proceedings in Physics. Springer-Verlag Berlin Heidelberg. Vol. 112. pp. 483-493.

Vanapalli, S.K., Oh, Won Taek, and Puppala, Anand J. 2007. Determination of the bearing capacity of unsaturated soils under undrained loading conditions. *In*

Proceedings of 60th Canadian Geotechnical Conference & 8th Joint CGS/IAH-CNC Groundwater Conference, T6-A, Ottawa, Canada.

Vanapalli, S.K., Sun, R., and Li, X. 2010. Bearing capacity of an unsaturated sand from model footing tests. *In* Proceedings of the 5th International Conference on Unsaturated Soils, Barcelona, Spain.

Vesić, A.S. 1963. Bearing capacity of deep foundations in sand. Highway Research Record, **39**: 112-153.

Vesić, A.S. 1973. Analysis of ultimate loads of shallow foundations. Journal of the Soil Mechanics and Foundation Division, ASCE, **99**(SM1): 45 – 73.

Yongfu Xu 2004. Bearing capacity of unsaturated expansive soils. Geotechnical and Geological Engineering, **22**: 611 – 625.

APPENDIX

Table A.1 Grain size distribution data of Filtration sand

Sieve No.	Opening diameter	Mass retained	% retained	% passing
	(mm)	(g)		Cumulative
12	1.7	0	0	100
20	0.85	164.01	16.401	83.599
25	0.71	235.39	23.539	60.06
30	0.6	359.32	35.932	24.128
40	0.425	201.5	20.15	3.978
60	0.25	29.15	2.915	1.063
Pan		6.13	0.613	0

Table A.2 Grain size distribution data of Quarry sand

Sieve No.	Opening diameter	Mass retained	% retained	% passing
	(mm)	(g)		Cumulative
30	0.6	9.91	0.991	99.009
40	0.425	10.68	1.068	97.941
60	0.25	175.5	17.55	80.391
80	0.18	339.81	33.981	46.41
100	0.15	175.61	17.561	28.849
200	0.075	247.04	24.704	4.145
Pan		36.15	3.615	0

Table A.3 Chemical analysis of Filtration sand

Chemical compound	% by weight
Silicon Dioxide (SiO_2)	99.230
Iron Oxide (Fe_2O_3)	0.110
Aluminum Oxide (Al_2O_3)	0.330
Calcium Oxide (CaO)	0.020
Titanium Dioxide (TiO_2)	0.010
Magnesium Oxide (MgO)	0.010
Potassium Oxide (K_2O)	0.010
Loss on Ignition (L.O.I.)	0.160

Table A.4 Suction profile data of Filtration sand

Depth of water table (mm)	Matric suction of 50 mm below soil suface (kPa)	Matric suction of 100 mm below soil suface (kPa)
0	0	0
50	0.8	0.8
150	1.8	1.8
250	2.2	2.2
350	3.6	3.6
450	4.4	4.4
550	6	5
650	7.8	5.6
750	9	6.2
850	11.6	7.4

Table A.5 Suction profile data of Quarry sand

Depth of water table (mm)	Matric suction of 50 mm below soil suface (kPa)	Matric suction of 100 mm below soil suface (kPa)
0	0	0
50	0.4	0.4
150	1.5	1.5
250	2.4	2.4
350	3.3	3.3
450	4	4
550	5.3	5.3
650	6.2	6.2
750	7	7

Table A.6 Typical Chemical Analysis of Sil-co-sil 106 (%)

Silicon Dioxide (total)	SiO_2	> 99.80
Aluminum Oxide	Al_2O_3	~ 0.05
Iron Oxide	Fe_2O_3	~ 0.04
Titanium Oxide	TiO_2	~ 0.02
Calcium Oxide	CaO	< 0.01
Loss On Ignitition	LOI	~ 0.10

Table A.7 Typical Physical Properties of Sil-co-sil 106

Colour	White	Mineral	Quartz
Hardness (Mohs)	7	Moisture	< 0.20%
Specific Gravity (g/cc)	2.65	Melting Point (°F)	~ 3100
pH	7	Melting Point (°C)	~ 1700

Table A.8 Suction profile data of Sil-co-sil 106

Depth of water table (mm)	Matric suction of 50 mm below soil suface (kPa)	Matric suction of 100 mm below soil suface (kPa)
0	0	0
50	0	0
150	1.8	1.8
250	2.8	2.8
350	4	4
450	4.8	4.8
550	5.8	5.8
650	7	7
750	8	8
850	9	9

Table A.9 Typical Chemical Analysis of Min-u-sil 30 (%)

SiO_2 (Silicon Dioxide)	99.5	MgO (Magnesium Oxide)	0.01
Fe_2O_3 (Iron Oxide)	0.024	Na_2O (Sodium Oxide)	0.01
Al_2O_3 (Aluminum Oxide)	0.30	K_2O (Potassium Oxide)	0.01
TiO_2 (Titanium Dioxide)	0.01	LOI (loss on Ignition)	0.2
CaO (Calcium Oxide)	0.02		

Table A.10 Typical Physical Properties of Min-u-sil 30

Bulk density-compacted (kg/m^3)	1009.16	pH	6.5
Bulk density-uncompacted (kg/m^3)	784.90	-30 Micron (%)	97
Hardness (Mohs)	7	+325 Mesh (%)	0.3
Median diameter (MICRONS)	8.0	Yellowness index	4.0
Oil absorption (D-1483)	23	Specific gravity	2.65

Table A.11 Suction profile data of Min-u-sil 30

Depth of water table (mm)	Matric suction of 50 mm below soil suface (kPa)	Matric suction of 100 mm below soil suface (kPa)
0	0	0
150	0.2	0.2
350	3.6	3.6
550	6.4	6.4
750	8.6	8.6